

Probabilistic rainfall nowcasting with Machine Learning models

Dina Pirone

Dipartimento di Ingegneria Civile, Edile e Ambientale

Università degli Studi di Napoli Federico II

Thesis submitted for the degree of PhD in Civil Systems Engineering

Napoli, March 2023

Supervisors

Prof. Giuseppe Del Giudice, Università degli Studi di Napoli Federico II,

Prof. Domenico Pianese, Università degli Studi di Napoli Federico II

Co-Supervisors

Prof. Patrick Willems, Katholieke Universiteit Leuven, Belgium

Prof. Luigi Cimorelli, Università degli Studi di Napoli Federico II

PhD Programme Coordinator - XXXV Cycle

Prof. Andrea Papola, Università degli Studi di Napoli Federico II

The Reading Committee

Prof. Claudia Teutschbein, Uppsala Universitet, Sweden

Prof. Maurizio Mazzoleni, Vrije Universiteit Amsterdam, Netherlands

Copyright © 2023 by Dina Pirone

All rights reserved. No part of this material may be copied or reproduced in any way without the author's prior permission.

Abstract

Nowcasting models use real-time data to predict rainfall with short lead times - from a few minutes up to six hours. They influence many aspects of daily life in hydrological, agricultural, and economic sectors. For example, they facilitate drivers by predicting road conditions, enhance flight safety by providing weather guidance, and prevent casualties by issuing rainfall alerts which can affect human life and cause environmental issues. However, short-term prediction is challenging because meteorological variables are strongly interconnected and rapidly change during events. In addition, the long computational times and low spatial and temporal resolution of nowcasting models do not often suit the short-term prediction requirements. This thesis focuses on developing an approach for probabilistic rainfall nowcasting with machine learning. Since machine learning does not require any previous physical assumption, this research investigates their ability to provide reliable and quick forecasts. A machine learning model for probabilistic rainfall nowcasting for short lead times - from a few minutes up to 6 hours - is proposed. The model employs cumulative rainfall fields from station data as inputs for feed-forward neural networks to predict rainfall intervals and the corresponding probabilities of occurrence. Using cumulative rainfall depths from station data overcomes the lack of temporal memory of the feed-forward neural networks. In this way, using only the current rain field as input, the model exploits pattern recognition techniques combining temporal - cumulative rainfall depth - and spatial - cumulative rainfall field - information. Several feed-forward neural networks were independently trained and tested on almost 360 rainfall events over the study area - one of the eight warning zones of the Campania Region. First, comprehensive nowcasts verifications were performed to analyze probabilistic nowcasts' reliability using continuous and categorical indicators. The performance of the models was also compared with the results of two different benchmarks: Eulerian Persistence and Pysteps. Then, to assess

the extendibility of the procedure to other regions, the model was applied to another study area that differed from southern Italy one: the Flanders Region of Belgium. Results showed that using temporal and spatial information enables the model to predict short-term rainfall using only the current measurements as input, resulting in a rapid, easily replicable, and convenient nowcasting approach. Therefore, the procedure effectively predicts multi-step rainfall fields and is suitable for operational early warning systems.

Keywords: Precipitation nowcasting; Multi-step predictions; Rain-gauge measurements; Pattern recognition; Feed-forward neural networks; Cumulative rainfall fields.

Abstract (Ita)

I modelli di *nowcasting* forniscono previsioni meteorologiche a breve termine, da pochi minuti fino a un massimo di sei ore. Essi influenzano molti aspetti della vita quotidiana, e sono decisivi durante le situazioni di emergenza. I modelli di *nowcasting*, infatti, condizionano la viabilità stradale, migliorano la sicurezza aerea fornendo indicazioni meteorologiche, e, soprattutto, supportano i sistemi di allerta meteo che possono salvaguardare la vita umana e prevenire disastri ambientali. Tuttavia, le variabili meteorologiche sono fortemente interconnesse tra di loro e cambiano rapidamente durante un evento. Inoltre, i lunghi tempi di elaborazione e la bassa risoluzione spaziale e temporale dei modelli previsionali spesso non si addicono alle esigenze di una previsione con associato un anticipo di non oltre 6 ore. Di conseguenza, i sistemi di *nowcasting* sono impegnativi da implementare e l'utilizzo di modelli numerici di previsione risulta spesso inadeguato. Recenti sviluppi nel campo dell'intelligenza artificiale hanno fornito un approccio innovativo per costruire modelli previsionali di grandezze idrologiche: le Reti Neurali Artificiali. L'innovazione consiste nella possibilità di individuare caratteristiche spaziali e temporali rilevanti nei dati forniti al modello e di utilizzarle per previsioni future, senza effettuare assunzioni a priori. In questo modo, si potrebbero cogliere le regole che spieghino le relazioni che intercorrono tra le variabili idrologiche coinvolte nell'evento piovoso, anche se non si conoscono le soluzioni dettagliate e analitiche che caratterizzano il problema sotto indagine. Il presente elaborato è volto allo sviluppo di un modello basato sugli algoritmi dell'intelligenza artificiale per la previsione delle piogge a breve termine. Viene di seguito proposto un modello per il *nowcasting* probabilistico delle precipitazioni, da pochi minuti a sei ore. Il modello impiega campi di pioggia cumulati come input a reti neurali di tipo *Feed Forward* per prevedere possibili intervalli di pioggia e le corrispondenti probabilità di realizzazione, dopo un fissato orizzonte temporale. In primo luogo, la procedura è

stata applicata a un'area di 1619 km² in una Regione dell'Italia meridionale. Diverse reti neurali di tipo feed forward sono state indipendentemente addestrate e testate su quasi 360 eventi pluviometrici verificatisi nell'area di studio, una delle otto zone di allerta della Regione Campania. Le prestazioni dei modelli sono state confrontate con i risultati di due diversi benchmark: la persistenza euleriana e Pysteps. Dopodiché, al fine di valutare l'estendibilità della procedura ad altre regioni, il modello è stato applicato a un'altra area di studio, diversa da quella dell'Italia meridionale: la regione delle Fiandre, in Belgio. Tutti i modelli hanno prodotto previsioni coerenti e hanno riprodotto l'evoluzione spazio-temporale delle precipitazioni. I risultati hanno dimostrato che l'utilizzo combinato di informazioni temporali e spaziali consente al modello di prevedere le precipitazioni a breve termine utilizzando solo le misurazioni attuali come input, risultando in un approccio di *nowcasting* rapido, facilmente replicabile e conveniente. Risultati che confermano con un certo successo che la strada delle Reti Neurali Artificiali, integrata con altre grandezze idrologiche, potrebbe essere foriera di significativi benefici per il miglioramento delle previsioni. Se da un lato questa caratteristica presenta notevoli vantaggi perché permette di affrontare molti problemi di cui non sono note le soluzioni analitiche; dall'altro vi è però il pericolo di rinunciare a cercare di comprendere a fondo la natura di un problema e di rifugiarsi in una soluzione di tipo data-driven. Il mondo della ricerca scientifica trova oggi nuovi stimoli per lo studio di queste tecniche, con l'obiettivo di portare a livelli sempre più accettabili l'affidabilità degli strumenti operativi di previsione.

Acknowledgements

Many people shaped my journey with their support, visions, generosity, and love, and I am delighted to thank them all.

This journey would not have been possible without the trust and motivation of Prof. Domenico Pianese. His mentoring and experience spurred new ideas and challenges, which turned into a doctoral thesis. I am grateful for the inspiring and constructive conversations and his forward-looking plans.

My profound appreciation goes to Prof. Giuseppe Del Giudice, his guidance and perspectives were impeccable during every part of the journey. With outstanding acumen and remarkable humour, he provided practical solutions and directed towards the right path at doubtful junctions.

I sincerely thank Prof. Patrick Willems, who considered me an effective team member. I was amazed by his multitasking capabilities and astonishing intellect. His hints and observations deeply influenced my research.

Special thanks go to Prof. Luigi Cimorelli, who provided a sound basis for the research topic and contributed to developing the initial idea, starting from scratch. His skills were awe-inspiring and mainly encouraged my progress as a researcher.

I want to express my gratitude to the reading committee for their time spent examining this thesis and for their thorough and constructive remarks regarding my research.

A sincere acknowledgement is extended to Professors Luca Cozzolino, Salvatore Manfreda, and Giovanni Menduni, who supported part of my journey, involving me in their research projects. Working with them allowed me to experience different points of view and develop novel and soft skills.

I am grateful to Ing. Andrea D'Aniello for his helping hand and sound advice. I appreciated his encouragement, attention to detail, listening skills, and ability to contextualize difficulties – at least part of them.

I want to thank my colleagues at DICEA, Francesco, Margherita, Maria Cristina, Mimmo, and Roberta, who made this journey enjoyable and enriched my days and life with friendship and affection. An inevitable thank goes to the late-night feedback sessions, moral support and countless tips and strategies, which built a one-in-a-lifetime friendship with Sara.

At DICEA, I also luckily crossed the path with bright spark Professors. Since I was a master student, their knowledge-transfer capacity and fascinating competence influenced my academic and research approach. I want to acknowledge Professors Mariano Buccino, Andrea Papola and Andrea Vacca for that.

Affectionately thanks go to Arda, Danitza, Daan, and Wilhem. Since the first day of my period at KU Leuven, they have been exceptionally inclusive and kind-hearted. We shared the office and unforgettable experiences.

Let me thank my best friends, Mariamalia and Veronica, for their authentic trustworthiness. They pushed away despair, encouraging insights and achievements.

The sweetest acknowledgement goes to my darling Carmine, my best friend, coach, and closer confidante. He took for granted all my achievements while impressively celebrating.

The last and greatest thank goes to my family for their encouragement. I am grateful to my sister, who did not miss the opportunity to make me feel her role model. I am deeply grateful to my mother and father, who taught me dedication to work, perseverance, compassion, and the values of emotions. They made all the efforts and sacrifices worth it. Infine, desidero ringraziare i miei amorevoli nonni, che mi hanno donato fiducia, ispirazione, e il privilegio di essere parte della loro famiglia.

Sincerely,

Dina

Napoli, 10th March 2023

A mia Mamma

Table of Contents

LIST OF FIGURES	i
------------------------	----------

LIST OF TABLES	v
-----------------------	----------

ABBREVIATIONS	vi
----------------------	-----------

CHAPTER 1 - INTRODUCTION	1
---------------------------------	----------

1.1 - RAINFALL NOWCASTING	1
---------------------------	---

1.2 - HYDRO-METEOROLOGICAL PROCESSES	2
--------------------------------------	---

1.3 - RAINFALL MEASUREMENTS	3
-----------------------------	---

1.4 - MACHINE LEARNING MODELS	4
-------------------------------	---

1.5 - PROBABILISTIC NOWCASTING	5
--------------------------------	---

1.6 - OBJECTIVE OF THE THESIS	5
-------------------------------	---

1.7 - OUTLINE OF THE THESIS	7
-----------------------------	---

REFERENCES	8
------------	---

CHAPTER 2 - NOWCASTING MODELS	13
--------------------------------------	-----------

2.1 - NUMERICAL WEATHER PREDICTION MODELS	14
---	----

2.2 - MACHINE LEARNING MODELS	14
-------------------------------	----

2.3 - PATTERN RECOGNITION TECHNIQUES	16
--------------------------------------	----

2.4 - BENCHMARK MODELS	17
------------------------	----

2.4.1 - <i>Eulerian Persistence</i>	17
-------------------------------------	----

2.4.2 - <i>STEPS</i>	17
----------------------	----

REFERENCES	19
------------	----

CHAPTER 3 - STUDY AREA AND DATASET	24
3.1 - STUDY AREA	24
3.2 - AVAILABLE DATA	26
3.3 - RAINFALL EVENT SELECTION	27
3.4 - RAINFALL EVENT CLASSIFICATION	28
REFERENCES	31
CHAPTER 4 - METHODOLOGY: THE MACHINE LEARNING MODEL	32
4.1 - WORKFLOW	32
4.2 - INPUT VARIABLES PRE-PROCESSING	36
4.3 - MODEL SETUP AND TRAINING STRATEGY	38
4.4 - OUTPUT VARIABLES POST-PROCESSING: A PROBABILISTIC APPROACH	41
4.5 - PERFORMANCE CRITERIA	42
REFERENCES	44
CHAPTER 5 - RESULTS AND DISCUSSION	45
5.1 - NOWCAST PERFORMANCE AND SKILL EVALUATION	45
5.2 - EVENT-BASED COMPARISON	52
5.2.1 - <i>Convective event - event on 1 October 2018</i>	54
5.2.2 - <i>Stratiform event - event on 19 December 2019</i>	56
REFERENCES	60
CHAPTER 6 - TRANSFERABILITY OF THE MODEL TO OTHER CONTEXTS	61
6.1 - STUDY AREA AND DATASET	62
6.2 - MODEL PARAMETERS IN BELGIUM	65
6.3 - RESULTS AND DISCUSSION	68
6.3.1 - <i>Nowcasts performance and skill evaluation</i>	68
6.3.2 - <i>Event-based results</i>	82
REFERENCES	95

CHAPTER 7 - SYNTHESIS AND CONCLUSIONS _____ **96**

7.1 - SYNTHESIS _____ 96

7.2 - OUTLOOKS OR IMPLICATIONS FOR FUTURE RESEARCH _____ 101

DATA AVAILABILITY _____ **103**

PUBLICATIONS _____ **104**

List of Figures

FIG. 3.1	THE LOCATION OF THE STUDY AREA (LEFT) WITHIN CAMPANIA REGION AND (RIGHT) WITH THE CORRESPONDING ELEVATION AND BOUNDARIES. THE LOCATION OF METEOROLOGICAL STATIONS IS ILLUSTRATED RIGHT.	25
FIG. 3.2	EXAMPLE OF STORM EVENT SEPARATION METHOD USING 1-H MINIMUM INTER-EVENT TIME MIT. Y AXIS INDICATES AVERAGE RAINFALL DEPTH OF THE RAIN-GAUGE STATIONS OVER THE STUDY AREA.	27
FIG. 3.3	NUMBER OF EVENTS SELECTED EACH YEAR ACCORDING TO MINIMUM INTER EVENT TIME (MIT) CRITERIA.	28
FIG. 3.4	BOX PLOT OF A) RAIN EVENT DURATION; B) TOTAL RAINFALL VOLUME; C) AVERAGE 10 MINUTES RAIN DEPTH; D) MAX 10 MINUTES RAIN DEPTH OBSERVED EACH MONTH BY ALL RAIN GAUGE STATIONS DURING THE SELECTED EVENTS.	30
FIG. 4.1	SCHEMATIC MODEL OVERVIEW REGARDING A GENERIC LEAD TIME DT AND RECORDING STATION N. 4.	34
FIG. 4.2	HISTOGRAM OF EXAMPLES WITHIN EACH RAIN CLASS	37
FIG. 4.3	FEED-FORWARD NEURAL NETWORK ARCHITECTURE WITH ONE HIDDEN LAYER	38
FIG. 4.4	TRAINING, TESTING, AND VALIDATION CURVES AS A FUNCTION OF THE EPOCHS. THE BEST VALIDATION PERFORMANCE IS AT EPOCH 498.	40
FIG. 5.1	BOXPLOTS OF RMSE AND RSE VALUES FOR EACH LEAD TIME BETWEEN OBSERVED AND PREDICTED VALUES OF THE 19 RAIN GAUGES. THE BLUE CROSSES ARE THE MEAN VALUES OF RMSE AND RSE FOR THE EULERIAN PERSISTENCE (EP) FOR EACH LEAD TIME.	46
FIG. 5.2	BOX PLOT OF POD, CSI, AND FAR VALUES FOR EACH LEAD TIME BETWEEN OBSERVED AND PREDICTED VALUES OF THE 19 RAIN GAUGES. THE BLUE CROSSES ARE THE MEAN VALUES OF POD, CSI, AND FAR FOR THE EULERIAN PERSISTENCE (EP) FOR EACH LEAD TIME.	48

FIG. 5.3	CONFUSION MATRIX FOR EACH LEAD TIME BETWEEN OBSERVATIONS AND PREDICTED CLASSES. THE COLOURS BEGIN WITH WHITE, RANGE THROUGH SHADES OF GREEN, AND THEN THROUGH SHADES OF BRIGHT GREEN. BRIGHTER GREEN MEANS A HIGHER PERCENTAGE OF ACTUAL PREDICTED.	49
FIG. 5.4	RAIN DEPTH REGISTERED DURING THE EVENT ON THE 1ST OF OCTOBER 2018 (TOP) AND 19TH OF DECEMBER 2019 (BOTTOM). THE RED LINES ARE REFERRED TO THE STATIONS WITH THE HIGHEST RAIN DEPTH PEAK IN 10 MINUTES: STATION N. 3 AND N. 5, RESPECTIVELY. THE DIFFERENT SHADES OF GREY ARE REFERRED TO THE OTHER STATION'S MEASUREMENTS.	53
FIG. 5.5	EVENT BASED COMPARISON BETWEEN OBSERVED VALUES AND MODELS PREDICTIONS OVER 5 LEAD TIMES FOR STATION N. 3.	54
FIG. 5.6	EVENT-BASED COMPARISON BETWEEN OBSERVED VALUES AND MODEL PREDICTIONS OVER FIVE LEAD TIMES FOR STATION N. 5.	57
FIG. 6.1	THE LOCATION OF THE STUDY AREA (FLANDERS) WITHIN BELGIAN BORDERS (DARK GREY LINE). RAIN GAUGE STATIONS ARE ILLUSTRATED WITH BLUE DOTS.	62
FIG. 6.2	NUMBER OF EVENTS SELECTED EACH YEAR ACCORDING TO MINIMUM INTER EVENT TIME (MIT) CRITERIA.	63
FIG. 6.3	BOX PLOT OF A) RAIN EVENT DURATION; B) TOTAL RAIN DEPTH; C) MEAN RAIN DEPTH; D) MAX RAIN DEPTH OBSERVED EACH MONTH BY ALL RAIN GAUGE STATIONS DURING THE SELECTED EVENTS.	64
FIG. 6.4	LOCATION OF MELSELE STATION (RED DOT) AND RECORDING STATIONS USED AS INPUT FOR MELSELE MODELS (BLACK DOTS) IN A RADIUS OF 50KM FROM MELSELE (SOLID RED LINE).	65
FIG. 6.5	HISTOGRAM OF EXAMPLES WITHIN EACH RAIN CLASS [%] AND CUMULATIVE PERCENTAGE.	67
FIG. 6.6	POD, FAR, PEARSON COEFFICIENT, AND MAE VALUES FOR MELSELE STATION. THE DASHED LINE INDICATES THE MODELS' LOWER (OR HIGHER) VALUE FOR TRAINING, VALIDATION, AND TESTING SETS.	69
FIG. 6.7	COMPARISON OF ACTUAL OBSERVED RAINFALL VALUES (REAL) AND THE PREDICTED ONES WITH 5 MINUTES LEAD TIME FOR THE TRAINING SET (YEARS 2017,2018, AND 2019), VALIDATION SET (2020) AND TESTING SET (2021).	71

FIG. 6.8	COMPARISON OF ACTUAL OBSERVED RAINFALL VALUES (REAL) AND THE PREDICTED ONES WITH 10 MINUTES LEAD TIME FOR THE TRAINING SET (YEARS 2017,2018 AND 2019), VALIDATION SET (2020) AND TESTING SET (2021).	73
FIG. 6.9	COMPARISON OF ACTUAL OBSERVED RAINFALL VALUES (REAL) AND THE PREDICTED ONES WITH 30 MINUTES LEAD TIME FOR THE TRAINING SET (YEARS 2017,2018 AND 2019), VALIDATION SET (2020) AND TESTING SET (2021).	75
FIG. 6.10	COMPARISON OF ACTUAL OBSERVED RAINFALL VALUES (REAL) AND THE PREDICTED ONES WITH 60 MINUTES LEAD TIME FOR THE TRAINING SET (2017,2018, AND 2019), VALIDATION SET (2020) AND TESTING SET (2021).	77
FIG. 6.11	COMPARISON OF ACTUAL OBSERVED RAINFALL VALUES (REAL) AND THE PREDICTED ONES WITH 120 MINUTES LEAD TIME FOR THE TRAINING SET (2017,2018, AND 2019), VALIDATION SET (2020) AND TESTING SET (2021).	79
FIG. 6.12	COMPARISON OF ACTUAL OBSERVED RAINFALL VALUES (REAL) AND THE PREDICTED ONES WITH 180 MINUTES LEAD TIME FOR THE TRAINING SET (2017,2018, AND 2019), VALIDATION SET (2020) AND TESTING SET (2021).	81
FIG. 6.13	RAIN DEPTHS REGISTERED DURING THE EVENT ON THE 4TH OF JULY 2021 FROM RAIN-GAUGE STATIONS OVER THE STUDY AREA.	83
FIG. 6.14	RAIN DEPTHS REGISTERED DURING THE EVENT ON THE 4TH OF JULY 2021 FROM MELSELE STATION (RAIN GAUGE) AND FROM WEATHER RADAR (9 CELLS/PIXELS AROUND MELSELE STATIONS).	84
FIG. 6.15	RESULT OF THE 5 MINUTES LEAD-TIME MODEL. COMPARISON BETWEEN RAIN GAUGE MEASUREMENTS (RG), REAL DISCRETIZED VALUES AND PREDICTED VALUES FOR MELSELE STATION.	86
FIG. 6.16	RESULT OF THE 10 MINUTES LEAD-TIME MODEL. COMPARISON BETWEEN RAIN GAUGE MEASUREMENTS (RG), REAL DISCRETIZED VALUES AND PREDICTED VALUES FOR MELSELE STATION.	86
FIG. 6.17	RESULT OF THE 30 MINUTES LEAD-TIME MODEL. COMPARISON BETWEEN RAIN GAUGE MEASUREMENTS (RG), REAL DISCRETIZED VALUES, AND PREDICTED VALUES FOR MELSELE STATION.	87
FIG. 6.18	RESULT OF THE 60 MINUTES LEAD-TIME MODEL. COMPARISON BETWEEN RAIN GAUGE MEASUREMENTS (RG), REAL DISCRETIZED VALUES AND PREDICTED VALUES FOR MELSELE STATION.	87

FIG. 6.19	RESULT OF THE 120 MINUTES LEAD-TIME MODEL. COMPARISON BETWEEN RAIN GAUGE MEASUREMENTS (RG), REAL DISCRETIZED VALUES AND PREDICTED VALUES FOR MELSELE STATION.	88
FIG. 6.20	RESULT OF THE 180 MINUTES LEAD-TIME MODEL. COMPARISON BETWEEN RAIN GAUGE MEASUREMENTS (RG), REAL DISCRETIZED VALUES AND PREDICTED VALUES FOR MELSELE STATION.	88
FIG. 6.21	COMPARISON BETWEEN 20 ENSEMBLES (ENS.) FROM PYSTEPS, OBSERVED RADAR VALUES AND RAIN GAUGE (RF) WITH INITIAL TIME AT 08:45.	90
FIG. 6.22	COMPARISON BETWEEN 20 ENSEMBLES (ENS.) FROM PYSTEPS, OBSERVED RADAR VALUES, AND RAIN GAUGE (RF) WITH INITIAL TIME AT 9:50.	90
FIG. 6.23	COMPARISON BETWEEN 20 ENSEMBLES (ENS.) FROM PYSTEPS, OBSERVED RADAR VALUES AND RAIN GAUGE (RF) WITH INITIAL TIME AT 10:50.	91
FIG. 6.24	COMPARISON BETWEEN 20 ENSEMBLES (ENS.) FROM PYSTEPS, OBSERVED RADAR VALUES AND RAIN GAUGE (RF) WITH INITIAL TIME AT 11:15.	91
FIG. 6.25	COMPARISON BETWEEN 20 ENSEMBLES (ENS.) FROM PYSTEPS, OBSERVED RADAR VALUES AND RAIN GAUGE (RF) WITH INITIAL TIME AT 11:35.	92
FIG. 6.26	COMPARISON BETWEEN 20 ENSEMBLES (ENS.) FROM PYSTEPS, OBSERVED RADAR VALUES AND RAIN GAUGE (RF) WITH INITIAL TIME AT 11:40.	92
FIG. 6.27	COMPARISON BETWEEN 20 ENSEMBLES (ENS.) FROM PYSTEPS, OBSERVED RADAR VALUES AND RAIN GAUGE (RF) WITH INITIAL TIME AT 11:45.	93

List of Tables

TABLE 3.1 BASIC PARAMETERS OF THE METEOROLOGICAL STATIONS OVER THE STUDY AREA.	26
TABLE 4.1 CONTINGENCY TABLE FOR THE DISCRETIZED INTERVALS OF PRECIPITATION.	36
TABLE 4.2 CONTINGENCY TABLE FOR METEOROLOGICAL INDICATORS.	43
TABLE 5.1 COMPARISON OF THE AVERAGE SCORES OF THE DIFFERENT MODELS OVER 5 LEAD TIMES. RSE, POD, FAR AND CSI ARE DIMENSIONLESS AND RANGE BETWEEN 0 AND 1 (THE VALUES ARE THE MEAN VALUES FROM THE BOXPLOTS IN FIG. 5.1 AND FIG. 5.2).	46
TABLE 5.2 ANALYSED RAIN EVENTS MAIN PROPERTIES.	52
TABLE 5.3 COMPARISON OF THE PERFORMANCE CRITERIA OF THE DIFFERENT MODELS OVER 5 LEAD TIMES FOR STATION N. 3. RSE, POD, FAR AND CSI ARE DIMENSIONLESS AND RANGE BETWEEN 0 AND 1.	55
TABLE 5.4 COMPARISON OF THE PERFORMANCE CRITERIA OF THE DIFFERENT MODELS OVER 5 LEAD TIMES FOR STATION N. 4. RSE, POD, FAR AND CSI ARE DIMENSIONLESS AND RANGE BETWEEN 0 AND 1.	58
TABLE 6.1 PARAMETERS OF THE METEOROLOGICAL STATIONS OVER THE STUDY AREA.	66
TABLE 6.2 CONTINGENCY TABLE FOR THE DISCRETIZED INTERVALS OF PRECIPITATION SCENARIO 1.	67
TABLE 6.3 MAIN CHARACTERISTICS OF EVENT 309 FROM THE TESTING SET.	82
TABLE 6.4 DEFAULT PYSTEPS CONFIGURATION USED IN THE EXPERIMENTS.	89

Abbreviations

ANFIS	Adaptive Neuro-Fuzzy Inference System
ANN	Artificial Neural Network
ANNs	Artificial Neural Networks
CSI	Critical Success Index
DCP	Department of Civil Protection
DDMs	Data-Driven Methods
EP	Eulerian Persistence
FAR	False Alarm Rate
FFNNs	Feed Forward Neural Networks
IQR	InterQuartile Range
MDMs	Model-Driven Methods
MIT	Minimum Inter-event Time
ML	Machine Learning
NWP	Numerical Weather Prediction
POD	Probability of Detection
Pysteps	Implementation of STEPS in python
RMI	Royal Meteorological Institute of Belgium
RMSE	Root Mean Square Error
RSE	Root Square Error
SOM	Self-Organizing Map
STEPS	Short-term ensemble prediction system
WMO	World Meteorological Organization

Chapter 1 - Introduction

The term *nowcasting* describes the expected changes in the current state of the weather on a timescale of a few hours (Browning, 1981). In 2010, the World Meteorological Organization (WMO) defined *nowcasting* as a forecasting technique from the present to 6 hours ahead, including a detailed description of the current weather. Over the years, the term has also found adoption in different fields outside the meteorological domain, such as economics, financial markets, or human mobility. In meteorology and hydrology, the main application of nowcasting is predicting events characterized by rapid evolution, such as thunderstorms, lightning, wind, and precipitations (Franch, 2021).

1.1 - Rainfall nowcasting

Rainfall nowcasting influences many aspects of daily life. For example, it facilitates drivers by predicting road conditions, enhances flight safety by providing weather guidance for regional aviation, and avoids casualties by issuing citywide rainfall alerts. During emergencies, rainfall nowcasting supports early-warning systems to reduce fatalities and economic losses, which can affect human life and cause environmental issues (Aakash Parmar, Kinjal Mistree, 2017; Ayzel et al., 2020;

Barrera-Animas et al., 2022; Chen et al., 2022; Foresti et al., 2016; Hammad et al., 2021; Liu et al., 2021; Luo et al., 2022; Ravuri et al., 2021).

However, early warning systems are beneficial only if the underlying nowcasts are accurate, timely, and reliable. Uncertainty in the nowcasts originates from either model structure, initial conditions, setup, calibration procedures, or the precipitation phenomenon itself (Beven, 1993; Clark et al., 2017; Melsen et al., 2016).

1.2 - Hydro-meteorological processes

Due to its high variability in time and space, precipitation nowcasting is among the most challenging tasks in hydrological fields (Moulin et al., 2009; Sampson et al., 2014). To experience the challenges in nowcasting models, it is essential to understand the processes governing precipitation formation. The precipitation cloud systems can be organized and structured in convective and stratiform movements. These two mechanisms exhibit different types of droplets and rain formation initiated by air motions with different magnitudes and, consequently, present different rainfall duration and intensities.

The convective precipitation comes from local solid vertical air motions (for instance, created by intense solar radiation) that can initiate in a short time (in the range of minutes) the formation of big droplets at the base of the cloud formation. On the other hand, stratiform precipitation is usually developed over a longer time (in the range of hours or even days), as the vertical air motion is feeble, causing tiny droplets at the top of the cloud formation. In the presence of mountains, at both stratiform or convective structures, a vertical movement of the air masses can occur due to the orographic lifting.

Observing needs to be quality controlled to capture space-time details of the precipitation processes. Indeed, nowcasting is highly dependent on observational data.

1.3 - Rainfall measurements

According to the spatial scale and, mainly, on the data availability, different rainfall measurements may be used for nowcasting. They include gridded data from radars/satellites or rain gauges.

Weather radar indirectly measures the rainfall field through reflectivity; the radar transmits microwave signals via pulses, and the energy reflected by hydro-meteors is captured back and converted into intensity. As the radar does a 360 scanning around itself, it builds up rainfall fields, usually at 1 km² and 5 min resolutions. Due to the radar's ability to capture rainfall structures at such fine scales, urban hydrologist has long recognized its potential for urban hydrology use. However, since the radar data does not measure the rainfall directly, it is subjected to several sources of errors, compromising the accuracy of the rain rates. Many studies have attempted to recognize and mitigate these sources of errors over the past decades, nevertheless since the right rainfall field is not known (radar rainfall rates at such scales do not necessarily meet the rain gauge measurement (Ochoa-Rodriguez et al., 2019), no conclusion can be reached regarding its accuracy.

On the other hand, rain gauges are considered reference devices for measuring the amount of precipitation at ground level (Duan et al., 2021; Moraux et al., 2019; Shehu and Haberlandt, 2021). They report precipitation rate and accumulation and provide information on instantaneous and heavy rainfall intensity over short periods. The main drawback of rain gauges is their lack of spatial representation, being point measurements (Yang et al., 2020). Indeed, if a storm occurs between the rain gauges, they can miss the peak rainfall intensity, automatically leading to an underestimation of the forecast. However, if a particularly dense network of rain gauges is available, it can be used for detection and nowcasting purposes (WMO, 2017).

1.4 - Machine Learning models

In addition to the inherent complexities of the atmosphere and relevant dynamical processes, the ever-growing need for real-time, large-scale, and fine-grained precipitation nowcasting poses extra challenges to the meteorological community. Consequently, it has aroused research interest in the machine-learning community. The recent application of machine learning and deep learning techniques in nowcasting has produced several advances in the accuracy of precipitation nowcasting systems. Machine Learning (ML) allows for unravelling hydrological problems, including forecasting rainfall (Hong, 2008; Ridwan et al., 2021; Valverde Ramírez et al., 2005).

ML models can identify the relationships between input and output data without making *a priori* assumptions about the physical processes. They can even recognize all the existing complex and typically non-linear relationships of the dynamical process. Disadvantages include their “black box” nature, proneness to over-fitting, and the empirical nature of model development (Bai et al., 2021; Liong and He, 2010). Among ML techniques, Feed Forward Neural Networks (FFNNs) has been propelled to the forefront in investigations of nowcasting methods (Prudden et al., 2020; Zhou et al., 2022). They have recently achieved outstanding predictive performance and have become an indispensable tools in various pattern recognition applications (Bai et al., 2021). Bishop (2006) stated that the most successful model in pattern recognition is the feed-forward neural network.

Indeed, ML's flexibility and conceptual simplicity make them attractive for nowcasting purposes (Asghari and Nasser, 2015). Although recent advances in weather forecasting models based on ML techniques, precipitation nowcasting is still a challenge for researchers and operational weather services (D. K. Kim et al., 2021; Lengfeld et al., 2020).

1.5 - Probabilistic nowcasting

Precipitation nowcasts issued by ML systems are often subject to uncertainties. There are many forms of uncertainty in modelling; thus, any sensible model will be uncertain when predicting unobserved data. At the lowest level, model uncertainty derives from measurement noise; at higher levels, a model may have many parameters, and there is uncertainty about which values of these parameters will be good at predicting new data. The probabilistic approach to modelling uses probability theory to express forms of uncertainty. Therefore, it is crucial to provide, together with a nowcast, an estimation of its uncertainty (Foresti et al., 2016).

Nowcasting techniques include deterministic and probabilistic methods. Deterministic methods lead to one nowcast for every time step, while probabilistic nowcasts often generate ensembles, i.e., multiple nowcasting scenarios for every time step, to quantify the predictability.

1.6 - Objective of the thesis

This study investigates the enhancement that can be reached in rainfall nowcasting by exploiting ML methods and using rain-gauge measurements as inputs. In particular, probabilistic machine learning approaches for rainfall nowcasting will be developed. The main objectives of this work are as follows.

1. Developing a new nowcasting approach based on machine learning models that suits many contexts and can be quickly reproduced. Indeed, ML models can identify the relationships between input and output data without making a priori assumptions about the physical processes. Moreover, they can even recognize all the existing complex and typically non-linear relationships of the dynamical process. In particular, the study will focus on feed-forward neural networks since they are commonly used neural network types in hydrology due to their simple architecture and ability to detect non-linear relationships among variables.

-
2. Considering recording stations and cumulative rainfall depths as inputs for feed-forward neural networks to overcome their lack of temporary memory. Indeed, feed-forward neural networks can not learn sequential or time-varying patterns (F. J. Chang et al., 2014). To overcome this drawback, this study would employ cumulative rainfall depths, which are non-decreasing variables. Unlike rainfall depths, which vary during an event, cumulative rainfall depth cannot decrease. Likewise, the model would employ rainfall depths measured in adjacent gauges, which could also provide valuable spatial information. As a result, temporal memory would be achieved through cumulative rainfall depth and cumulative rainfall depth from adjacent gauges.
 3. Providing an estimation of the uncertainty of the nowcasts, giving a probabilistic interpretation of the outputs. The probabilistic prediction would be achieved by employing the Softmax function in the ML model, which solves nonlinear multiple classification problems (Huang and Xiang, 2018). The Softmax function turns a vector into a vector of values between 0 and 1 that sum one. Thus, they can be interpreted as probabilities; therefore, the model would supply the most likely forecast as long as the associated probability. Since probabilistic predictions provide greater economic and decision-making value than deterministic ones (Ravuri et al., 2021)
 4. Enhancing model operational utility and reliability. Thus, analyse the flexibility and conceptual simplicity of the proposed approach and verify if it can be a promising tool for nowcasting purposes.

1.7 - Outline of the Thesis

This section serves as an introduction to the research work. **Chapter 2** introduces nowcasting approaches and presents a review of current methods. Next, existing models are described, highlighting their strengths and predictability limits. In **Chapter 3**, the study area and the dataset are presented. The procedure to select relevant rainfall events is described, and a description of the selected rainfall events is provided. **Chapter 4** describes the methodology and all the steps developed to obtain the final configuration. It lists all the processes, from raw rainfall data reading to final probabilistic predictions. **Chapter 5** reports the results of the models. Both performance and the training strategy are assessed. The first part of the chapter is devoted to analyzing all the rain events that were not used to train the models to evaluate the generalization abilities. Then, to highlight the ability of the models to predict differently, some rainfall events with different characteristics are analyzed. **Chapter 6** deals with the possibility of applying the model in another region: the Flanders region in Belgium. Here, two benchmark models, taken from the scientific literature, are used to assess the novelty of the procedure: Eulerian Persistence and Pysteps. Finally, **Chapter 7** provides a synthesis of the research work, in which the main findings are summarised and discussed together with the implications for future research.

References

- Aakash Parmar, Kinjal Mistree, M.S., 2017. Machine Learning Techniques for rainfall prediction: A Review. *Int. Conf. Innov. Inf. Embed. Commun. Syst.*
- Asghari, K., Nasserli, M., 2015. Spatial rainfall prediction using optimal features selection approaches. *Hydrol. Res.* 46, 343–355. <https://doi.org/10.2166/nh.2014.178>
- Ayzel, G., Scheffer, T., Heistermann, M., 2020. RainNet v1.0: A convolutional neural network for radar-based precipitation nowcasting. *Geosci. Model Dev.* 13, 2631–2644. <https://doi.org/10.5194/gmd-13-2631-2020>
- Bai, X., Wang, X., Liu, X., Liu, Q., Song, J., Sebe, N., Kim, B., 2021. Explainable deep learning for efficient and robust pattern recognition: A survey of recent developments. *Pattern Recognit.* 120, 108102. <https://doi.org/10.1016/j.patcog.2021.108102>
- Barrera-Animas, A.Y., Oyedele, L.O., Bilal, M., Akinosho, T.D., Delgado, J.M.D., Akanbi, L.A., 2022. Rainfall prediction: A comparative analysis of modern machine learning algorithms for time-series forecasting. *Mach. Learn. with Appl.* 7, 100204. <https://doi.org/10.1016/j.mlwa.2021.100204>
- Bishop, C. M., 2006. *Pattern Recognition and Machine Learning*. Springer, Science Business Media, LLC.
- Capozzi, V., Picciotti, E., Mazzarella, V., Marzano, F.S., Budillon, G., 2018. Fuzzy-logic detection and probability of hail exploiting short-range X-band weather radar. *Atmos. Res.* 201, 17–33. <https://doi.org/10.1016/j.atmosres.2017.10.006>
- Chang, F.J., Chen, P.A., Lu, Y.R., Huang, E., Chang, K.Y., 2014. Real-time multi-step-ahead water level forecasting by recurrent neural networks for urban flood control. *J. Hydrol.* 517, 836–846. <https://doi.org/10.1016/j.jhydrol.2014.06.013>
- Chang, K.Y., Tsai, M.J., 2016. A nonlinear spatio-temporal lumping of radar rainfall for modeling multi-step-ahead inflow forecasts by data-driven techniques. *J. Hydrol.* 239, 256–269. <https://doi.org/10.1016/j.jhydrol.2004.06.028>
- Chang, L.C., Shen, H.Y., Chang, F.J., 2014. Regional flood inundation nowcast using hybrid SOM and dynamic neural networks. *J. Hydrol.* 519, 476–489. <https://doi.org/10.1016/j.jhydrol.2014.07.036>
- Chao, Z., Pu, F., Yin, Y., Han, B., Chen, X., 2018. Research on real-time local rainfall prediction based on MEMS sensors. *J. Sensors* 2018, 1–9. <https://doi.org/10.1155/2018/6184713>
- Chen, S., Xu, X., Zhang, Y., Shao, D., Zhang, S., Zeng, M., 2022. Two-stream convolutional LSTM for precipitation nowcasting. *Neural Comput. Appl.* 9. <https://doi.org/10.1007/s00521-021-06877-9>

-
- De Luca, D.L., Capparelli, G., 2022. Rainfall nowcasting model for early warning systems applied to a case over Central Italy. *Nat. Hazards*. <https://doi.org/10.1007/s11069-021-05191-w>
- Dolciné, L., Andrieu, H., French, M.N., 1998. Evaluation of a conceptual rainfall forecasting model from observed and simulated rain events. *Hydrol. Earth Syst. Sci.* <https://doi.org/10.5194/hess-2-173-1998>
- Dolciné, L., Andrieu, H., French, M.N., 1997. Rainfall forecasting in a mountainous region using a weather radar and ground meteorological observations. *Phys. Chem. Earth* 22, 247–252. [https://doi.org/10.1016/S0079-1946\(97\)00148-1](https://doi.org/10.1016/S0079-1946(97)00148-1)
- Duan, Z., Duggan, E., Chen, C., Gao, H., Dong, J., Liu, J., 2021. Comparison of traditional method and triple collocation analysis for evaluation of multiple gridded precipitation products across Germany. *J. Hydrometeorol.* 2983–3000. <https://doi.org/10.1175/jhm-d-21-0049.1>
- Fogler, H. R., 1974. A pattern recognition model for forecasting. *Management science*, 20, 8, 1178–1189.
- Foresti, L., Reyniers, M., Seed, A., Delobbe, L., 2016. Development and verification of a real-time stochastic precipitation nowcasting system for urban hydrology in Belgium. *Hydrol. Earth Syst. Sci.* 20, 505–527. <https://doi.org/10.5194/hess-20-505-2016>
- Gaál, L., Molnar, P., Szolgay, J., 2014. Selection of intense rainfall events based on intensity thresholds and lightning data in Switzerland. *Hydrol. Earth Syst. Sci.* 18, 1561–1573. <https://doi.org/10.5194/hess-18-1561-2014>
- Ghaemi, E., Foelsche, U., Kann, A., Fuchsberger, J., 2021. Evaluation of Integrated Nowcasting through Comprehensive Analysis (INCA) precipitation analysis using a dense rain-gauge network in southeastern Austria. *Hydrol. Earth Syst. Sci.* 25, 4335–4356. <https://doi.org/10.5194/hess-25-4335-2021>
- Haile, A.T., Rientjes, T.H.M., Habib, E., Jetten, V., Gebremichael, M., 2011. Rain event properties at the source of the Blue Nile River. *Hydrol. Earth Syst. Sci.* 15, 1023–1034. <https://doi.org/10.5194/hess-15-1023-2011>
- Hammad, M., Shoaib, M., Salahudin, H., Baig, M.A.I., Khan, M.M., Ullah, M.K., 2021. Rainfall forecasting in upper Indus basin using various artificial intelligence techniques. *Stoch. Environ. Res. Risk Assess.* 35, 2213–2235. <https://doi.org/10.1007/s00477-021-02013-0>
- Heneker, T.M., Lambert, M.F., Kuczera, G., 2001. A point rainfall model for risk-based design. *J. Hydrol.* 247, 54–71. [https://doi.org/10.1016/S0022-1694\(01\)00361-4](https://doi.org/10.1016/S0022-1694(01)00361-4)
- Heuvelink, D., Berenguer, M., Brauer, C.C., Uijlenhoet, R., 2020. Hydrological application of radar rainfall nowcasting in the Netherlands. *Environ. Int.* 136, 105431. <https://doi.org/10.1016/j.envint.2019.105431>

-
- Hong, W.C., 2008. Rainfall forecasting by technological machine learning models. *Appl. Math. Comput.* 200, 41–57. <https://doi.org/10.1016/j.amc.2007.10.046>
- Huang, L., Xiang, L. yang, 2018. Method for Meteorological Early Warning of Precipitation-Induced Landslides Based on Deep Neural Network. *Neural Process. Lett.* 48, 1243–1260. <https://doi.org/10.1007/s11063-017-9778-0>
- Imhoff, R.O., Brauer, C.C., Overeem, A., Weerts, A.H., Uijlenhoet, R., 2020. Spatial and Temporal Evaluation of Radar Rainfall Nowcasting Techniques on 1,533 Events. *Water Resour. Res.* 56, 1–22. <https://doi.org/10.1029/2019WR026723>
- Imhoff, R.O., Brauer, C.C., van Heeringen, K.J., Uijlenhoet, R., Weerts, A.H., 2022. Large-Sample Evaluation of Radar Rainfall Nowcasting for Flood Early Warning. *Water Resour. Res.* 58. <https://doi.org/10.1029/2021WR031591>
- Jasper-Tönnies, A., Hellmers, S., Einfalt, T., Strehz, A., Fröhle, P., 2018. Ensembles of radar nowcasts and COSMO-DE-EPS for urban flood management. *Water Sci. Technol.* 2017, 27–35. <https://doi.org/10.2166/wst.2018.079>
- Kim, D.K., Suezawa, T., Mega, T., Kikuchi, H., Yoshikawa, E., Baron, P., Ushio, T., 2021. Improving precipitation nowcasting using a three-dimensional convolutional neural network model from Multi Parameter Phased Array Weather Radar observations. *Atmos. Res.* 262, 105774. <https://doi.org/10.1016/j.atmosres.2021.105774>
- Kim, S., Hong, S., Joh, M., Song, S., 2017. DeepRain: ConvLSTM Network for Precipitation Prediction using Multichannel Radar Data 3–6.
- Kim, T., Yang, T., Gao, S., Zhang, L., Ding, Z., Wen, X., Gourley, J.J., Hong, Y., 2021. Can artificial intelligence and data-driven machine learning models match or even replace process-driven hydrologic models for streamflow simulation?: A case study of four watersheds with different hydro-climatic regions across the CONUS. *J. Hydrol.* 598, 126423. <https://doi.org/10.1016/j.jhydrol.2021.126423>
- Lengfeld, K., Kirstetter, P.E., Fowler, H.J., Yu, J., Becker, A., Flamig, Z., Gourley, J., 2020. Use of radar data for characterizing extreme precipitation at fine scales and short durations. *Environ. Res. Lett.* 15. <https://doi.org/10.1088/1748-9326/ab98b4>
- Lin, G.F., Chen, G.R., Wu, M.C., Chou, Y.C., 2009. Effective forecasting of hourly typhoon rainfall using support vector machines. *Water Resour. Res.* 45, 1–11. <https://doi.org/10.1029/2009WR007911>
- Liong, S.Y., He, S., 2010. Raingauge-based rainfall nowcasting with artificial neural network. *Adv. Geosci. Vol. 17 Hydrol. Sci.* 1–9. <https://doi.org/10.1142/7158-vol17>
- Liu, J., Xu, L., Chen, N., 2022. A spatiotemporal deep learning model ST-LSTM-SA for hourly rainfall forecasting using radar echo images. *J. Hydrol.* 609, 127748. <https://doi.org/10.1016/j.jhydrol.2022.127748>
-

-
- Liu, Y., Wang, H., Lei, X., 2021. Real-time forecasting of river water level in urban based on radar rainfall: A case study in Fuzhou City. *J. Hydrol.* 603, 126820. <https://doi.org/10.1016/j.jhydrol.2021.126820>
- Luo, C., Zhao, X., Sun, Y., Li, X., Ye, Y., 2022. PredRANN: The spatiotemporal attention Convolution Recurrent Neural Network for precipitation nowcasting. *Knowledge-Based Syst.* 239, 107900. <https://doi.org/10.1016/j.knosys.2021.107900>
- Mcarthur, R. C., 1987. Scenario-Driven Automatic Pattern Recognition in Nowcasting. *Journal of Atmospheric and Oceanic Technology*, 29-35. [https://doi.org/10.1175/1520-0426\(1987\)004<0029:SDAPRI>2.0.CO;2](https://doi.org/10.1175/1520-0426(1987)004<0029:SDAPRI>2.0.CO;2)
- Moon, S.H., Kim, Y.H., Lee, Y.H., Moon, B.R., 2019. Application of machine learning to an early warning system for very short-term heavy rainfall. *J. Hydrol.* 568, 1042–1054. <https://doi.org/10.1016/j.jhydrol.2018.11.060>
- Moraux, A., Dewitte, S., Cornelis, B., Munteanu, A., 2019. Deep learning for precipitation estimation from satellite and rain gauges measurements. *Remote Sens.* 11, 1–22. <https://doi.org/10.3390/rs11212463>
- Nguyen, D.H., Bae, D.H., 2020. Correcting mean areal precipitation forecasts to improve urban flooding predictions by using long short-term memory network. *J. Hydrol.* 584, 124710. <https://doi.org/10.1016/j.jhydrol.2020.124710>
- Pelosi, A., Furcolo, P., Rossi, F., Villani, P., 2020. The characterization of extraordinary extreme events (EEEs) for the assessment of design rainfall depths with high return periods. *Hydrol. Process.* 34, 2543–2559. <https://doi.org/10.1002/hyp.13747>
- Piciullo, L., Siano, I., Calvello, M., 2016. Calibration of rainfall thresholds for landslide early warning purposes: Applying the EDuMaP method to the system deployed in Campania region (Italy). *Landslides Eng. Slopes. Exp. Theory Pract.* 3, 1621–1629. <https://doi.org/10.1201/b21520-201>
- Prudden, R., Adams, S., Kangin, D., Robinson, N., Ravuri, S., Mohamed, S., Arribas, A., 2020. A review of radar-based nowcasting of precipitation and applicable machine learning techniques.
- Pulkkinen, S., Nerini, D., Pérez Hortal, A.A., Velasco-Forero, C., Seed, A., Germann, U., Foresti, L., 2019. Pysteps: An open-source Python library for probabilistic precipitation nowcasting (v1.0). *Geosci. Model Dev.* 12, 4185–4219. <https://doi.org/10.5194/gmd-12-4185-2019>
- Ravuri, S., Lenc, K., Willson, M., Kangin, D., Lam, R., Mirowski, P., Fitzsimons, M., Athanassiadou, M., Kashem, S., Madge, S., Prudden, R., Mandhane, A., Clark, A., Brock, A., Simonyan, K., Hadsell, R., Robinson, N., Clancy, E., Arribas, A., Mohamed, S., 2021. Skilful precipitation nowcasting using deep generative models of radar. *Nature* 597, 672–677. <https://doi.org/10.1038/s41586-021-03854-z>

-
- Ridwan, W.M., Sapitang, M., Aziz, A., Kushiar, K.F., Ahmed, A.N., El-Shafie, A., 2021. Rainfall forecasting model using machine learning methods: Case study Terengganu, Malaysia. *Ain Shams Eng. J.* 12, 1651–1663. <https://doi.org/10.1016/j.asej.2020.09.011>
- Shehu, B., Haberlandt, U., 2021. Relevance of merging radar and rainfall gauge data for rainfall nowcasting in urban hydrology. *J. Hydrol.* 594, 125931. <https://doi.org/10.1016/j.jhydrol.2020.125931>
- Simonin, D., Pierce, C., Roberts, N., Ballard, S.P., Li, Z., 2017. Performance of Met Office hourly cycling NWP-based nowcasting for precipitation forecasts. *Q. J. R. Meteorol. Soc.* 143, 2862–2873. <https://doi.org/10.1002/qj.3136>
- Sokol, Z., Szturc, J., Orellana-Alvear, J., Popová, J., Jurczyk, A., Célleri, R., 2021. The role of weather radar in rainfall estimation and its application in meteorological and hydrological modelling —A review. *Remote Sens.* 13, 1–38. <https://doi.org/10.3390/rs13030351>
- Suyatno, J.A., Nhita, F., Rohmawati, A.A., 2018. Rainfall forecasting in Bandung regency using C4.5 algorithm. 2018 6th Int. Conf. Inf. Commun. Technol. ICoICT 2018 324–328. <https://doi.org/10.1109/ICoICT.2018.8528725>
- Theodoridis, S., Koutroumbas, K., 2009. *Pattern Recognition*, fourth ed. Elsevier/Academic Press, Amsterdam.
- Thorndahl, S., Einfalt, T., Willems, P., Ellerbæk Nielsen, J., Ten Veldhuis, M.C., Arnbjerg-Nielsen, K., Rasmussen, M.R., Molnar, P., 2017. Weather radar rainfall data in urban hydrology. *Hydrol. Earth Syst. Sci.* 21, 1359–1380. <https://doi.org/10.5194/hess-21-1359-2017>
- Valverde Ramírez, M.C., De Campos Velho, H.F., Ferreira, N.J., 2005. Artificial neural network technique for rainfall forecasting applied to the São Paulo region. *J. Hydrol.* 301, 146–162. <https://doi.org/10.1016/j.jhydrol.2004.06.028>
- WMO, 2017. *Guidelines for Nowcasting Techniques*, World Meteorological Organization.
- Yang, Q., Dai, Q., Han, D., Zhu, Z., Zhang, S., 2020. Uncertainty analysis of radar rainfall estimates induced by atmospheric conditions using long short-term memory networks. *J. Hydrol.* 590, 125482. <https://doi.org/10.1016/j.jhydrol.2020.125482>
- Zhang, Z., Sabuncu, M.R., 2018. Generalized cross entropy loss for training deep neural networks with noisy labels. *Adv. Neural Inf. Process. Syst.* 2018-Decem, 8778–8788.
- Zhou, S., Wang, Y., Yuan, Q., Yue, L., Zhang, L., 2022. Spatiotemporal estimation of 6-hour high-resolution precipitation across China based on Himawari-8 using a stacking ensemble machine learning model. *J. Hydrol.* 609, 127718. <https://doi.org/10.1016/j.jhydrol.2022.127718>

Chapter 2 - Nowcasting models

This chapter presents the more common techniques used worldwide for forecasting rainfall. **Section 2.1** introduces Numerical Weather Prediction (NWP) methods and discusses their performance and predictability limits. Next, **section 2.2** describes machine learning tools generally used for rainfall nowcasting. The gap between NWP and ML models is illustrated, and conclusions are derived about the need and room for improvement of the existing nowcast methods. Then, **Section 2.3** focuses on Pattern Recognition techniques for nowcasting purposes. Finally, the selected nowcast benchmark methods are described shortly in **Section 2.4** and **section 2.5**.

To evaluate possible critical situations, an effective nowcasting model requires a succession of nowcasts characterized by high update frequency and short computational time (Imhoff et al., 2022; WMO, 2017). Prior investigations queried several approaches to meet nowcasting model requirements. The prevailing ones are 1) Model-Driven Methods (MDMs), which entail the identification of the relationships among variables involved; 2) Data-Driven Methods (DDMs), which comprise all the models that employ available data in order to identify patterns and classify new ones, without making a priori assumptions (De Luca and Capparelli, 2022).

2.1 - Numerical Weather Prediction models

MDMs encompass Numerical Weather Prediction (NWP) models, which appeal to the water community because of their proven effectiveness and robustness through the years (De Luca and Capparelli, 2022; Liu et al., 2021). NWP models solve mathematical equations to simulate the dynamics and physics of the atmosphere, producing reliable forecasts. Regardless of their exact applications, NWP implementation is nontrivial due to the high dimensionality of the spatiotemporal relationship between meteorological variables. Nevertheless, they represent proper rainfall forecasting tools for daily temporal scale and over the spatial scale of 1000 km (De Luca and Capparelli, 2022). However, NWP models can capture mesoscale weather patterns such as fronts, not smaller-scale convective patterns within mesoscale systems (Chao et al., 2018). As a result, convective heavy precipitation cells are difficult to predict with NWP models mainly because their lifetimes are often shorter than 30 min (Jasper-Tönnies et al., 2018). Thus a level of nowcast accuracy at the convective scale is challenging to reach with NWP (Simonin et al., 2017). Moreover, adequate observations of meteorological variables are not regularly available within the area of interest, which makes it challenging to define accurate initial and boundary conditions (Dolciné et al., 1997).

2.2 - Machine Learning models

On the other hand, DDMs have also been widely used to unravel hydrological problems, including rainfall forecasting (Hong, 2008; Ridwan et al., 2021; Valverde Ramírez et al., 2005). They can identify the relationships between input and output data without making a priori assumptions about the physical processes. They can even recognize all the existing complex and typically non-linear relationships of the dynamical process. Disadvantages of DDMs include their “black box” nature, proneness to over-fitting, and the empirical nature of model development (Bai et al., 2021; Liong and He, 2010).

Among DDMs, Machine Learning (ML) techniques have been propelled to the forefront in investigations of nowcasting methods (Prudden et al., 2020; Zhou et al., 2022). L. C. Chang et al. (2014) illustrate the benefit of using a hybrid ML model based on a Self-Organizing Map (SOM) and Dynamic Neural Networks for forecasting inundation maps based solely on rainfall data and historical inundation depths. Chang, K.Y. and Tsai, M.J. (2016) propose an Adaptive Neuro-Fuzzy Inference System (ANFIS) model for flood forecasting and demonstrate its capability in modeling the complex rainfall–runoff process. With a temporal resolution of 10 min and a spatial resolution of 1.25 km, they reveal that the approach alleviates the timing error problem and improves the accuracy and reliability of the forecast. A ML model to estimate 6-hour precipitation at a spatial resolution of 5 km based on Himawari-8 and ground station data over China was recently developed by Zhou et al. (2022). Also, Liu et al. (2022) show how a Deep Neural Network model for hourly rainfall forecasting using radar echo images can predict over 40% of rainfall events and forecast well on small-scale intense rainfall.

It is still unknown whether the DDMs will gradually prevail over the MDMs or vice versa and how the traditional models will further develop, given the distinct philosophy used in those two groups of models (T. Kim et al., 2021). In recent studies, researchers have used ML techniques for rainfall nowcasting, and some studies have performed better than traditional methods (D. K. Kim et al., 2021). Indeed, ML's flexibility and conceptual simplicity make them attractive for nowcasting purposes (Asghari and Nasser, 2015). Nevertheless, despite recent advances in weather forecasting models based on ML techniques, precipitation nowcasting is still challenging for researchers and operational weather services (D. K. Kim et al., 2021; Lengfeld et al., 2020).

2.3 - Pattern Recognition techniques

Since machine learning does not require any previous assumption, they have become an indispensable tool in a wide range of pattern recognition applications. Pattern recognition is the scientific discipline whose goal is classifying objects or classes. Depending on the application, the objects can be images, signals, or any measurements that need to be classified. The objects are usually referred to as patterns, hence the name pattern recognition (Theodoridis and Koutroumbas, 2009). Even though the specific pattern recognition technique varies depending on the structure of the problem, the aim is always concerned with developing algorithms and decision rules that classify patterns into different categories (Fogler, 1974). According to McArthur (1987), the typical approach to developing pattern recognition techniques is bottom-up: a set of processes is established to identify all features of interest in a dataset and aggregate them into patterns. If the approach relies on rules, it may lead to a proliferation of rules, exceptions to the rules, and so on.

Feed- forward neural networks are considered one of the most successful models in pattern recognition (Bishop, 2006). Implementing a feed-forward neural network for pattern recognition techniques requires examples of patterns, thanks to which the network can learn and apply the learnt rule to future, unseen examples. The learning process is supervised learning if the examples of patterns (input vectors) are provided along with their corresponding categories (target). The concept of supervised learning encompasses using examples to develop a tool that can identify and extract regularities in input vectors to classify them into the corresponding target vectors according to found regularities. Once the learning process is completed, the tool will classify new unseen data according to found regularities. A model is considered well-defined if it can make forecasts or predictions about unobserved data having been trained on observed data.

Moreover, FFNNs are commonly used neural network types in hydrology due to their simple architecture and ability to backpropagate the error while training over network structure (McGarry et al. 1999).

2.4 - Benchmark models

The Eulerian Persistence (EP) and the Short-Term Ensemble Prediction System (STEPS) are used as a reference for estimating and improving the proposed models' predictability.

2.4.1 - Eulerian Persistence

Eulerian Persistence (EP) refers to keeping the most recent observation frozen in space and considering it as all predictions up to a desired lead time. EP is shown mathematically as (Zawadzki,1973):

$$\varphi(t_0 + DT, x) = \varphi(t_0, x) \quad (2.1)$$

where $\varphi(t_0, x)$ is the observed data field, t_0 is the start time of the forecast, $\varphi(t_0 + DT, x)$ is the forecast at lead time DT , x is the position. Eulerian persistence represents the most straightforward forecast and is typically used as a reference for more sophisticated nowcasting methods (Pierce et al., 2004; Ebert et al., 2004).

2.4.2 - STEPS

Several methods have been developed for probabilistic rainfall nowcasting based on extrapolation of radar data, which are especially suited for short-term (0–3 h) rainfall forecasts at spatial resolutions as fine as 1 km² (Bowler et al., 2006, Berenguer et al., 2011). The Short-Term Ensemble Prediction System is an example of a method for creating short-term probabilistic rainfall nowcasts (STEPS; Bowler et al., 2006). This method produces an ensemble of equally likely rainfall nowcasts by perturbing the rainfall patterns for every ensemble member with a second-order autoregressive process.

Pysteps (Pulkkinen et al., 2019) is a modular framework that allows users to use different parts and concepts of (probabilistic) nowcasting methods and to develop them further. Initially, Pysteps entailed STEPS (Bowler et al., 2006; Seed et al., 2013),

but nowadays, it also supports more recent approaches by, for example, Nerini et al. (2017) and Pulkkinen et al. (2020).

References

- Aakash Parmar, Kinjal Mistree, M.S., 2017. Machine Learning Techniques for rainfall prediction: A Review. *Int. Conf. Innov. Inf. Embed. Commun. Syst.*
- Asghari, K., Nasser, M., 2015. Spatial rainfall prediction using optimal features selection approaches. *Hydrol. Res.* 46, 343–355. <https://doi.org/10.2166/nh.2014.178>
- Ayzel, G., Scheffer, T., Heistermann, M., 2020. RainNet v1.0: A convolutional neural network for radar-based precipitation nowcasting. *Geosci. Model Dev.* 13, 2631–2644. <https://doi.org/10.5194/gmd-13-2631-2020>
- Bai, X., Wang, X., Liu, X., Liu, Q., Song, J., Sebe, N., Kim, B., 2021. Explainable deep learning for efficient and robust pattern recognition: A survey of recent developments. *Pattern Recognit.* 120, 108102. <https://doi.org/10.1016/j.patcog.2021.108102>
- Barrera-Animas, A.Y., Oyedele, L.O., Bilal, M., Akinosho, T.D., Delgado, J.M.D., Akanbi, L.A., 2022. Rainfall prediction: A comparative analysis of modern machine learning algorithms for time-series forecasting. *Mach. Learn. with Appl.* 7, 100204. <https://doi.org/10.1016/j.mlwa.2021.100204>
- Bishop, C. M., 2006. *Pattern Recognition and Machine Learning*. Springer, Science Business Media, LLC.
- Capozzi, V., Picciotti, E., Mazzarella, V., Marzano, F.S., Budillon, G., 2018. Fuzzy-logic detection and probability of hail exploiting short-range X-band weather radar. *Atmos. Res.* 201, 17–33. <https://doi.org/10.1016/j.atmosres.2017.10.006>
- Chang, F.J., Chen, P.A., Lu, Y.R., Huang, E., Chang, K.Y., 2014. Real-time multi-step-ahead water level forecasting by recurrent neural networks for urban flood control. *J. Hydrol.* 517, 836–846. <https://doi.org/10.1016/j.jhydrol.2014.06.013>
- Chang, K.Y., Tsai, M.J., 2016. A nonlinear spatio-temporal lumping of radar rainfall for modeling multi-step-ahead inflow forecasts by data-driven techniques. *J. Hydrol.* 239, 256–269. <https://doi.org/10.1016/j.jhydrol.2004.06.028>
- Chang, L.C., Shen, H.Y., Chang, F.J., 2014. Regional flood inundation nowcast using hybrid SOM and dynamic neural networks. *J. Hydrol.* 519, 476–489. <https://doi.org/10.1016/j.jhydrol.2014.07.036>
- Chao, Z., Pu, F., Yin, Y., Han, B., Chen, X., 2018. Research on real-time local rainfall prediction based on MEMS sensors. *J. Sensors* 2018, 1–9. <https://doi.org/10.1155/2018/6184713>
- Chen, S., Xu, X., Zhang, Y., Shao, D., Zhang, S., Zeng, M., 2022. Two-stream convolutional LSTM for precipitation nowcasting. *Neural Comput. Appl.* 9. <https://doi.org/10.1007/s00521-021-06877-9>

-
- De Luca, D.L., Capparelli, G., 2022. Rainfall nowcasting model for early warning systems applied to a case over Central Italy. *Nat. Hazards*. <https://doi.org/10.1007/s11069-021-05191-w>
- Dolciné, L., Andrieu, H., French, M.N., 1998. Evaluation of a conceptual rainfall forecasting model from observed and simulated rain events. *Hydrol. Earth Syst. Sci.* <https://doi.org/10.5194/hess-2-173-1998>
- Dolciné, L., Andrieu, H., French, M.N., 1997. Rainfall forecasting in a mountainous region using a weather radar and ground meteorological observations. *Phys. Chem. Earth* 22, 247–252. [https://doi.org/10.1016/S0079-1946\(97\)00148-1](https://doi.org/10.1016/S0079-1946(97)00148-1)
- Duan, Z., Duggan, E., Chen, C., Gao, H., Dong, J., Liu, J., 2021. Comparison of traditional method and triple collocation analysis for evaluation of multiple gridded precipitation products across Germany. *J. Hydrometeorol.* 2983–3000. <https://doi.org/10.1175/jhm-d-21-0049.1>
- Fogler, H. R., 1974. A pattern recognition model for forecasting. *Management science*, 20, 8, 1178–1189.
- Foresti, L., Reyniers, M., Seed, A., Delobbe, L., 2016. Development and verification of a real-time stochastic precipitation nowcasting system for urban hydrology in Belgium. *Hydrol. Earth Syst. Sci.* 20, 505–527. <https://doi.org/10.5194/hess-20-505-2016>
- Gaál, L., Molnar, P., Szolgay, J., 2014. Selection of intense rainfall events based on intensity thresholds and lightning data in Switzerland. *Hydrol. Earth Syst. Sci.* 18, 1561–1573. <https://doi.org/10.5194/hess-18-1561-2014>
- Ghaemi, E., Foelsche, U., Kann, A., Fuchsberger, J., 2021. Evaluation of Integrated Nowcasting through Comprehensive Analysis (INCA) precipitation analysis using a dense rain-gauge network in southeastern Austria. *Hydrol. Earth Syst. Sci.* 25, 4335–4356. <https://doi.org/10.5194/hess-25-4335-2021>
- Haile, A.T., Rientjes, T.H.M., Habib, E., Jetten, V., Gebremichael, M., 2011. Rain event properties at the source of the Blue Nile River. *Hydrol. Earth Syst. Sci.* 15, 1023–1034. <https://doi.org/10.5194/hess-15-1023-2011>
- Hammad, M., Shoaib, M., Salahudin, H., Baig, M.A.I., Khan, M.M., Ullah, M.K., 2021. Rainfall forecasting in upper Indus basin using various artificial intelligence techniques. *Stoch. Environ. Res. Risk Assess.* 35, 2213–2235. <https://doi.org/10.1007/s00477-021-02013-0>
- Heneker, T.M., Lambert, M.F., Kuczera, G., 2001. A point rainfall model for risk-based design. *J. Hydrol.* 247, 54–71. [https://doi.org/10.1016/S0022-1694\(01\)00361-4](https://doi.org/10.1016/S0022-1694(01)00361-4)
- Heuvelink, D., Berenguer, M., Brauer, C.C., Uijlenhoet, R., 2020. Hydrological application of radar rainfall nowcasting in the Netherlands. *Environ. Int.* 136, 105431. <https://doi.org/10.1016/j.envint.2019.105431>

-
- Hong, W.C., 2008. Rainfall forecasting by technological machine learning models. *Appl. Math. Comput.* 200, 41–57. <https://doi.org/10.1016/j.amc.2007.10.046>
- Huang, L., Xiang, L. yang, 2018. Method for Meteorological Early Warning of Precipitation-Induced Landslides Based on Deep Neural Network. *Neural Process. Lett.* 48, 1243–1260. <https://doi.org/10.1007/s11063-017-9778-0>
- Imhoff, R.O., Brauer, C.C., Overeem, A., Weerts, A.H., Uijlenhoet, R., 2020. Spatial and Temporal Evaluation of Radar Rainfall Nowcasting Techniques on 1,533 Events. *Water Resour. Res.* 56, 1–22. <https://doi.org/10.1029/2019WR026723>
- Imhoff, R.O., Brauer, C.C., van Heeringen, K.J., Uijlenhoet, R., Weerts, A.H., 2022. Large-Sample Evaluation of Radar Rainfall Nowcasting for Flood Early Warning. *Water Resour. Res.* 58. <https://doi.org/10.1029/2021WR031591>
- Jasper-Tönnies, A., Hellmers, S., Einfalt, T., Strehz, A., Fröhle, P., 2018. Ensembles of radar nowcasts and COSMO-DE-EPS for urban flood management. *Water Sci. Technol.* 2017, 27–35. <https://doi.org/10.2166/wst.2018.079>
- Kim, D.K., Suezawa, T., Mega, T., Kikuchi, H., Yoshikawa, E., Baron, P., Ushio, T., 2021. Improving precipitation nowcasting using a three-dimensional convolutional neural network model from Multi Parameter Phased Array Weather Radar observations. *Atmos. Res.* 262, 105774. <https://doi.org/10.1016/j.atmosres.2021.105774>
- Kim, S., Hong, S., Joh, M., Song, S., 2017. DeepRain: ConvLSTM Network for Precipitation Prediction using Multichannel Radar Data 3–6.
- Kim, T., Yang, T., Gao, S., Zhang, L., Ding, Z., Wen, X., Gourley, J.J., Hong, Y., 2021. Can artificial intelligence and data-driven machine learning models match or even replace process-driven hydrologic models for streamflow simulation?: A case study of four watersheds with different hydro-climatic regions across the CONUS. *J. Hydrol.* 598, 126423. <https://doi.org/10.1016/j.jhydrol.2021.126423>
- Lengfeld, K., Kirstetter, P.E., Fowler, H.J., Yu, J., Becker, A., Flamig, Z., Gourley, J., 2020. Use of radar data for characterizing extreme precipitation at fine scales and short durations. *Environ. Res. Lett.* 15. <https://doi.org/10.1088/1748-9326/ab98b4>
- Lin, G.F., Chen, G.R., Wu, M.C., Chou, Y.C., 2009. Effective forecasting of hourly typhoon rainfall using support vector machines. *Water Resour. Res.* 45, 1–11. <https://doi.org/10.1029/2009WR007911>
- Liong, S.Y., He, S., 2010. Raingauge-based rainfall nowcasting with artificial neural network. *Adv. Geosci. Vol. 17 Hydrol. Sci.* 1–9. <https://doi.org/10.1142/7158-vol17>
- Liu, J., Xu, L., Chen, N., 2022. A spatiotemporal deep learning model ST-LSTM-SA for hourly rainfall forecasting using radar echo images. *J. Hydrol.* 609, 127748. <https://doi.org/10.1016/j.jhydrol.2022.127748>

-
- Liu, Y., Wang, H., Lei, X., 2021. Real-time forecasting of river water level in urban based on radar rainfall: A case study in Fuzhou City. *J. Hydrol.* 603, 126820. <https://doi.org/10.1016/j.jhydrol.2021.126820>
- Luo, C., Zhao, X., Sun, Y., Li, X., Ye, Y., 2022. PredRANN: The spatiotemporal attention Convolution Recurrent Neural Network for precipitation nowcasting. *Knowledge-Based Syst.* 239, 107900. <https://doi.org/10.1016/j.knosys.2021.107900>
- Mcarthur, R. C., 1987. Scenario-Driven Automatic Pattern Recognition in Nowcasting. *Journal of Atmospheric and Oceanic Technology*, 29-35. [https://doi.org/10.1175/1520-0426\(1987\)004<0029:SDAPRI>2.0.CO;2](https://doi.org/10.1175/1520-0426(1987)004<0029:SDAPRI>2.0.CO;2)
- Moon, S.H., Kim, Y.H., Lee, Y.H., Moon, B.R., 2019. Application of machine learning to an early warning system for very short-term heavy rainfall. *J. Hydrol.* 568, 1042–1054. <https://doi.org/10.1016/j.jhydrol.2018.11.060>
- Moraux, A., Dewitte, S., Cornelis, B., Munteanu, A., 2019. Deep learning for precipitation estimation from satellite and rain gauges measurements. *Remote Sens.* 11, 1–22. <https://doi.org/10.3390/rs11212463>
- Nguyen, D.H., Bae, D.H., 2020. Correcting mean areal precipitation forecasts to improve urban flooding predictions by using long short-term memory network. *J. Hydrol.* 584, 124710. <https://doi.org/10.1016/j.jhydrol.2020.124710>
- Pelosi, A., Furcolo, P., Rossi, F., Villani, P., 2020. The characterization of extraordinary extreme events (EEEs) for the assessment of design rainfall depths with high return periods. *Hydrol. Process.* 34, 2543–2559. <https://doi.org/10.1002/hyp.13747>
- Piciullo, L., Siano, I., Calvello, M., 2016. Calibration of rainfall thresholds for landslide early warning purposes: Applying the EDuMaP method to the system deployed in Campania region (Italy). *Landslides Eng. Slopes. Exp. Theory Pract.* 3, 1621–1629. <https://doi.org/10.1201/b21520-201>
- Prudden, R., Adams, S., Kangin, D., Robinson, N., Ravuri, S., Mohamed, S., Arribas, A., 2020. A review of radar-based nowcasting of precipitation and applicable machine learning techniques.
- Pulkkinen, S., Nerini, D., Pérez Hortal, A.A., Velasco-Forero, C., Seed, A., Germann, U., Foresti, L., 2019. Pysteps: An open-source Python library for probabilistic precipitation nowcasting (v1.0). *Geosci. Model Dev.* 12, 4185–4219. <https://doi.org/10.5194/gmd-12-4185-2019>
- Ravuri, S., Lenc, K., Willson, M., Kangin, D., Lam, R., Mirowski, P., Fitzsimons, M., Athanassiadou, M., Kashem, S., Madge, S., Prudden, R., Mandhane, A., Clark, A., Brock, A., Simonyan, K., Hadsell, R., Robinson, N., Clancy, E., Arribas, A., Mohamed, S., 2021. Skilful precipitation nowcasting using deep generative models of radar. *Nature* 597, 672–677. <https://doi.org/10.1038/s41586-021-03854-z>

-
- Ridwan, W.M., Sapitang, M., Aziz, A., Kushiar, K.F., Ahmed, A.N., El-Shafie, A., 2021. Rainfall forecasting model using machine learning methods: Case study Terengganu, Malaysia. *Ain Shams Eng. J.* 12, 1651–1663. <https://doi.org/10.1016/j.asej.2020.09.011>
- Shehu, B., Haberlandt, U., 2021. Relevance of merging radar and rainfall gauge data for rainfall nowcasting in urban hydrology. *J. Hydrol.* 594, 125931. <https://doi.org/10.1016/j.jhydrol.2020.125931>
- Simonin, D., Pierce, C., Roberts, N., Ballard, S.P., Li, Z., 2017. Performance of Met Office hourly cycling NWP-based nowcasting for precipitation forecasts. *Q. J. R. Meteorol. Soc.* 143, 2862–2873. <https://doi.org/10.1002/qj.3136>
- Sokol, Z., Szturc, J., Orellana-Alvear, J., Popová, J., Jurczyk, A., Célleri, R., 2021. The role of weather radar in rainfall estimation and its application in meteorological and hydrological modelling —A review. *Remote Sens.* 13, 1–38. <https://doi.org/10.3390/rs13030351>
- Suyatno, J.A., Nhita, F., Rohmawati, A.A., 2018. Rainfall forecasting in Bandung regency using C4.5 algorithm. 2018 6th Int. Conf. Inf. Commun. Technol. ICoICT 2018 324–328. <https://doi.org/10.1109/ICoICT.2018.8528725>
- Theodoridis, S., Koutroumbas, K., 2009. *Pattern Recognition*, fourth ed. Elsevier/Academic Press, Amsterdam.
- Thorndahl, S., Einfalt, T., Willems, P., Ellerbæk Nielsen, J., Ten Veldhuis, M.C., Arnbjerg-Nielsen, K., Rasmussen, M.R., Molnar, P., 2017. Weather radar rainfall data in urban hydrology. *Hydrol. Earth Syst. Sci.* 21, 1359–1380. <https://doi.org/10.5194/hess-21-1359-2017>
- Valverde Ramírez, M.C., De Campos Velho, H.F., Ferreira, N.J., 2005. Artificial neural network technique for rainfall forecasting applied to the São Paulo region. *J. Hydrol.* 301, 146–162. <https://doi.org/10.1016/j.jhydrol.2004.06.028>
- WMO, 2017. *Guidelines for Nowcasting Techniques*, World Meteorological Organization.
- Yang, Q., Dai, Q., Han, D., Zhu, Z., Zhang, S., 2020. Uncertainty analysis of radar rainfall estimates induced by atmospheric conditions using long short-term memory networks. *J. Hydrol.* 590, 125482. <https://doi.org/10.1016/j.jhydrol.2020.125482>
- Zhang, Z., Sabuncu, M.R., 2018. Generalized cross entropy loss for training deep neural networks with noisy labels. *Adv. Neural Inf. Process. Syst.* 2018-Decem, 8778–8788.
- Zhou, S., Wang, Y., Yuan, Q., Yue, L., Zhang, L., 2022. Spatiotemporal estimation of 6-hour high-resolution precipitation across China based on Himawari-8 using a stacking ensemble machine learning model. *J. Hydrol.* 609, 127718. <https://doi.org/10.1016/j.jhydrol.2022.127718>

Chapter 3 - Study area and dataset

This chapter presents the study area – **section 3.1** – and the available data – **section 3.2** – used to investigate the predictability of the proposed nowcast method. Next, **section 3.3** summarizes the procedure employed for identifying relevant rainfall events used for training and validating the method. Finally, as the nowcast methods are expected to behave differently based on the event types, a classification scheme of the selected rainfall events is described in **section 3.4**.

3.1 - Study area

The Campania region (Southern Italy) has an area of 13'600 km² and a population of about 5.8 million people. It is currently divided into 8 “meteorological warning zones” according to homogeneity criteria considering the following factors: hydrography, morphology, rainfall, geology, land-use, hydraulic and hydrogeological events, and administrative boundaries (Piciullo et al., 2016). The study area is zone 1 of the Campania region (**Fig. 3.1, left**). It covers 1619 km² and includes 109 municipalities and 19 rain-gauges (**Fig. 3.1, right**).

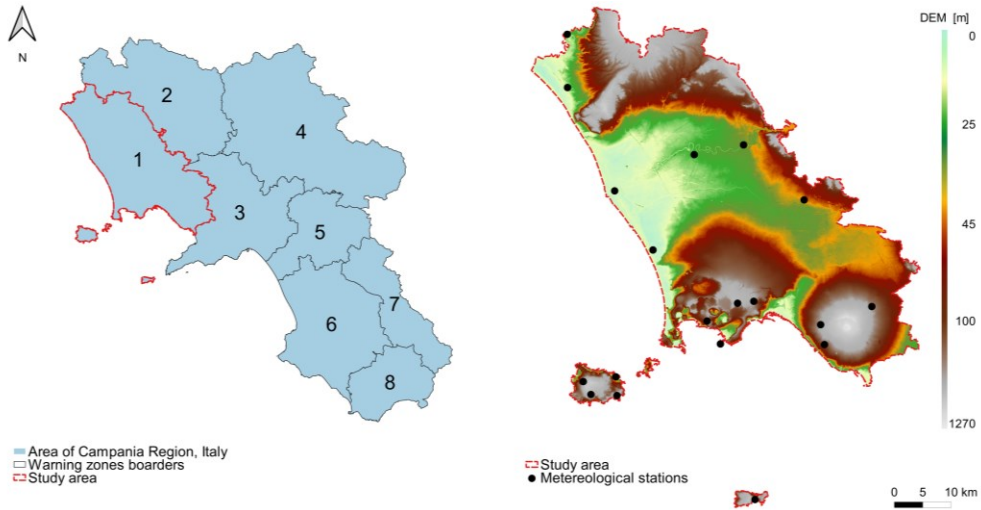


Fig. 3.1 The location of the study area (left) within Campania Region and (right) with the corresponding elevation and boundaries. The location of meteorological stations is illustrated right.

The area has a complex highlands system and two main volcanic structures, Vesuvius and the Phlegrean Fields. These two orographic features constitute an essential factor in the mesoscale meteorology of the region, enhancing convection systems development, especially in the summer.

The study area is near the Mediterranean Sea; thus, the prevailing climate is the Mediterranean, characterized by long dry summer periods and rainy winters with mild temperatures. In particular, the winter exhibits stratiform rainfall events lasting up to a few days. In summer, there are stratiform events, convective events, and combinations. Furthermore, in the cold season, the region is sometimes affected by polar maritime air masses coming from the North Atlantic, which can lead to the development of thunderstorm cells over the sea surface and the coastal sectors. On the other hand, in the warm season, thunderstorm events are mainly triggered by the interaction between small-scale mechanisms and synoptic-scale flow (Capozzi et al., 2018).

3.2 - Available data

The rain-gauge data used in this study are registered by tipping bucket devices with 0.2 mm resolution. For every rain gauge station over the study area (**Table 2.1**), the Campania Region Department of Civil Protection (DPC) provided rainfall measurements every 10 minutes.

In events determination, all intervals with only 0.2 mm in 10 min were ignored because these are often artefacts of condensation at the end of events, increasing the duration of events with minimal increase in rainfall depth (Gaál et al., 2014).

Table 3.1 Basic parameters of the meteorological stations over the study area.

ID	Sensor	Station Name	Longitude [UTM]	Latitude [UTM]	Z [m a.s.l.]
1	18919	Capri	14.2386	40.5483	195
2	37534	Capua	14.2083	41.1086	24
3	20881	Castel Volturno	13.9397	41.0338	9
4	36309	Cellole	13.8383	41.1961	9
5	21760	Ercolano	14.3722	40.8255	209
6	33430	Forio	13.8791	40.7319	340
7	12243	Grazzanise	14.1052	41.0925	14
8	33436	Ischia	13.9469	40.7400	35
9	40341	Lago Patria	14.0211	40.9411	1
10	18955	Monte Epomeo	13.8955	40.7116	370
11	18891	Napoli Camaldoli	14.1988	40.8583	390
12	18949	Napoli Capodimonte	14.2325	40.8616	176
13	36128	Nisida	14.1638	40.7937	88
14	18901	Ottaviano	14.4786	40.8547	180
15	33433	Piano Liguori	13.9497	40.7105	320
16	18953	Pozzuoli	14.1355	40.8298	127
17	21520	S.Castrese	13.8361	41.2802	750
18	38667	S.Marco Evangelista	14.3359	41.0225	31
19	18929	Torre del Greco	14.3805	40.7941	50

3.3 - Rainfall event selection

Rain events are a convenient way of summarizing rainfall time series into meaningful entities regarding a particular application (Haile et al., 2011). Therefore, it is essential to define a rain event and the duration considered to distinguish it. Since this study aims at predicting punctual rainfall with short lead times, the definition of spatial events was revised.

It is common to define punctual rainfall events by the Minimum Inter-arrival Time index, hereafter referred to as MIT. Regarding a single station, a storm is a rainfall period with preceding and succeeding dry periods more than MIT (Heneker et al., 2001). Many application-based criteria for identifying rainfall events using a fixed MIT exist in the literature, with values ranging from 3 min to 24 h.

Since the model employs precipitation fields, the MIT criteria were adapted for them. Thus, regarding meteorological stations over an area, a rainfall event is defined as a period of rainfall with preceding and succeeding dry periods more than MIT for the total number of stations in the area. According to climate characteristics, precipitation events were identified separately for the warm (April–September) and cold (October–March) seasons. A MIT of 2 hours was chosen for the warm season and 1 hour for the cold season. **Fig. 2.2** depicts two so-defined rainfall events.

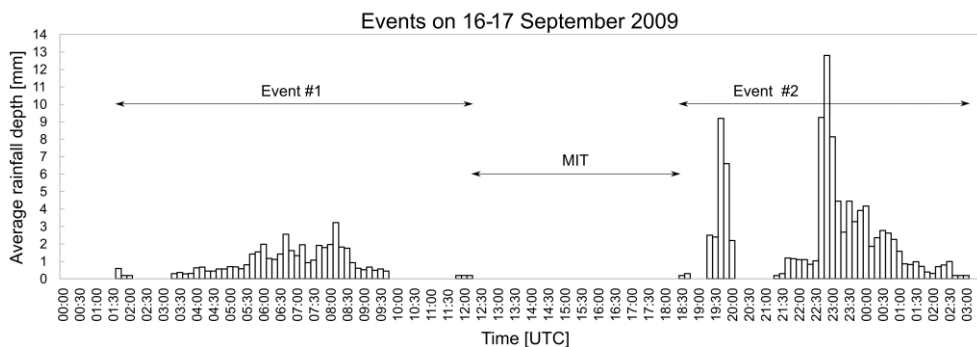


Fig. 3.2 Example of storm event separation method using 1-h minimum inter-event time MIT. Y axis indicates average rainfall depth of the rain-gauge stations over the study area.

Almost 32 events per year, for a total of 359 rainfall events, occurred in the study area from 2009 to 2019 and were registered by the 19 rain-gauge stations (**Fig. 3.3**).

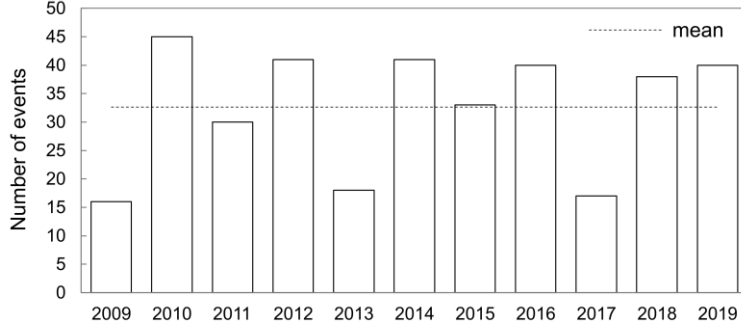


Fig. 3.3 Number of events selected each year according to Minimum Inter Event Time (MIT) criteria.

3.4 - Rainfall event classification

For each month, the main characteristics of the selected rainfall events were computed (**Fig. 3.4**):

- **rain event duration** $\{T_1, T_2, \dots, T_M\}$ where M is the number of events.
- **maximum total rainfall volume** registered during the M rain events $\{H_{max}^1, H_{max}^2, \dots, H_{max}^M\}$ (**Eq. 1**):

$$H_{max}^k = \max\{H_1^k, H_2^k, \dots, H_i^k, \dots, H_n^k\} = \max\{\sum_{t=1}^{T_k} h_{1,t}^k, \sum_{t=1}^{T_k} h_{2,t}^k, \dots, \sum_{t=1}^{T_k} h_{i,t}^k, \dots, \sum_{t=1}^{T_k} h_{n,t}^k\} \quad (3.1)$$

where H_{max}^k is the maximum total rainfall volume registered during k-th rain event among the n station over the study area, H_i^k is the total rainfall volume registered by the i-th station during k-th rain event, $h_{i,t}^k$ is the rain depth registered by i-th station during t-th instant of k-th rain event, T_k is the duration of the k-th event, and n is the number of stations.

-
- **average 10 minutes rain depth** $\{\bar{h}^1, \bar{h}^2, \dots, \bar{h}^M, \}$, according to Eq. 2:

$$\bar{h}^k = \frac{1}{n} \sum_{i=1}^n \bar{h}_i^k \quad (3.2)$$

where n is the number of stations, \bar{h}_i the average 10 minutes rain depth registered by n-th station during the k-th rain event, calculated according to **Eq. 3.3**:

$$\bar{h}_i^k = \sum_{t=1}^{T_k} h_{1,t}^k \quad (3.3)$$

where $h_{1,t}^k$ is the rain depth registered by i-th station during t-th instant of k-th rain event and T_k is the duration of the k-th event.

- **maximum 10 minutes of rain depth**, among the measurements registered by the stations during the event $\{h_{max}^1, h_{max}^2, \dots, h_{max}^M\}$ (**Eq. 3.4**):

$$h_{max}^k = \max\{h_{max,1}^k, h_{max,2}^k, \dots, h_{max,n}^k\} \quad (3.4)$$

where h_{max}^k is the maximum 10 minutes depth registered during k-th rain event among the n station over the study area, $h_{max,i}^k$ is the maximum 10 minutes depth registered by the i-th station during k-th rain event.

Based on these characteristics, rainfall events were distinguished into three groups:

- stratiform;
- convective;
- mixed.

The third group was introduced because, according to event duration, both stratiform and convective storms were present during an event. Thus, a clear separation was not possible.

Most of the events were contemporary registered by all the stations, typical of stratiform events. However, during some events, more than one convective cell was observed. In particular, during the winter, rain events have smaller rain depths and can last up to a few days, typical of stratiform events. While in summer, rain events

occur predominantly in the form of more localized rain showers, with shorter durations and higher rain depths, according to convective event type formation.

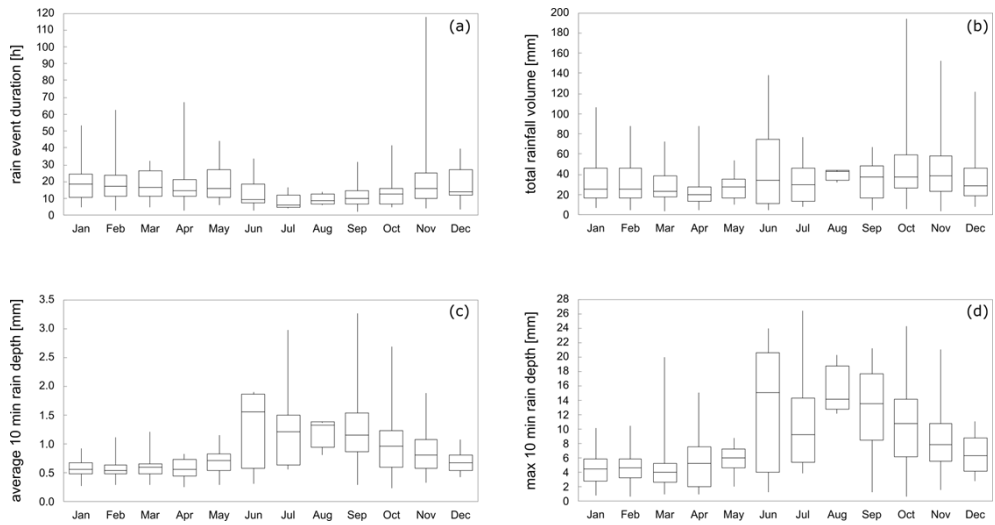


Fig. 3.4 Box plot of a) rain event duration; b) total rainfall volume; c) average 10 minutes rain depth; d) max 10 minutes rain depth observed each month by all rain gauge stations during the selected events.

References

- Capozzi, V., Picciotti, E., Mazzarella, V., Marzano, F.S., Budillon, G., 2018. Fuzzy-logic detection and probability of hail exploiting short-range X-band weather radar. *Atmos. Res.* 201, 17–33. <https://doi.org/10.1016/j.atmosres.2017.10.006>
- Gaál, L., Molnar, P., Szolgay, J., 2014. Selection of intense rainfall events based on intensity thresholds and lightning data in Switzerland. *Hydrol. Earth Syst. Sci.* 18, 1561–1573. <https://doi.org/10.5194/hess-18-1561-2014>
- Haile, A.T., Rientjes, T.H.M., Habib, E., Jetten, V., Gebremichael, M., 2011. Rain event properties at the source of the Blue Nile River. *Hydrol. Earth Syst. Sci.* 15, 1023–1034. <https://doi.org/10.5194/hess-15-1023-2011>
- Heneker, T.M., Lambert, M.F., Kuczera, G., 2001. A point rainfall model for risk-based design. *J. Hydrol.* 247, 54–71. [https://doi.org/10.1016/S0022-1694\(01\)00361-4](https://doi.org/10.1016/S0022-1694(01)00361-4)
- Piciullo, L., Siano, I., Calvello, M., 2016. Calibration of rainfall thresholds for landslide early warning purposes: Applying the EDuMaP method to the system deployed in Campania region (Italy). *Landslides Eng. Slopes. Exp. Theory Pract.* 3, 1621–1629. <https://doi.org/10.1201/b21520-201>

Chapter 4 - Methodology: the Machine Learning model

This chapter illustrates the proposed model and all the steps to obtain the final configuration. First, **section 4.1** gives an overview of the workflow and lists all the processes: from raw rainfall data reading to final probabilistic predictions. Then, in the following sections, every step is explored, and a detailed description is given. First, **section 4.2** defines how to pre-process rainfall data to make them usable for the models. Next, **section 4.3** illustrates the architecture of the models and the training strategy adopted to achieve competitive training. Then, **section 4.4** describes output post-processing. Finally, **section 4.5** defines the performance criteria considered to evaluate the models.

4.1 - Workflow

The proposed ML model employs cumulative rainfall depth from recording stations over the study area as inputs to predict rainfall interval and the corresponding probability of occurrence in one of the stations after DT lead-time. In particular, a model was independently developed and trained from the others for each station and each lead time. The stations were 19, and the lead times were 5, so a total of 95 models. **Fig. 4.1** shows the nowcasts workflow regarding one station and one lead-time.

First, let t_0 be the time when a rain event starts; the first step is reading the cumulative rainfall depths (observation) of the stations over the study area

$$\mathbf{h}_{t_0} = h_1, h_2, \dots, h_n \quad (4.1)$$

where n is the number of stations.

According to contingency **Table 2**, the observations \mathbf{h}_{t_0} are discretized into *rain intervals* or *rain classes* \mathbf{x}_{t_0} (as better explained in **section 4.2** – input variable pre-processing) to form the input pattern. After the discretization, the difference between two values within the same interval is neglected.

$$\mathbf{x}_{t_0} = x_1, x_2, \dots, x_n \quad (4.2)$$

where n is the number of stations.

Then, the input pattern at t_0 (\mathbf{x}_{t_0}) pass through the nowcasting model (**section 4.2**) to predict the probabilities of occurrence $\mathbf{P}(\mathbf{y}_{t_0+DT})$ for every rain interval \mathbf{y}_{t_0+DT} , at $t_0 + DT$ with DT being equal to the lead time (**section 4.4**):

$$\mathbf{P}(\mathbf{y}_{t_0+DT}) = P(y_1), P(y_2), \dots, P(y_N) \quad (4.3)$$

Where y_i is the rain interval, N is the number of rain intervals, and $P(y_i)$, the probability of occurrence of y_i . The probability of occurrence $P(y_i)$, is calculated through the Softmax, which ensures that the sum of the $P(y_i)$ is equal to one:

$$\sum_{i=1}^N P(y_i) = 1 \quad (4.4)$$

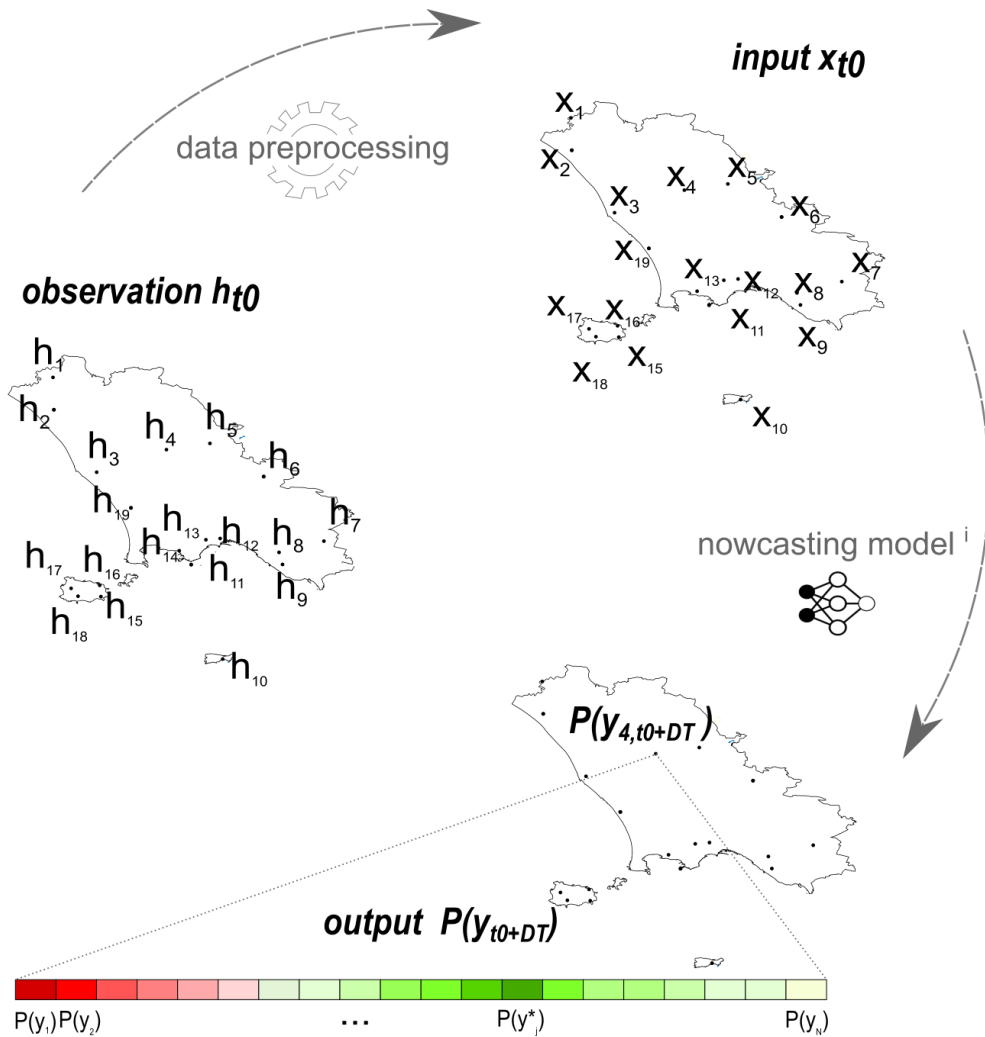


Fig. 4.1 - Schematic model overview regarding a generic lead time DT and recording station n . ⁴¹

¹ The n observations (h_{t_0}) at t_0 are discretized into rain intervals (x_{t_0}), according to input variable pre-processing, where n is the number of recording station over the study area. The input pass through the i -th nowcasting models to predict the corresponding probability of occurrence $P(y + DT)$ of the N rain intervals $y_{t_0 + DT}$, where N is the number of rain interval and DT is the lead time. The model selects the rain interval with the highest probability of occurrence y^* . The colours of the probability vector begin with bright green through shades of bright red: brighter green means a higher probability of occurrence, while brighter red lower.

Finally, the model selects the rain class y_t^* with the highest probability:

$$y_t^* | P_{y_t^*} \max \{P(y_1), P(y_2), \dots, P(y_N)\} \quad (4.5)$$

Where N is the number of rain classes.

At time t_1 , new registrations are available \mathbf{h}_{t_1} , which are added up to the previous registrations \mathbf{h}_0 and discretized in \mathbf{x}_{t_1} , according to the corresponding rain class. Then, \mathbf{x}_{t_1} are employed by the model to provide new nowcasts, thus the associated probability of occurrence $P(\mathbf{y}_{t_1+DT})$.

The update frequency is 10 minutes; thus, $t_0-t_1=10$ minutes. Each model has its parameters, but the input pattern is the same for each of them, which means that the input at time t_0 (vector \mathbf{x}_{t_0}) is passed through each model, but each model predicts different outputs. A numerical example of the input-output pattern is given below: assuming that the vector \mathbf{h}_t is

$$\mathbf{h}_t = \{ 0.2, 1.0, 3.2, 0.2, 4.2, 4.6, 5.8, 1.2, 1.2, 0.2, 0.4, 1.4, 1.6, 2.4, 1.2, 0.2, 0.4, 0.2, 0.4 \}$$

it will be discretized into the corresponding vector \mathbf{x}_t :

$$\mathbf{x}_t = \{ 1, 1, 2, 1, 2, 2, 3, 1, 1, 1, 1, 1, 1, 1, 1, 1, 1, 1, 1 \}.$$

The nowcast after DT lead time for station number 4 will be the vector $P_{y_{4,t+DT}}$:

$$P_{y_{4,t+DT}} = \{ 0, 0.02, 0.04, 0.89, 0.01, 0.01, 0.01, 0.01, 0, 0, 0, 0, 0, 0, 0, 0, 0, 0, 0 \}.$$

Thus, the highest probability for station number 4 is associated with class third (89 %), i.e., the most probable rain interval is between 5 and 10 mm, according to contingency **Table 4.1**.

Table 4.1 Contingency table for the discretized intervals of precipitation.

Class ID (x)	Interval [mm]	No. Examples	Percentage [%]	Cumulative percentage [%]
1	0-2	231408	0.2782	0.2782
2	2-5	135316	0.1627	0.4408
3	5-10	146280	0.1758	0.6166
4	10-15	96427	0.1159	0.7325
5	15-20	67726	0.0814	0.8140
6	20-25	47105	0.0566	0.8706
7	25-30	32564	0.0391	0.9097
8	30-35	23334	0.0280	0.9378
9	35-40	16271	0.0196	0.9573
10	40-45	9537	0.0115	0.9688
11	45-50	6538	0.0079	0.9766
12	50-60	9854	0.0118	0.9885
13	60-70	5153	0.0062	0.9947
14	70-80	2217	0.0027	0.9974
15	80-90	1068	0.0013	0.9986
16	90-100	504	0.0006	0.9992
17	100-125	337	0.0004	0.9996
18	125-150	170	0.0002	0.9999
19	150-175	54	0.0001	0.9999
20	175-200	70	0.0001	1.0000

4.2 - Input variables pre-processing

According to Moon et al. (2019), we discretized continuous data (h_t) into intervals (x_t), thus, after the discretization, the difference between two values within the same interval is neglected. **Table 4.1** is the contingency table for the discretized precipitation intervals, hereafter referred to as rain classes or classes. Twenty classes with different widths, ranging from 2 mm to 25 mm, were defined.

The upper limit of the highest class is 200 mm, which depends on the employed data set, thus, on the rainfall events. According to MIT criteria for rainfall events determination, the maximum total rainfall volume observed during the 359 events was

almost 194 mm. As a result, when an observed value is higher than 200 mm, the rainfall event is considered finished.

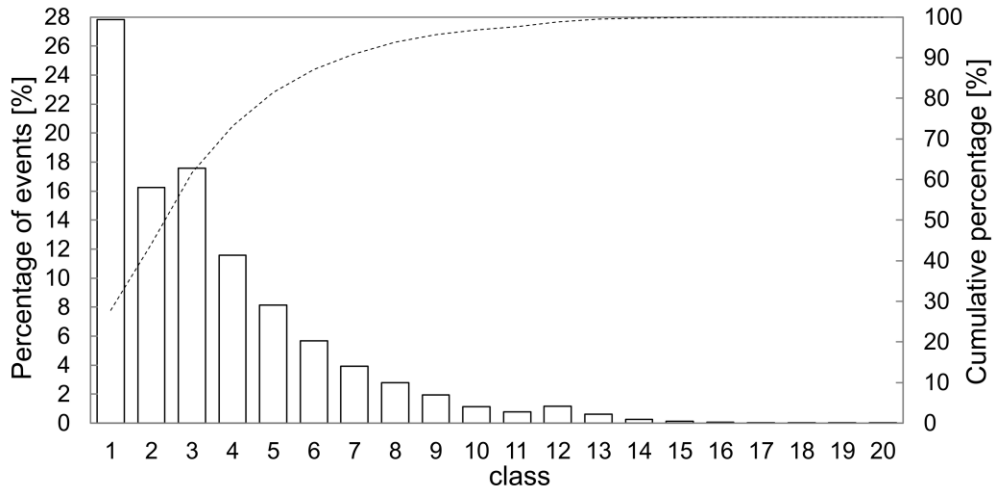


Fig. 4.2 Histogram of examples within each rain class

Our discretization is narrower than the ones done by (Moon et al., 2019; Suyatno et al., 2018), resulting in higher intervals and accuracy. However, it is worth highlighting that the 20 classes have different percentages of examples, resulting in an asymmetrical distribution with higher frequency for the first classes. To achieve uniform distribution, intervals should have been narrower for lower classes and wider for higher ones. However, on the one hand, further discrimination among first classes would have led to an interval of less than 1 mm width, resulting in a useless precision for operational nowcasting. On the other hand, higher classes would have been joined into a wider one, leaking valuable information. Therefore, this study prefers intervals with variable width rather than a uniform class distribution.

4.3 - Model setup and Training Strategy

A neural network is defined by its structure, including the hidden layers number, the number of nodes in each hidden layer, how the layers are linked, the activation function, and the weights. A feed-forward neural network was independently developed and trained from the others for each station and lead time.

Feed-forward neural networks pass the data forward from input to output. As illustrated in **Fig. 4.3**, it consists of interconnected layers with nodes and weights, where the flow of information is in the forward direction only. Thus, there is no backward flow, hence the name feed-forward network.

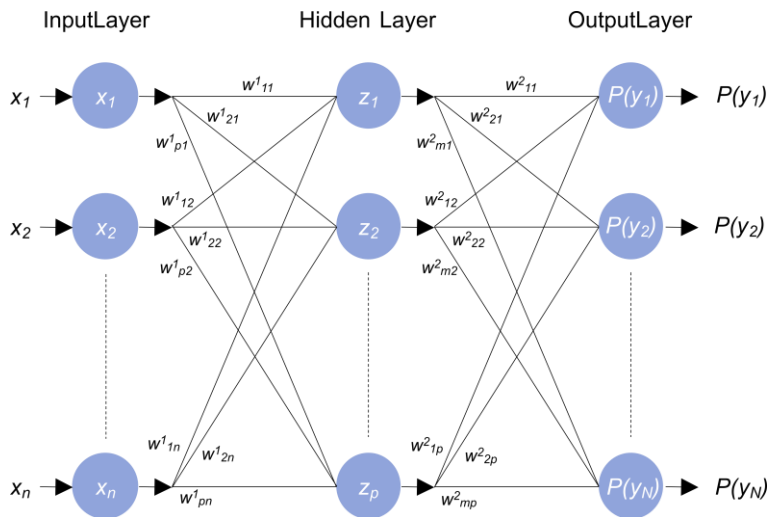


Fig. 4.3 Feed-forward neural network architecture with one hidden layer

The n number of input data is assigned to the nodes in the input layer ($x_i, i = 1, 2, \dots, n$), and is propagated through the interconnected nodes in the hidden layer, with weight parameters and biases. Each j hidden node ($j = 1, 2, \dots, p$) receives the weighted sum of the input nodes, adds the bias, and transfers to the output layer through an activation function. It can be described in

$$z_j = f_z \left(\sum_{i=1}^n x_i W_{ji} + c_j \right) = f_z(u_j) \quad (4.6)$$

where z_j is the j -th node in the hidden layer ($j=1, 2, \dots, p$), W_{ji} is the weight parameter between the hidden and input node, c_j is the bias, u_j is the symbol for the term in brackets, and f_z is the activation function, which is the hyperbolic tangent function:

$$f_z(u_j) = \frac{2}{1 + e^{-2u_j}} - 1 \quad (4.7)$$

Similarly, this process is also performed between the hidden and output layer.

$$P(y_k) = f_y \left(\sum_{j=1}^p z_j W_{kj} + b_k \right) = f_y(s_k) \quad (4.8)$$

where y_k is the output variable ($k = 1, 2, \dots, N$), W_{kj} is the weight parameter between the hidden and output nodes, b_k is the bias, s_k is the symbol for the term in brackets, and f_y is the activation function, which is the normalized exponential function, also known as the softmax function:

$$f_y(s_k) = \frac{e^{s_k}}{\sum_{k=1}^N e^{s_k}} \quad (4.9)$$

The training problem consists of finding the optimal combination of weights of the ML model. The most common training strategy is backpropagation, which adjusts the weights of connections between neurons in hidden and output layers to reduce the error in the output. However, when the dataset consists of experimental points, usually, there is some noise in the data. Therefore, reproducing the dataset precisely as it is not the best strategy because the noise will be reproduced, too. Moreover, one of the main drawbacks of ML models is overfitting, which happens when the model performs well on the dataset but poorly on new unseen data.

The early stop technique is applied while training the models to avoid those problems. The dataset, thus the rainfall events, were split into three groups: the period 2009-2014 was used for training (60%), the period 2015-2016 for validation (10%), and 2017-2019 for testing (30%). The training set was used to train the model by tuning its parameters with the back-propagation algorithm; the validation set asserted generalizing ability and avoided overfitting, which happens when the model is performing well on the data used during training but performs poorly on new unseen

data (Nguyen and Bae, 2020). As shown in **Fig. 4.4**, the network stops training when the error over the validation set (red line) increases while the error over the training set (blue line) is still decreasing; in this way, the network avoids overfitting.

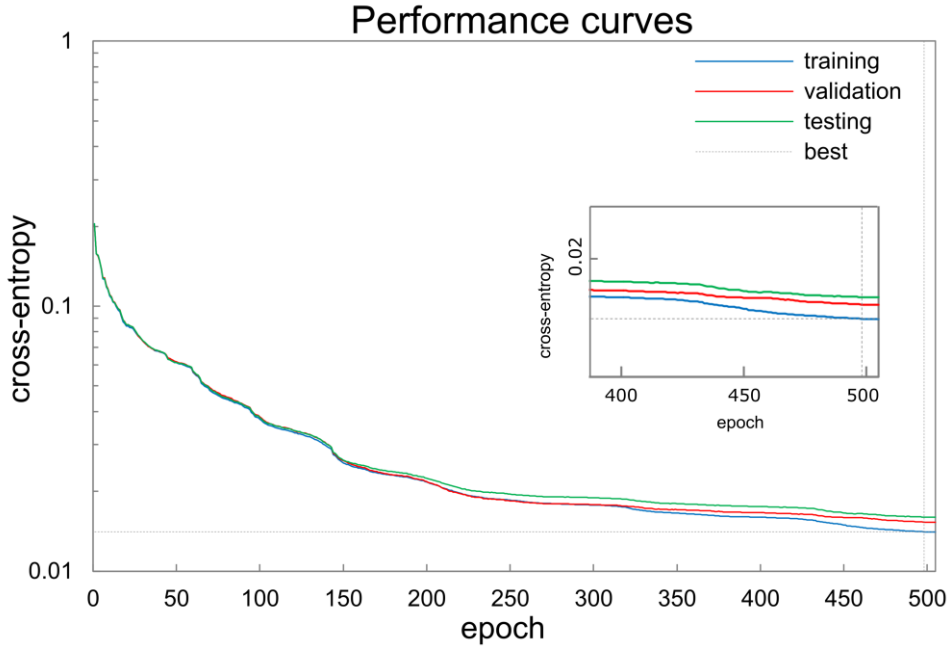


Fig. 4.4 Training, testing, and validation curves as a function of the epochs. The best validation performance is at epoch 498.

Evaluating the performance of the validation set is done to determine and optimize different network architectures and training strategies. Selecting the model and training method performing the best on the validation set introduces the risk of overfitting this dataset. Finally, the testing set allows the final model evaluation. We trained all the models by minimizing the cross-entropy loss (**Eq. 4.10**), which is most commonly used for classification (Zhang and Sabuncu, 2018).

$$\text{loss}_j = -O_j \ln P_j - (1 - O_j) \ln(1 - P_j) \quad (4.10)$$

where P_j is the corresponding predicted value to O_j (observed value) at epoch j , an epoch refers to one cycle through the dataset is passed forward and backward the neural network

4.4 - Output variables post-processing: a probabilistic approach

Once trained, each ML model predicts an output vector of the probability of occurrence $P(\mathbf{y}_{t+DT})$ associated with the vector of rain classes \mathbf{y}_{t+DT} . The probabilistic output from ML models is achieved by employing the Softmax function in the output layer. The Softmax is helpful because it provides a normalized probability distribution conditioned on the input (Huang and Xiang, 2018). The input values can be positive, negative, zero, or greater than one, but the softmax transforms them into values between 0 and 1. Many multi-layer neural networks end in a penultimate layer that outputs real-valued scores that are not conveniently scaled and may be challenging. The probability of occurrence enhances the ML model's operational utility and reliability. From an operational perspective, it is crucial to provide, together with the nowcast, an estimation of its uncertainty. Hence, probabilistic predictions provide greater economic and decision-making value than deterministic ones.

4.5 - Performance criteria

The nowcasts are verified against the observed values using continuous and categorical scores. The continuous scores include the Root Mean Square Error (**RMSE**) and Root Square Error (**RSE**). Since the model predicts a rain class, thus an interval, the continuous metrics are evaluated concerning the mean values of the classes.

$$\text{RMSE} = \sqrt{\frac{\sum_{i=1}^N (P_i - O_i)^2}{N}} \text{ [mm]} \quad (4.11)$$

$$\text{RSE} = \frac{\sum_{i=1}^N (P_i - O_i)^2}{\sum_{i=1}^N (\mu_0 - O_i)^2} [-] \quad (4.12)$$

where P_i and O_i are the predicted and observed rainfall classes, N is the number of observations, μ is the mean of observations (μ_0).

The categorical scores include three indicators commonly used in the meteorological community: Probability Of Detection (**POD**), False Alarm Ratio (**FAR**), and Critical Success Index (**CSI**). They are skill scores similar to precision and recall commonly used by machine learning researchers (Kim et al., 2017). The values of the scoring indicators range from 0 to 1. The lower FAR, the better, and the higher the value of CSI and POD, the better.

$$\text{POD} = \frac{\text{Hits}}{\text{Hits} + \text{Misses}} \quad (4.13)$$

$$\text{FAR} = \frac{\text{False Alarm}}{\text{False Alarm} + \text{Hits}} \quad (4.14)$$

$$\text{CSI} = \frac{\text{Hits}}{\text{Hits} + \text{False Alarm} + \text{Misses}} \quad (4.15)$$

where Hit indicates that the observed rainfall class is correctly predicted; False Alarm indicates that the predicted rainfall class is greater than the observed one; Miss indicates that the predicted rainfall interval is lower than the observed one (**Table 4.2**). According to how categorical indicators were defined, a threshold was not needed. Indeed, the model nowcasts a rainfall class, thus a categorical value.

Table 4.2 Contingency table for meteorological indicators.

Observation	Nowcasting	
	Present	Absent
Present	Hit	Miss
Absent	False Alarm	

All the performance criteria are calculated per station by pooling together the information from all the events. Moreover, a confusion matrix is used to find the level of accuracy of the multiclass classification model. It shows the accuracy of a machine learning algorithm, especially in the supervised learning method (Suyatno et al., 2018). The confusion matrix consists of columns representing predicted data classes and rows representing the original data class.

Finally, the verification results are compared with those from Eulerian Persistence (EP), which assumes that for any lead time $t+DT$, the nowcasts are the observation at time t .

References

- Huang, L., Xiang, L. yang, 2018. Method for Meteorological Early Warning of Precipitation-Induced Landslides Based on Deep Neural Network. *Neural Process. Lett.* 48, 1243–1260. <https://doi.org/10.1007/s11063-017-9778-0>
- Kim, S., Hong, S., Joh, M., Song, S., 2017. DeepRain: ConvLSTM Network for Precipitation Prediction using Multichannel Radar Data 3–6.
- Moon, S.H., Kim, Y.H., Lee, Y.H., Moon, B.R., 2019. Application of machine learning to an early warning system for very short-term heavy rainfall. *J. Hydrol.* 568, 1042–1054. <https://doi.org/10.1016/j.jhydrol.2018.11.060>
- Nguyen, D.H., Bae, D.H., 2020. Correcting mean areal precipitation forecasts to improve urban flooding predictions by using long short-term memory network. *J. Hydrol.* 584, 124710. <https://doi.org/10.1016/j.jhydrol.2020.124710>
- Suyatno, J.A., Nhita, F., Rohmawati, A.A., 2018. Rainfall forecasting in Bandung regency using C4.5 algorithm. 2018 6th Int. Conf. Inf. Commun. Technol. ICoICT 2018 324–328. <https://doi.org/10.1109/ICoICT.2018.8528725>

Chapter 5 - Results and Discussion

The following results assess the performance of the models and the training strategy. First, to evaluate the generalization abilities of the models, **section 5.1** is devoted to analyzing all the rain events that were not used to train the models, i.e., the events of the testing set. Each model is evaluated and compared using continuous (RMSE and RSE) and categorical (POD, CSI, and FAR) metrics. In addition, the Eulerian Persistence (EP) is considered a benchmark. **Section 5.2** compared two events of the testing set whose characteristics are similar to convective events - characterized by high intensities and short durations - and stratiform ones - characterized by more significant areas of influences, higher durations, and lower rainfall intensities - respectively.

5.1 - Nowcast performance and skill evaluation

For the testing set (years 2017, 2018, and 2019), the RMSE and RSE for all the 95 ML models were computed (**Fig. 5.1**). RMSE mean values increase from 1.67 mm to 6.15 mm, while RSE values range between 0.158 and 0.186 from 30-minutes to 6-hours lead time models, respectively (**Table 5.1**).

The boxplot's interquartile range (IQR) is narrow for 30min lead times but wider for 6 hours lead times. This result suggests that the models perform similarly for all rain gauges at short lead times but differently for higher lead times. The RMSE and RSE of the EP nowcast are significantly higher than the ones obtained by the proposed models. The difference is accentuated for increasing lead times and highlights the ability of the proposed models to provide better estimation than the simple EP model.

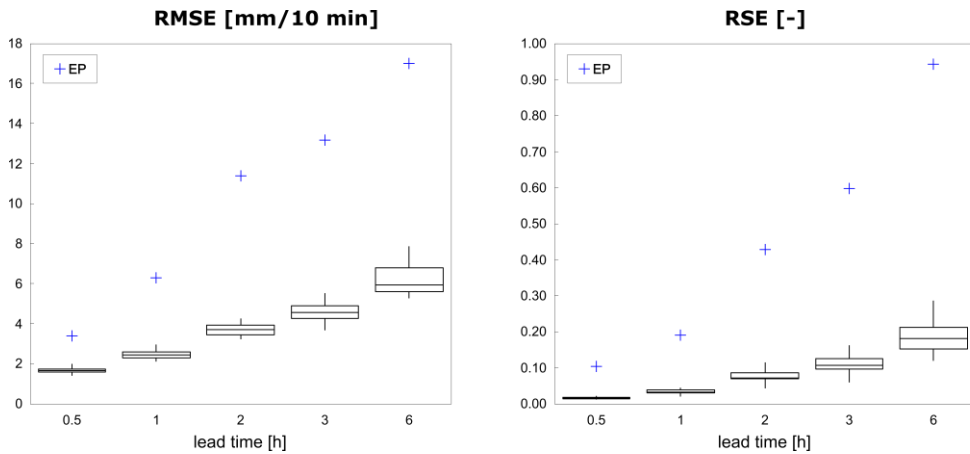


Fig. 5.1 Boxplots of RMSE and RSE values for each lead time between observed and predicted values of the 19 rain gauges. The blue crosses are the mean values of RMSE and RSE for the Eulerian Persistence (EP) for each lead time.

As expected, 30-minutes lead time models produce the best performance, while 6-hours ones perform the worst. These trends are broadly consistent with physical behavior. Thus, it is widely recognized that as the nowcast lead time increases, the correlation between the desired output and available input decreases (Lin et al., 2009), and rainfall nowcasts deteriorate (Heuvelink et al., 2020).

Table 5.1 Comparison of the average scores of the different models over five lead times. RSE, POD, FAR, and CSI are dimensionless and range between 0 and 1 (the values are the mean values from the boxplots in Fig. 5.1 and Fig. 5.2).

Lead-time [h]	0.5	1	2	3	6
RMSE [mm/10 min]	1.6735	2.4559	3.6998	4.5373	6.1506
RSE [-]	0.0158	0.0339	0.0751	0.1100	0.1864
POD [-]	0.9164	0.8584	0.7813	0.7504	0.7445
FAR [-]	0.0082	0.0182	0.0506	0.0775	0.1225
CSI [-]	0.9094	0.8450	0.7502	0.7060	0.6748

Model accuracy analysis reveals the same trends mentioned above: POD and CSI decrease from 0.5 h to 6 h lead-time model, while FAR increase (Fig. 5.2). The 30-minutes lead times models achieve the highest CSI (90.94%) and POD (91.64%) and lowest FAR (0.82%), giving better performance (**Table 4**).

Notwithstanding the decreasing trend, POD and CSI are all higher than 74.45 and 67.48%, and FAR lower than 12.25%, which means they all are, on average, close to their ideal values (100, 100 and 0%, respectively), confirming the goodness-of-fit of the models. In particular, low values of FAR are desirable for early warning systems since they cause financial losses and may result in people losing confidence in weather services and civil protection authorities (Liu et al., 2021).

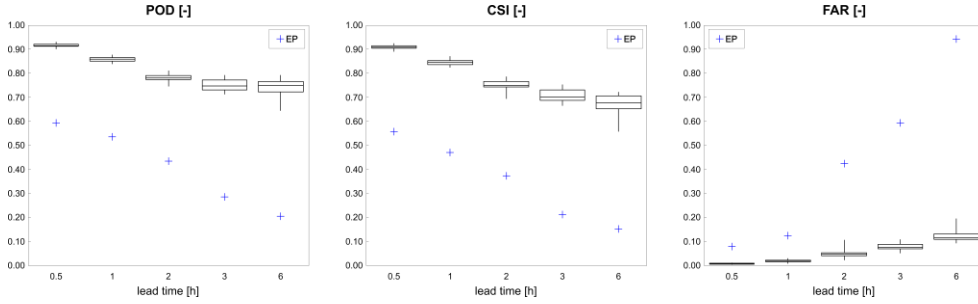


Fig. 5.2 Box plot of POD, CSI, and FAR values for each lead time between observed and predicted values of the 19 rain gauges. The blue crosses are the mean values of POD, CSI, and FAR for the Eulerian Persistence (EP) for each lead time.

The proposed models outperformed the benchmark EP for all the lead time and performance criteria (**Fig. 5.2**). Indeed, the EP approach is suitable for precipitation fields with negligible advection but can lead to significant errors in predicting the intensity of moving rainfall patterns.

Moreover, the models show an underestimation of the observations, as better depicted in confusion matrixes (**Fig. 5.3**). The dispersion of the values from the main diagonal provides accurate insights about the error made by the models. Even though the dispersion from the correctly predicted class (diagonal cells) is slightly appreciable for 30 minutes lead-times model, it considerably increases for the higher lead-times models. Also, Heuvelink et al. (2020) found that the rainfall forecasting skill decreased with increasing lead time, often associated with underestimating the nowcast rainfall. This was probably related to the fact that the nowcasting schemes do not explicitly consider the possible growth of rain cells. In the proposed models, the observed tendency to underestimate is mainly due to one reason. First, the output variables were discretized into intervals, which have a different number of examples. Almost 60% of the time steps (**Table 4.1**) fall in the first three classes (1,2,3).

Consequently, the models have more low classes examples and are willing to predict them rather than higher classes. To have equally size intervals, boundary intervals might have been set differently. However, this would have given too wide intervals

and would have been useless for nowcasting purposes. Thus, confusion matrixes highlighted that the model is influenced by the discretization of the rainfall into classes.

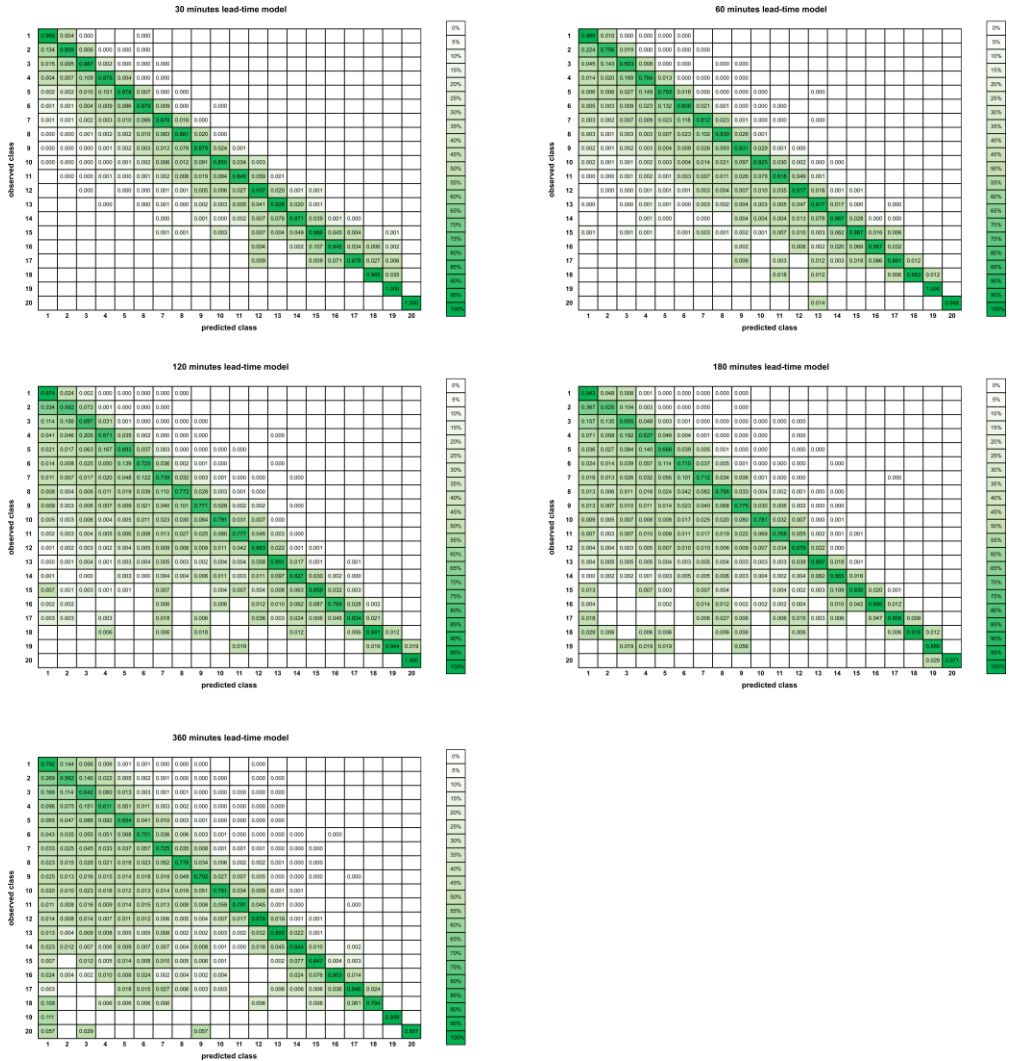


Fig. 5.3 Confusion matrix for each lead time between observations and predicted classes. The colours begin with white, range through shades of green, and then through shades of bright green. Brighter green means a higher percentage of actual predicted.

The result of the proposed model could be compared with that obtained by Shehu (2021), who investigated how to extend the predictability limit of rainfall at a fine scale (5 minutes and 1 km²) by improving the radar rainfall field fed into the nowcast models. Regarding a lead time of up to 3 hours, Shehu (2021) illustrated that the temporal RMSE between the nowcast time series and actual input field varies up to 0.5 mm/5min (6 mm/h). On the other hand, the RMSE obtained with our model ranges between 3.64 and 5.53 mm/10 minutes, i.e., 21.84 and 33.18 mm/h (**Fig. 5.1**). According to the results, Shehu's model provided better results than ours—an explanation for why the RMSE of our models were higher lies in how they were calculated. Indeed, the RMSE considered the mean of the rainfall classes. Therefore, even though a hit is registered (in terms of categorical criteria), the observed intensities can still deviate from the rainfall class mean. However, even though this comparison may not be entirely reliable since the spatial resolution of our model is coarser than Shehu's (2021), our model is competitive for several reasons. First, we employed rain gauge data—the reference devices for hydrological application - thus, the nowcasts were not affected by the conversion error from radar measurement, which allowed our model to obtain reliable prediction in real-time without further processing of the data.

Furthermore, weather radar real-time adjustment is tough at the beginning of rainfall events, with no prior rain gauge data recordings. In contrast, Shehu (2021) used radar data, which offered almost full spatial coverage but inevitably displayed a discrepancy with the gauge that will propagate and increase with the lead time. As a result, Shehu (2021) identified a predictability limit of the model, which was up to 3 hours of lead time.

Moreover, not only our models provided a nowcast but also the corresponding probability of occurrence. This is probably the model's main strength since it allows an estimation of the uncertainty of the nowcast – which is crucial for early warning purposes. Another advantage could be attributed to the easy-replicability and cost-effective times to run. Indeed, once the models are trained, the nowcasts are provided in real-time, i.e., the computational time is of the order of the millisecond. Our models

seem promising, but further correction must be performed to account for the lack of spatial representation. Since the models make a punctual prediction, if a storm occurs between the rain gauges, they can miss the peak rainfall intensity and automatically lead to an underestimation of the forecast. Indeed, depending on the specific velocity or advection, when a storm is captured at some stations, the others will capture it with a time shift. However, since our models do not consider the time shift, the performance criteria penalized the results. If criteria with a specific threshold were implemented (and time-independent), the performance would have differed.

Nevertheless, according to the overall result, it is evident that there is consistent physical behaviour, which is not obvious when dealing with machine learning techniques (Liu et al., 2022). As already stated, one of the main drawbacks of artificial intelligence algorithms is their tendency to produce results that cannot be rationally explained. As a result, users are unwilling to use them. In addition, it can be said that the training strategy was successful. Not only the model allows the evaluation of rainfall information but also the estimation of the transition from non-rain to rain conditions and prediction of short rainfall patterns, which are not easy to evaluate in advance. These features allow good quality in rainfall nowcasting, ensuring a practical warning issue.

5.2 - Event-based comparison

To highlight the ability of the model to predict different types of events, the performances of the proposed nowcasting models are shown and compared for two of them that differ in terms of (1) duration, (2) average total rain depth among the stations, (3) maximum total rain depth, (4) maximum 10 min rain depth, and (5) average 10 min rain depth (**Table 5.2**).

Table 5.2 Analysed rain events' main properties.

Event No.	311	357
Start [CET]	01 Oct 2018 04:00	19 Dec 2019 04:00
End [CET]	01 Oct 2018 23:00	20 Dec 2019 04:20
Duration [h]	19.16	24.33
Average total rain depth [mm]	26.16	46.65
Maximum total rain depth [mm]	59.60	122.00
Max 10 minutes rain depth [mm]	16.40	9.00
Average 10 min rain depth [mm]	1.84	0.82

The characteristics of the rain depth registered during event n. 311 were similar to convective cells, characterized by high intensities and short durations. Even though the event lasted almost 19 hours, the measurements were intermittent and lasted around one hour (**Fig. 5.4**). On the other hand, event n. 357 was related to the mechanism that generates stratiform rainfall, characterized by more significant areas of influence, higher durations, and lower rainfall intensities compared to the convective precipitation (**Fig. 5.4**).

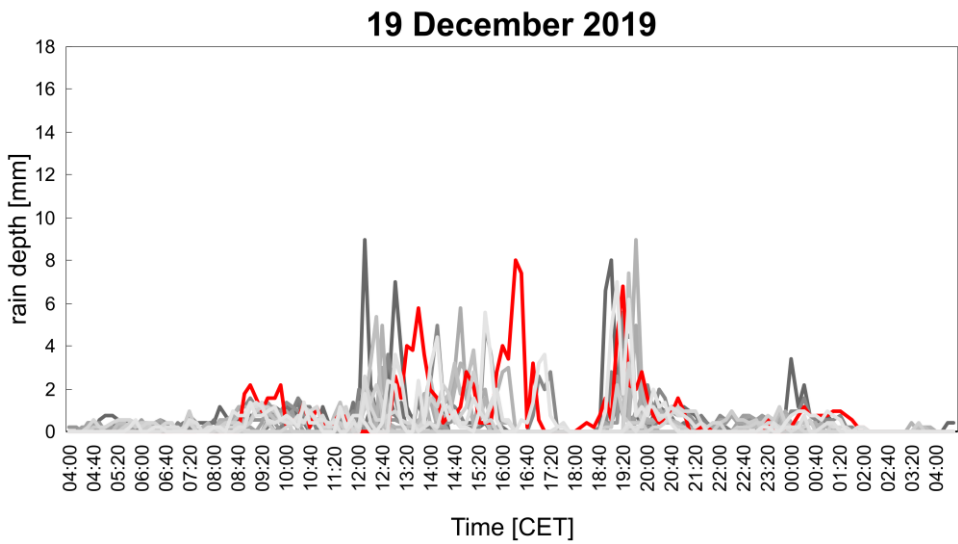
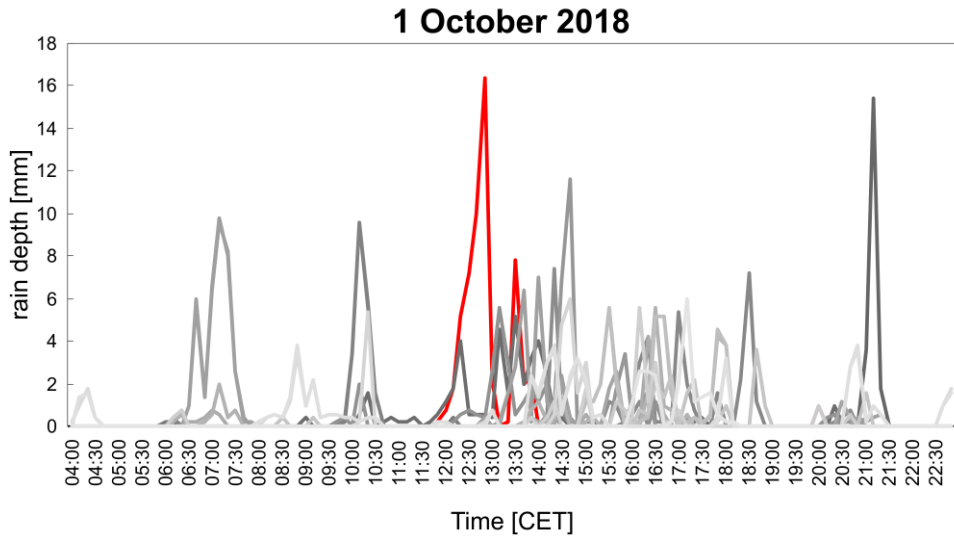


Fig. 5.4 Rain depth registered during the event on the 1st of October 2018 (top) and 19th of December 2019 (bottom). The red lines are referred to the stations with the highest rain depth peak in 10 minutes: station n. 3 and n. 5, respectively. The different shades of grey are referred to the other station's measurements.

5.2.1 - Convective event - event on 1 October 2018

The event on 1st October 2018 occurred with two earlier rain bursts, followed by almost 7 hours of continuous rain period, discontinuously measured by the stations over the study area (**Fig. 5.4**). An average of 26.16 mm fell in 19 h, with the highest total depth value of 59.60 mm registered by station number 6. While station number 3 detected the highest peak at 12:50 CET (Central European Time) of 16.40 mm (**Fig. 5.4 – red line**). The peak value lasted less than 1 hour and was exceptionally high - the maximum annual value registered by the station. To emphasize the ability of the models to detect local peaks, results are presented in terms of the mean values of the rain depth between observed and predicted rain classes (**Fig. 5.5**).

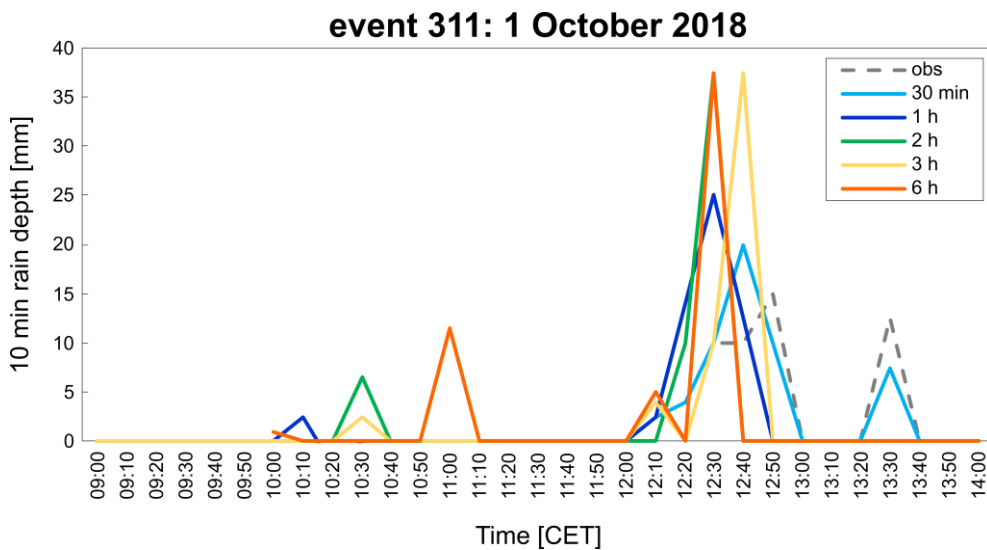


Fig. 5.5 Event based comparison between observed values and models predictions over 5 lead times for station n. 3.

Among the five models, 30 minutes lead-time one performed the most remarkable result. It achieved an RMSE of 1.92 mm and an RSE of 2.79 %. In contrast, the 6-hour lead time model nowcasts deviated from the observed data, resulting in an RMSE of 11.50 mm and an RSE of 16.71 %. Similarly, POD decreased from 100% to 13%, CSI from 96 % to 9 %, and FAR increased from 4% to 75%.

Table 5.3 Comparison of the performance criteria of the different models over five lead times for station n. 3. RSE, POD, FAR, and CSI are dimensionless and range between 0 and 1.

Lead-time [h]	0.5	1	2	3	6
RMSE [mm]	1.92	7.69	9.96	5.69	11.50
RSE [-]	0.03	0.11	0.14	0.08	0.17
POD [-]	1.00	0.73	0.36	0.32	0.13
FAR [-]	0.04	0.50	0.78	0.70	0.75
CSI [-]	0.96	0.42	0.16	0.18	0.09

The decline of the performance criteria within the five models was partly due to the short evolution of the rainfall registered by station 3. Indeed, the peak value occurred quickly after a no-rain burst– typical of convective cells (Capozzi et al., 2018). As a result, the 6-hours models had not enough stored information about the last time step; thus, the cumulative rain depths registered by station 3 were zero.

Even though the proposed models failed to nowcast the actual values at the correct time for higher lead times, they provided notable nowcasts for a lead time of up to 1 hour, which is valuable for dispatching decision-making. POD, CSI, and FAR suggest that the models could support Early Warning Systems to increase preparedness until more data becomes available. We believe these results were possible thanks to the joint use of cumulative rain depth from nearby stations. Even though station 3 started recording a no-zero value of rain depths only around 12:00 CET, the models already provided nowcasts because the rain event had already started over the study area – according to rainfall event selection (**Section 3.3**).

This performance is also consistent with the result obtained by Ghaemi et al. (2021), who evaluated the nowcasting product of 2 km resolution gridded data from 2007 to 2018. They observed that during four extreme convective short-duration events, there was a time shift in peak intensity detection, as happened in our models (**Fig. 5.4**). It is worth highlighting that, without further information from the nearby stations, the nowcast of the such isolated peak would have been trivial. Introducing cumulative rain depths from nearby stations as inputs to the model allowed to capture of spatiotemporal features. In this way, the models learned the rainfall process without storing antecedent time steps but according to the spatial characteristics.

5.2.2 - Stratiform event - event on 19 December 2019

All stations over the study area homogenously registered the event on 19th December 2019: an average of 50.57 mm fell in 22 h, with the highest values detected during the ten central hours (From 11:00 to 21:00) (**Fig. 5.3**). Results are shown for meteorological station number 5 that registered the highest cumulative rain depth value of 122.00 mm, almost gradually increasing during the event (**Fig. 5.3**). To highlight the ability of the model to predict the increasing rain depth during the event, results are presented in terms of cumulative rain depth between observed and predicted rain classes.

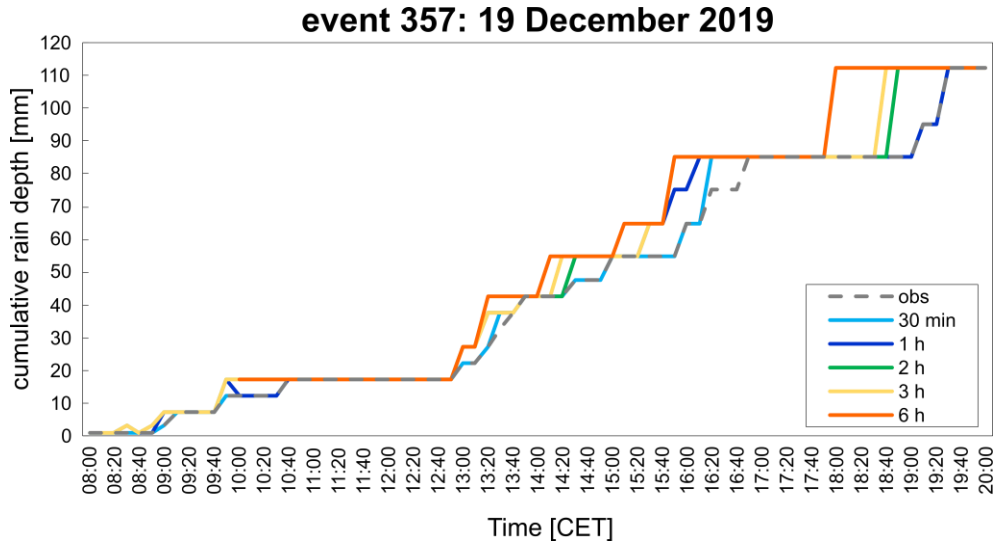


Fig. 5.6 Event-based comparison between observed values and model predictions over five lead times for station n. 5.

All the models recognised the increasing rainfall pattern registered by station n. 5. However, for higher lead-times models, the nowcasts were more significant than the observed values, resulting in an overestimation. Once again, as the lead time increased, the performance of the models decreased. For example, the 30-minute lead time model showed an RMSE of 0.35 mm, which increased to 4.50 mm for the 6 hours lead time one (**Table 5.4**), while RSE increased from 3 to 36 %. Also, meteorological indicators trends are consistent with previous results: POD, FAR, and CSI changed from 98, 3, and 95 to 69, 29, and 53, respectively.

Table 5.4 Comparison of the performance criteria of the different models over five lead times for station n. 4. RSE, POD, FAR, and CSI are dimensionless and range between 0 and 1.

Lead-time [h]	0.5	1	2	3	6
RMSE [mm/10min]	0.35	1.46	2.55	2.95	4.50
RSE [-]	0.03	0.12	0.20	0.23	0.36
POD [-]	0.98	0.95	0.90	0.85	0.69
FAR [-]	0.03	0.13	0.20	0.22	0.29
CSI [-]	0.95	0.84	0.74	0.68	0.53

Comparing the evaluation metric of the two events, we found that the model predicted the 2nd better than the 1st. We believe these results were possible thanks to gradual, light rain evolution. Furthermore, the stratiform events displayed a higher correlation than the simple convective ones and had many more timesteps to choose from in the training phase. As a result, the models favour the stratiform ones. Moreover, the results are compatible with (Imhoff et al., 2020), who showed that longer rain events durations, consisting of larger, more persistent systems, have higher predictability than the shortest durations, which generally consist of short-lifetime high-intensity convective precipitation events. Finally, they demonstrated that the average Mean Absolute Error (MAE) of the nowcasting model for stratiform rainfall becomes three times lower than those achieved during more convective rainfall with higher intensities.

Ayzel et al. (2020) proposed a neural network for radar-based precipitation nowcasting to predict continuous precipitation intensities at a lead time of five minutes. They found that the models had a limited ability to predict high rainfall intensities, probably due to a remarkable level of spatial smoothing in their predictions. Moreover, that smoothing becomes increasingly apparent at longer lead times. As suggested by their results, the nowcast performance is quite sensitive to the type of the event, and thus the results shown here do not contradict the fact that stratiform-type events may perform better than the convective type.

To conclude the comparison between the analysed events, the models provided better precipitation nowcasts when the event extension is homogeneous but failed to catch local precipitation events sufficiently in advance successfully. Thus, as expected, the potential lead time is short for convective rain events, where the rain evolves rapidly (Dolciné et al., 1998).

References

- Ayzel, G., Scheffer, T., Heistermann, M., 2020. RainNet v1.0: A convolutional neural network for radar-based precipitation nowcasting. *Geosci. Model Dev.* 13, 2631–2644. <https://doi.org/10.5194/gmd-13-2631-2020>
- Capozzi, V., Picciotti, E., Mazzarella, V., Marzano, F.S., Budillon, G., 2018. Fuzzy-logic detection and probability of hail exploiting short-range X-band weather radar. *Atmos. Res.* 201, 17–33. <https://doi.org/10.1016/j.atmosres.2017.10.006>
- Dolciné, L., Andrieu, H., French, M.N., 1998. Evaluation of a conceptual rainfall forecasting model from observed and simulated rain events. *Hydrol. Earth Syst. Sci.* <https://doi.org/10.5194/hess-2-173-1998>
- Ghaemi, E., Foelsche, U., Kann, A., Fuchsberger, J., 2021. Evaluation of Integrated Nowcasting through Comprehensive Analysis (INCA) precipitation analysis using a dense rain-gauge network in southeastern Austria. *Hydrol. Earth Syst. Sci.* 25, 4335–4356. <https://doi.org/10.5194/hess-25-4335-2021>
- Heuvelink, D., Berenguer, M., Brauer, C.C., Uijlenhoet, R., 2020. Hydrological application of radar rainfall nowcasting in the Netherlands. *Environ. Int.* 136, 105431. <https://doi.org/10.1016/j.envint.2019.105431>
- Imhoff, R.O., Brauer, C.C., Overeem, A., Weerts, A.H., Uijlenhoet, R., 2020. Spatial and Temporal Evaluation of Radar Rainfall Nowcasting Techniques on 1,533 Events. *Water Resour. Res.* 56, 1–22. <https://doi.org/10.1029/2019WR026723>
- Imhoff, R.O., Brauer, C.C., van Heeringen, K.J., Uijlenhoet, R., Weerts, A.H., 2022. Large-Sample Evaluation of Radar Rainfall Nowcasting for Flood Early Warning. *Water Resour. Res.* 58. <https://doi.org/10.1029/2021WR031591>
- Lin, G.F., Chen, G.R., Wu, M.C., Chou, Y.C., 2009. Effective forecasting of hourly typhoon rainfall using support vector machines. *Water Resour. Res.* 45, 1–11. <https://doi.org/10.1029/2009WR007911>
- Liu, J., Xu, L., Chen, N., 2022. A spatiotemporal deep learning model ST-LSTM-SA for hourly rainfall forecasting using radar echo images. *J. Hydrol.* 609, 127748. <https://doi.org/10.1016/j.jhydrol.2022.127748>
- Liu, Y., Wang, H., Lei, X., 2021. Real-time forecasting of river water level in urban based on radar rainfall: A case study in Fuzhou City. *J. Hydrol.* 603, 126820. <https://doi.org/10.1016/j.jhydrol.2021.126820>
- Shehu, B., Haberlandt, U., 2021. Relevance of merging radar and rainfall gauge data for rainfall nowcasting in urban hydrology. *J. Hydrol.* 594, 125931. <https://doi.org/10.1016/j.jhydrol.2020.125931>

Chapter 6 - Transferability of the model to other contexts

This chapter investigates the extendibility of the model to other regions that differ from southern Italy. The Flanders Region of Belgium, with its typical lowland catchments, is considered. The chapter is structured as the thesis. First, **section 6.1** describes the Belgian study area and the available rain data used to implement the model. One rain-gauge station is considered: Melsele station, near the city of Antwerp. In **section 6.2**, the parameters of the models are described, as well as the training strategy. **Section 6.3** shows the results of the models and compares them to two different benchmarks: Eulerian Persistence (EP) and pySTEPS. To assess the training strategy and evaluate the generalization abilities of the models, **section 6.3.1** shows the training, validation, and testing set results. Each model is evaluated using POD, FAR, Pearson coefficient, and MAE and compared to the EP result. Finally, **section 6.3.2** analyses a single rainfall event and compares it to the results of pySTEPS.

6.1 - Study area and dataset

The considered study area is the Flanders Region of Belgium (**Fig. 6.1**). It has an area of 13'624 km² and comprises sixty meteorological stations administrated by the Royal Meteorological Institute of Belgium (RMI)².

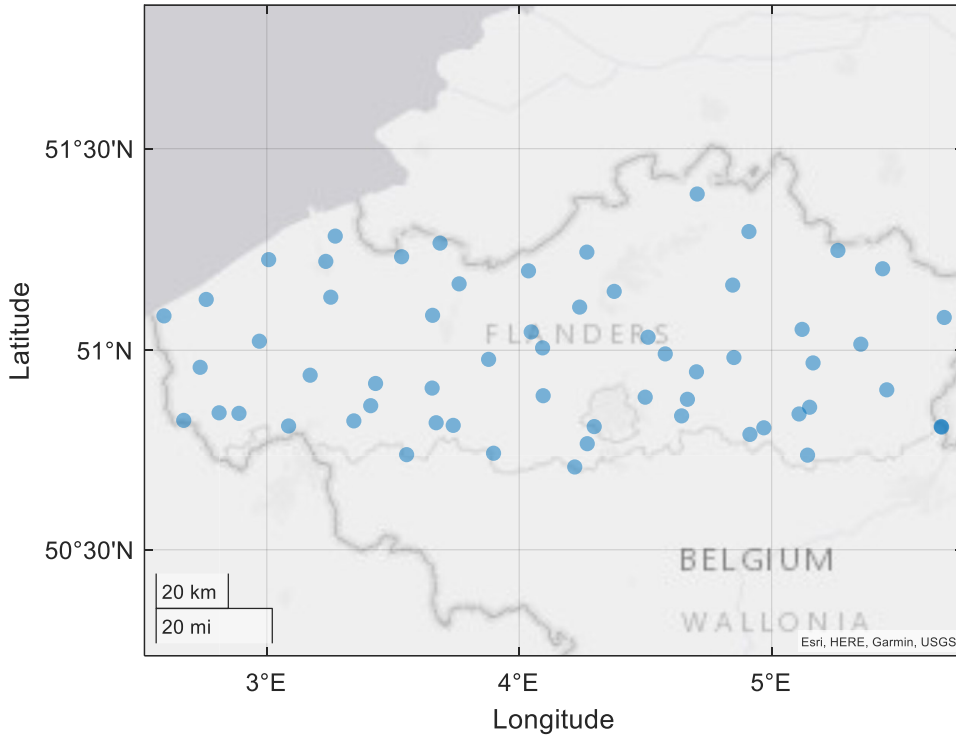


Fig. 6.1 The location of the study area (Flanders) within Belgian borders (dark grey line). Rain gauge stations are illustrated with blue dots.

This region has a temperate maritime climate with cool summers and moderate winters, high humidity during the year, and low sunshine duration in winter (Hosseinzadehtalaei et al., 2021). The precipitation is mainly of a) stratiform type in winter - caused by the Westerlies Air Masses (from the Atlantic) and characterized by

² <https://www.meteo.be/en/weather/forecasts/precipitation>

extended rainfall with low intensities; b) convective type in summer - caused by the radiation instabilities which occur at local scales and for a short duration of time. Owing to the flat topography of Flanders, precipitations at the stations follow a similar and homogeneous pattern.

Three hundred sixty rainfall events were selected from the 5-min rain-gauges time series for 2017–2021 (**Fig. 6.2**). Rain-gauge data is accessible online via the website: www.waterinfo.be³. The Minimum Inter-arrival Time index (MIT) selected the rainfall events. In particular, a MIT of 3 hours was chosen for the warm season (April, May, June, July, August, and September) and 2 hours for the cold one (October, November, December, January, February, and March).

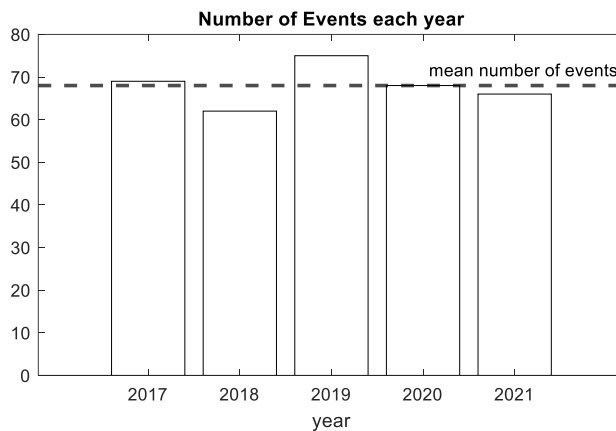


Fig. 6.2 Number of events selected each year according to Minimum Inter Event Time (MIT) criteria.

³ In association with other Flemish water managers, the Flemish Environment Agency has launched a widget-based web portal www.waterinfo.be, combining all real-time measurements and flood forecasts generated by the forecasting systems for the navigable and unnavigable rivers in Flanders. The data are presented as animated, forecasted flood maps and graphs of water levels, discharges and displayed on an interactive map of Flanders. In addition to floods, the website provides information on 3 other themes: tides, precipitation, and drought.

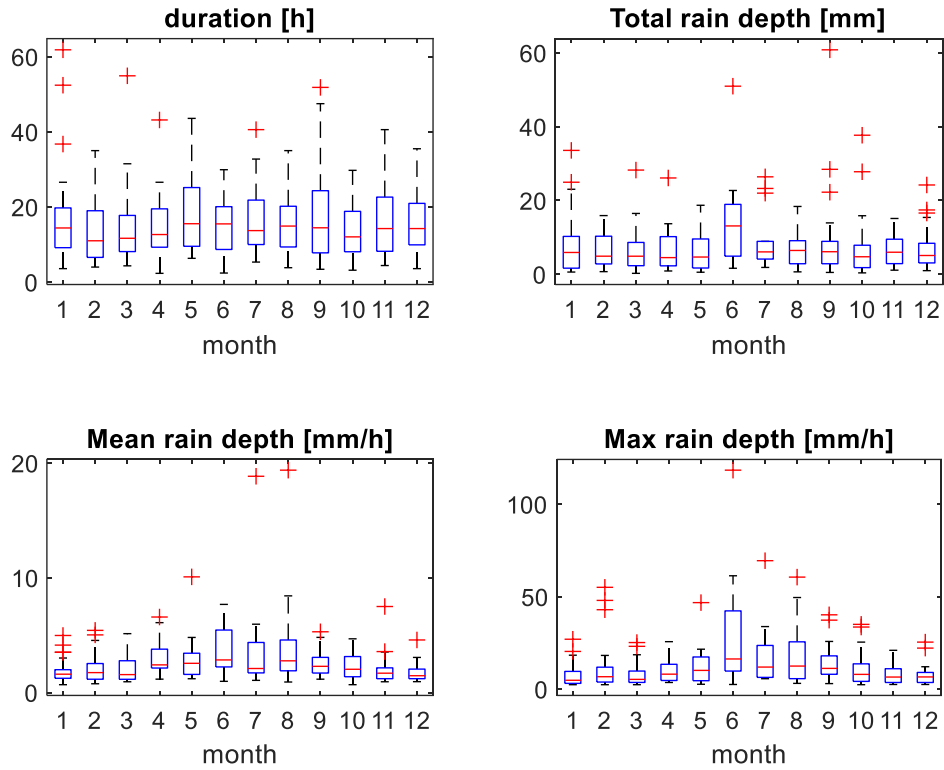


Fig. 6.3 Box plot of a) rain event duration; b) total rain depth; c) mean rain depth; d) max rain depth observed each month by all rain gauge stations during the selected events.

6.2 - Model parameters in Belgium

The ML model employs cumulative rainfall depths as inputs to predict rainfall intervals and the corresponding probability of occurrence in Melsele station after DT lead time. For six lead times (5, 10, 30, 60, 120, and 180 minutes), a model was independently developed and trained from the others for a total of 6 models.

The input data for the Melsele station model are the cumulative rainfall depths from recording stations (**Table 6.1**), which are in an area of 50 km radius from the Melsele station (**Fig. 6.2**).

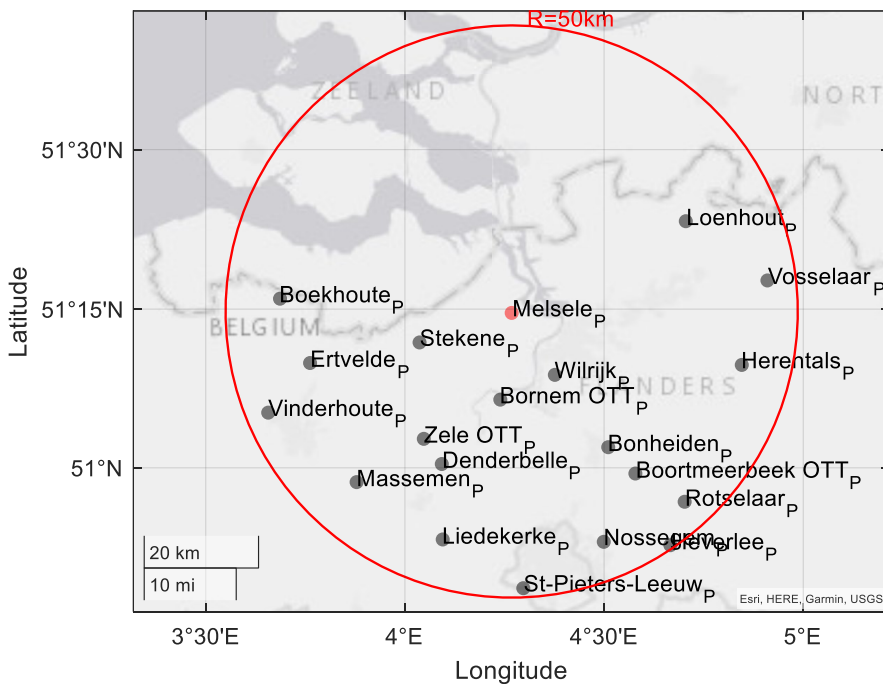


Fig. 6.4 Location of Melsele station (red dot) and recording stations used as input for Melsele models (black dots) in a radius of 50km from Melsele (solid red line).

Table 6.1 Parameters of the meteorological stations over the study area.

ID	Sensor ID	Station Name	Longitude [UTM]	Latitude [UTM]
1	210409042	Herentals_P	4.845694	51.162243
2	210397042	Bonheiden_P	4.510400	51.032543
3	210392042	Liedekerke_P	4.094898	50.886632
4	210381042	Boekhoute_P	3.686456	51.266411
5	210399042	Rotselaar_P	4.702251	50.946299
6	210412042	Loenhout_P	4.705126	51.387974
7	210400042	Heverlee_P	4.666340	50.877581
8	210394042	Denderbelle_P	4.092621	51.005996
9	210383042	Ertvelde_P	3.761918	51.165276
10	210382042	Stekene_P	4.036754	51.197620
11	210401042	Nossegem_P	4.499203	50.882903
12	210395042	St-Pieters-Leeuw_P	4.297130	50.809367
13	210385042	Massemen_P	3.878704	50.977371
14	210386042	Wilrijk_P	4.376359	51.146589
15	210410042	Vosselaar_P	4.910008	51.295069
16	207608042	Vinderhoute_P	3.656799	51.087051
17	14148010	Bornem OTT_P	4.239464	51.107571
18	13770010	Zelee OTT_P	4.047454	51.045712
19	13781010	Boortmeerbeek OTT_P	4.578555	50.990965

The cumulative rain depths are discretized into intervals; thus, the difference between two values within the same interval is neglected after the discretisation. **Table 6.2** is the contingency table for the discretized precipitation intervals, hereafter referred to as rain classes or classes. The discretization is different from the one in **section 3.3**. However, each class has a similar number of examples (Fig. 6.5), with a percentage never lower than 4 %. Therefore, in contrast to the previous discretization, 16 classes with different widths but similar numerosity were identified.

Table 6.2 Contingency table for the discretized intervals of precipitation scenario 1.

Class ID (x)	Interval [mm]	Interval width [mm]	Percentage [%]	Cumulative percentage [%]
1	0.1-0.5	0.40	0.090	0.090
2	0.5-1	0.50	0.087	0.176
3	1-1.5	0.50	0.071	0.247
4	1.5-2	0.50	0.064	0.312
5	2-2.5	0.50	0.057	0.368
6	2.5-3	0.50	0.053	0.421
7	3-3.5	0.50	0.046	0.467
8	3.5-4.5	1.00	0.081	0.548
9	4.5-5.5	1.00	0.070	0.618
10	5.5-6.5	1.00	0.058	0.675
11	6.5-7.5	1.00	0.048	0.723
12	7.5-9.5	2.00	0.069	0.792
13	9.5-12	2.50	0.058	0.850
14	12-15.5	3.50	0.052	0.902
15	15.5-20	4.50	0.041	0.943
16	20-120	100.00	0.057	1.000

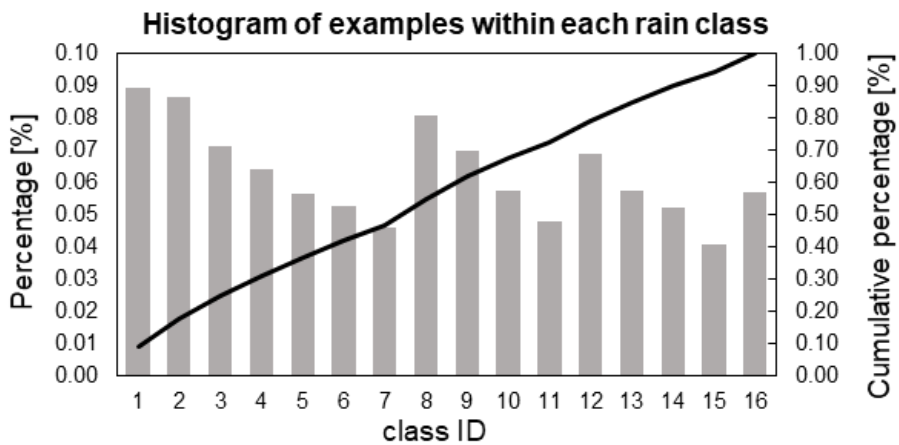


Fig. 6.5 Histogram of examples within each rain class [%] and cumulative percentage.

6.3 - Results and Discussion

To assess the training strategy and evaluate the generalization abilities of the models, **section 6.3.1** shows the training, validation, and testing set results. Each model is evaluated using POD, FAR, Pearson coefficient, and MAE and compared to the EP result. Finally, **section 6.3.2** analyses a single rainfall event and compares it to the results of pySTEPS.

6.3.1 - Nowcasts performance and skill evaluation

For training, validation, and testing sets, **Fig. 6.6** shows performance indicators for the six models as a function of lead time. As expected, the training set achieved the best results, while the performance of validation and testing sets was slightly lower. These trends indicate that the training strategy was successful; thus, the models achieved a competitive generalization ability. Indeed, the results of the validation and testing sets did not overly underperform the training set, but they followed a similar trend. All the indicators deteriorated with the lead time: POD and Pearson coefficient decreased, while FAR and MAE increased. This also means that the physical behaviour was fulfilled.

Even though the indicators declined with the lead time, they all outperformed the benchmark model EP. In contrast to the trends of the model, the trend of EP with lead times is unstable. Even though for a lead time of 5 minutes, the indicators for EP achieved better results, as soon as the lead time increased, the indicators sharply deteriorated. The main reason for this poor performance is probably due to the chaotic and rapid evolution of the rainfall. Indeed, EP is sensitive to the previous observation; thus, when the rainfall quickly evolves and changes, the values are weakly correlated, and the EP is no longer valuable.

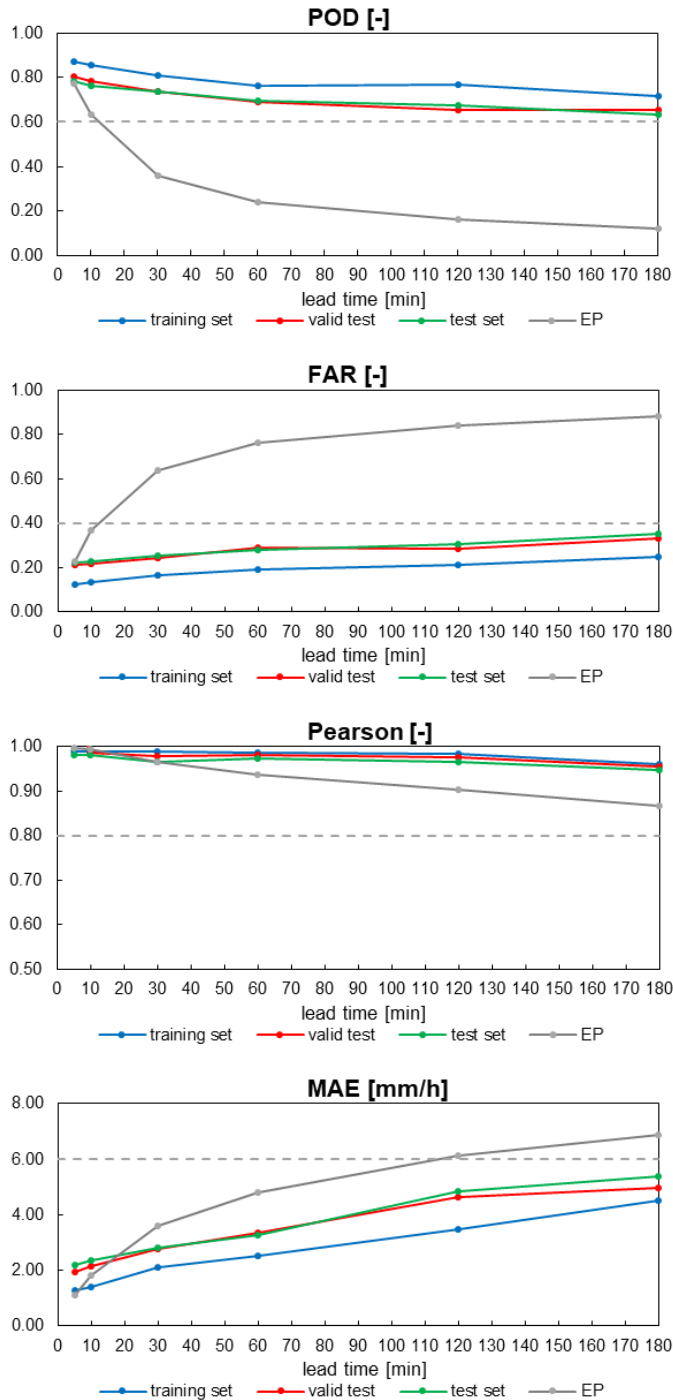


Fig. 6.6 POD, FAR, Pearson coefficient, and MAE values for Melsele station. The dashed line indicates the models' lower (or higher) value for training, validation, and testing sets.

Fig. 6.7, 6.8, 6.9, 6.10, 6.11, and 6.12⁴ compare the actual and predicted rainfall depth values for 5, 10, 30, 120, and 180 minutes ahead of lead time, respectively. In particular, 2017, 2018, and 2019 were used for the training set, 2020 for validation, and 2021 for testing. These figures indicate that the shape and the tendency of rainfall time series could be successfully predicted using the proposed model. However, once again, it is evident that the performance of the models decreased with increasing lead time.

⁴ Between each figure, one page is left blank in order to allow the reader to compare different models.

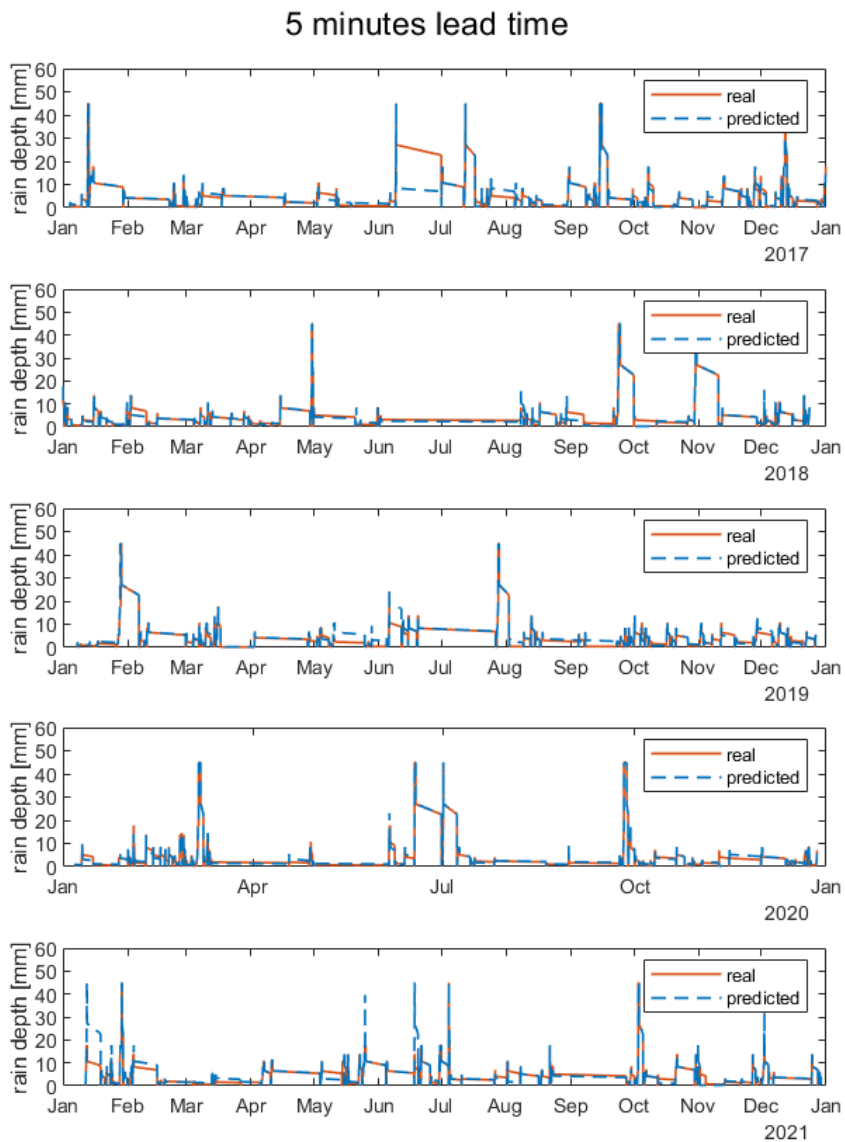


Fig. 6.7 Comparison of actual observed rainfall values (real) and the predicted ones with 5 minutes lead time for the training set (years 2017,2018, and 2019), validation set (2020) and testing set (2021).

10 minutes lead time

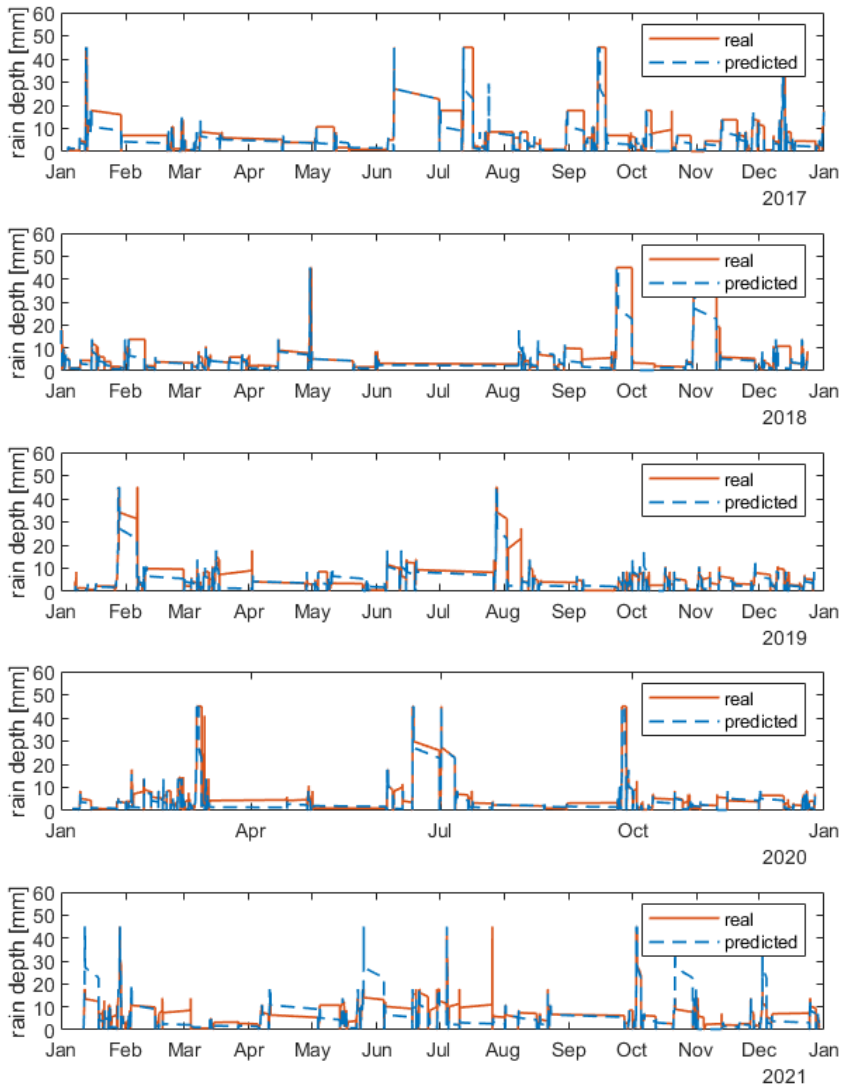


Fig. 6.8 Comparison of actual observed rainfall values (real) and the predicted ones with 10 minutes lead time for the training set (years 2017,2018 and 2019), validation set (2020) and testing set (2021).

30 minutes lead time

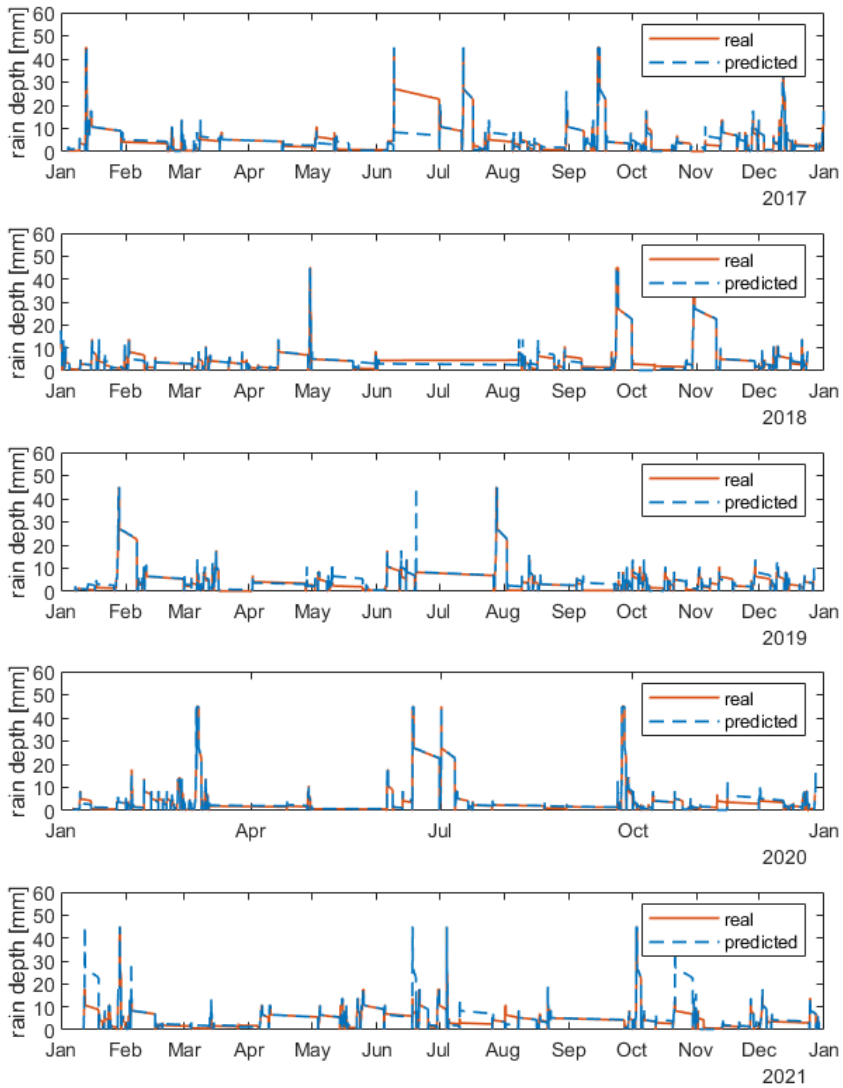


Fig. 6.9 Comparison of actual observed rainfall values (real) and the predicted ones with 30 minutes lead time for the training set (years 2017,2018 and 2019), validation set (2020) and testing set (2021).



60 minutes lead time

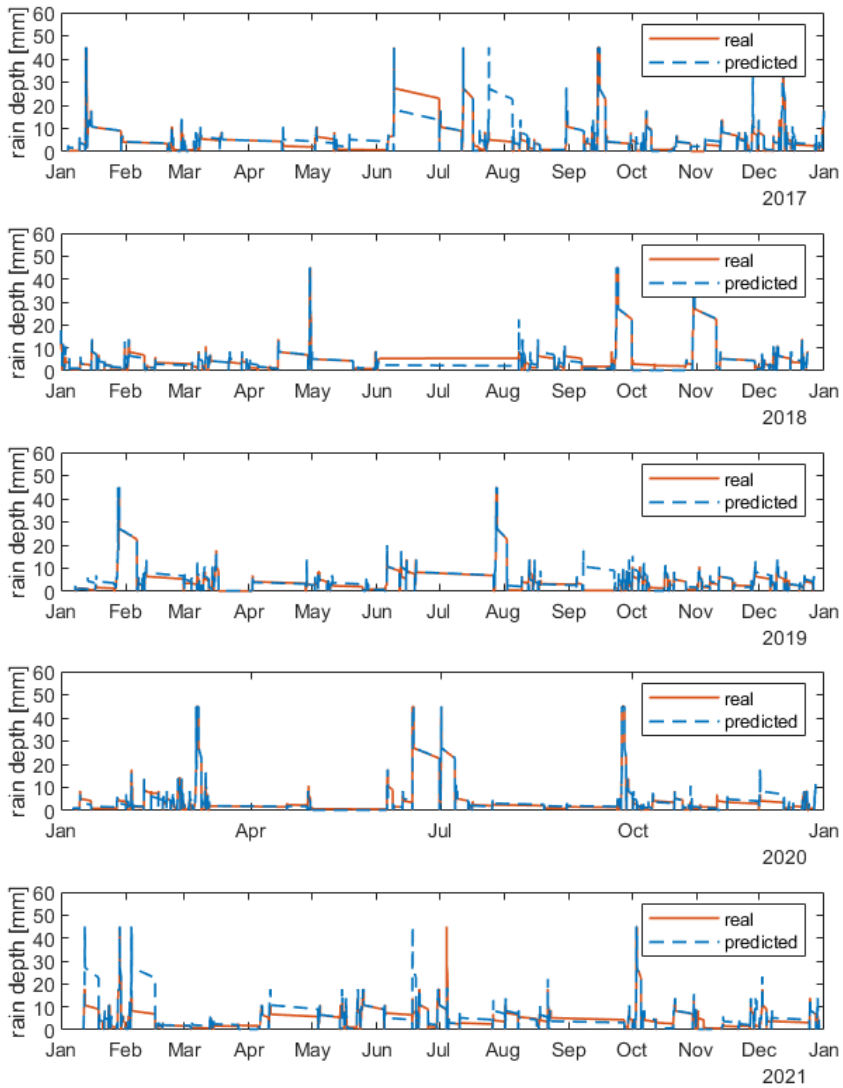


Fig. 6.10 Comparison of actual observed rainfall values (real) and the predicted ones with 60 minutes lead time for the training set (2017,2018 and 2019), validation set (2020) and testing set (2021).



120 minutes lead time

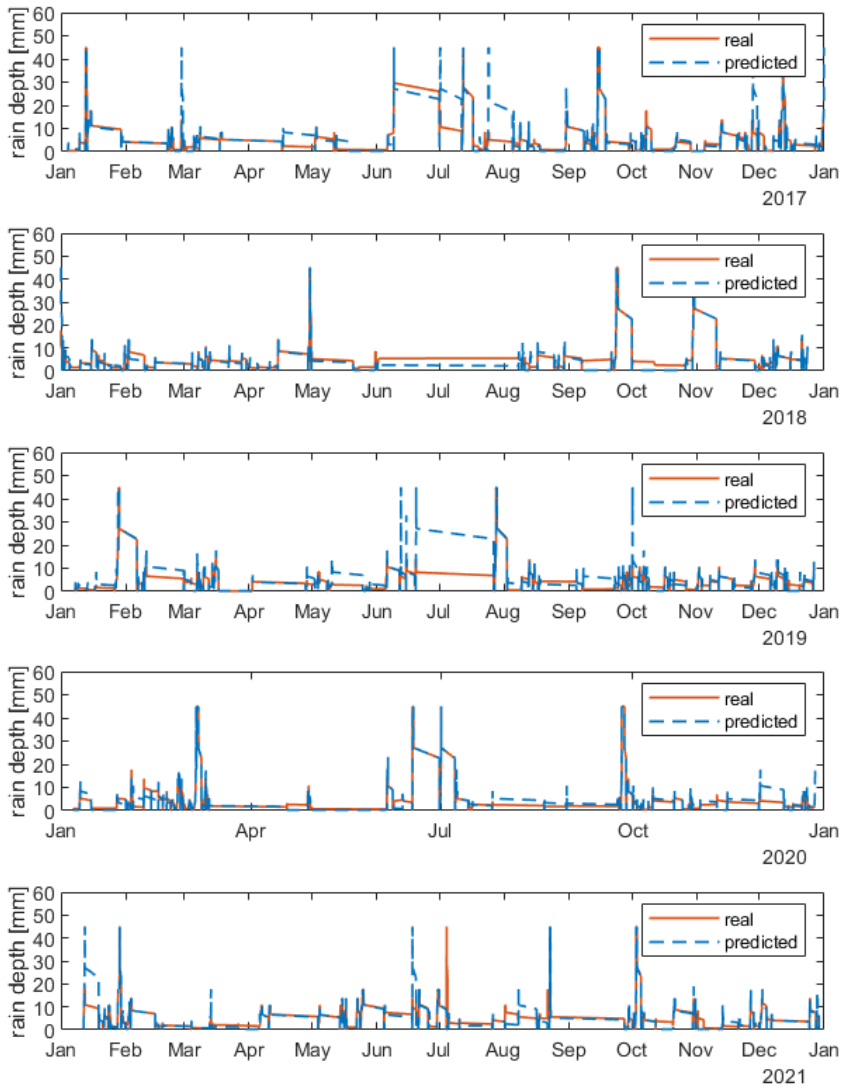


Fig. 6.11 Comparison of actual observed rainfall values (real) and the predicted ones with 120 minutes lead time for the training set (2017,2018, and 2019), validation set (2020) and testing set (2021).

180 minutes lead time

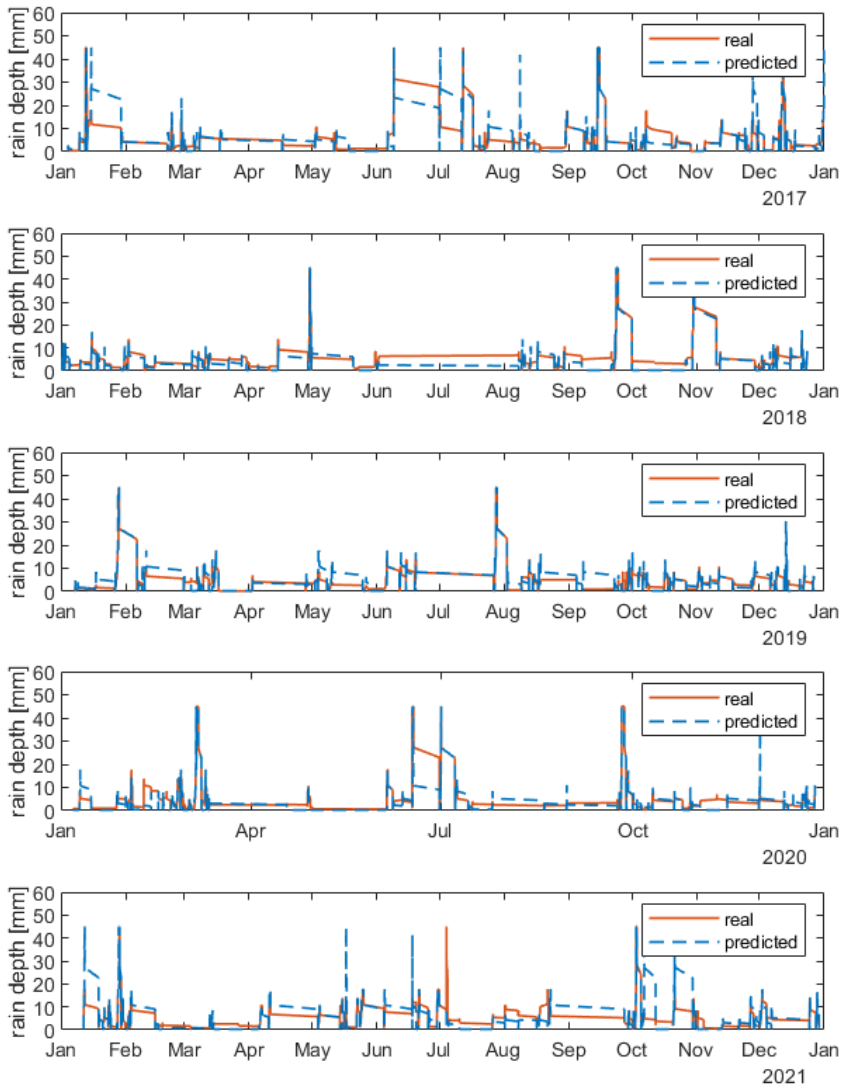


Fig. 6.12 Comparison of actual observed rainfall values (real) and the predicted ones with 180 minutes lead time for the training set (2017,2018 and 2019), validation set (2020) and testing set (2021).

6.3.2 - Event-based results

To highlight some typical differences between the proposed model and the output of pySTEPS, we analyze one event from the testing set (**Tab. 6.3**). First, the event is characterized: duration, peak time, and the number of involved stations are described. Next, since our proposed models use rainfall data from rain-gauge stations and pySTEPS uses radar data, the measurements from these two types of instruments are compared. Then, the parameters used to implement pySTEPS are described. Finally, a comparison between of two models is provided.

Table 6.3 Main characteristics of event 309 from the testing set.

Event No.	309
Start [CET]	04 July 2021 08:30
End [CET]	04 July 2021 13:30
Duration [h]	5
Max 10 minutes rain depth [mm/h]	140

It is worth mentioning that the comparison is more qualitative than quantitative. Indeed, the models are based on opposing approaches and use different input data with different spatial and temporal resolutions. Therefore, more than defining the best model, this comparison would highlight their suitability in different contexts.

The characteristics of the selected event are similar to convective cells, characterized by high intensities and short durations (**Table 6.3**). Even though the event officially lasted 4 hours, the higher rainfall bursts occurred in 2 hours: from 10:30 to 12:30. All the stations over the study area registered high rainfall peaks, with the highest value of 140 mm/h (**Fig. 6.13**). On the other hand, Melsele station registered a lower peak, almost 80 mm/h.

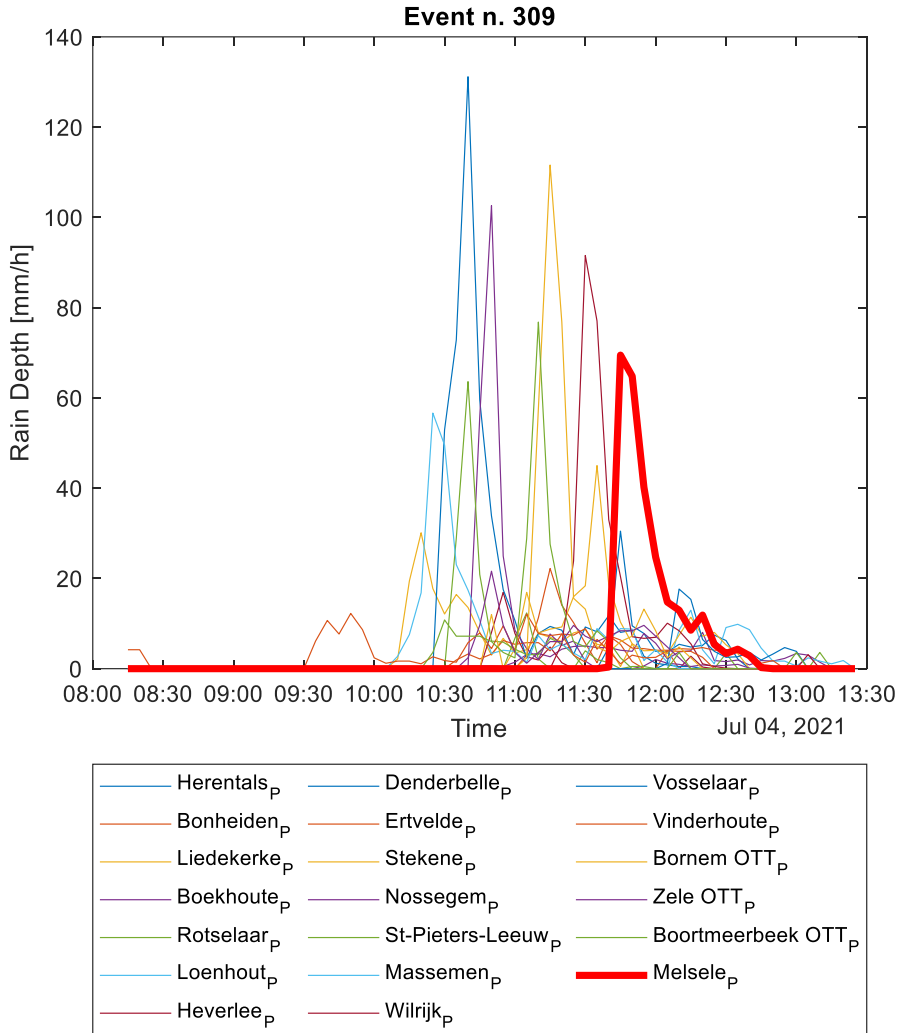


Fig. 6.13 Rain depths registered during the event on the 4th of July 2021 from rain-gauge stations over the study area.

To appreciate the differences between rain-gauge measurements from Melsele station and weather radar ones, **Fig. 6.14** shows both. In particular, the radar registrations of the 9 pixels around Melsele stations are considered. Rainfall measurements from radar sharply deviated from rain-gauge ones: radar rain depths are almost twice the actual values. As expected, for convective events, the rainfall is usually overestimated (Asghari et al., 2021). Indeed, the performance of the interpolation methods depends

on the available station density; a higher station density yields better results than a lower station density. However, the high density needed is not usually provided (Berne et al., 2004). Therefore, when comparing the prediction of pySTEPS, it is crucial to consider the already existing deviation of the radar measurements from the rain-gauge ones.

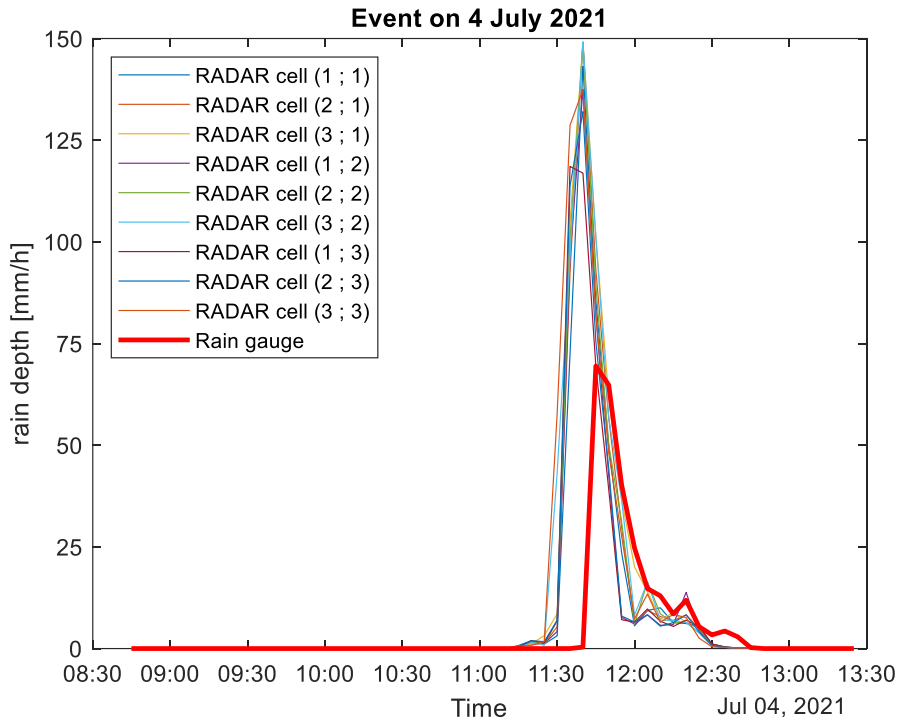


Fig. 6.14 Rain depths registered during the event on the 4th of July 2021 from Melsele station (rain gauge) and from weather radar (9 cells/pixels around Melsele stations).

To emphasize the ability of the models to detect local peaks, results are presented in terms of the mean values of the rain depths between observed and predicted rain classes **Fig. 6.15, Fig. 6.16, Fig. 6.17, Fig. 6.18, Fig. 6.19, Fig. 6.20** show the predictions of the 5, 10, 30, 60 and 120 lead-times model, respectively. In addition, to enhance the interpretability of the output, those graphs also show the original rain-gauges measurements (RG).

All the models with a lead time of up to 60 minutes correctly predicted the peak value at 11:45. The model with 120 minutes lead time predicted it with a time-shift of 5 minutes, while the model with 180 minutes lead time wholly underperformed. As expected, short lead times models performed the most remarkable result. Therefore, according to the proposed models, the peak value could have been predicted up to 1 hour before.

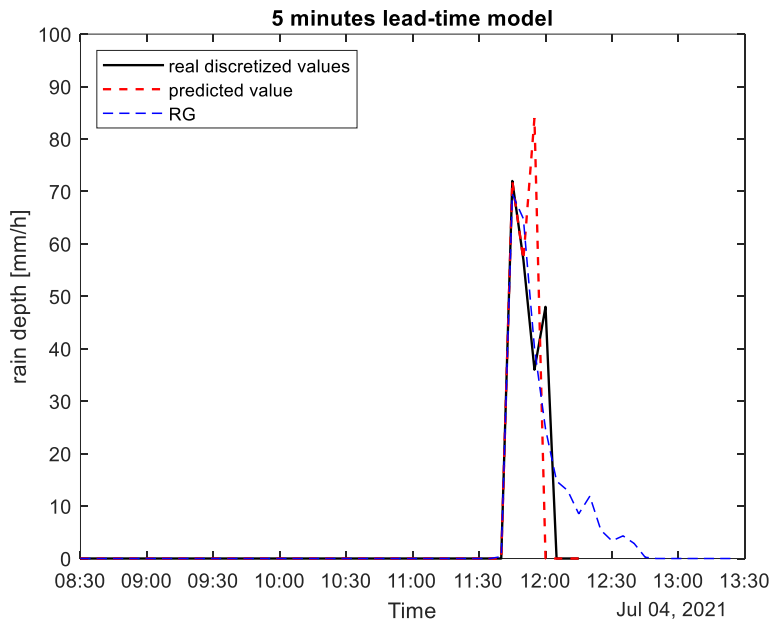


Fig. 6.15 Result of the 5 minutes lead-time model. Comparison between rain gauge measurements (RG), real discretized values and predicted values for Melsele station.

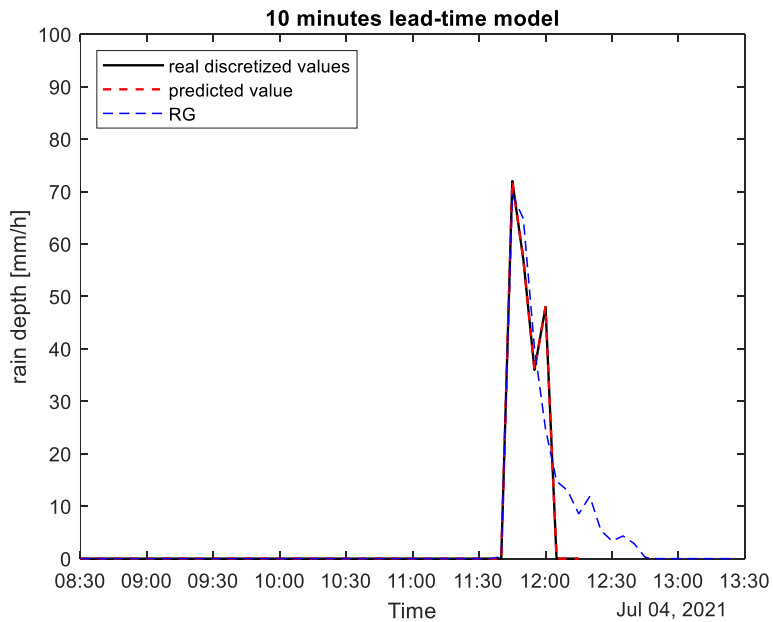


Fig. 6.16 Result of the 10 minutes lead-time model. Comparison between rain gauge measurements (RG), real discretized values and predicted values for Melsele station.

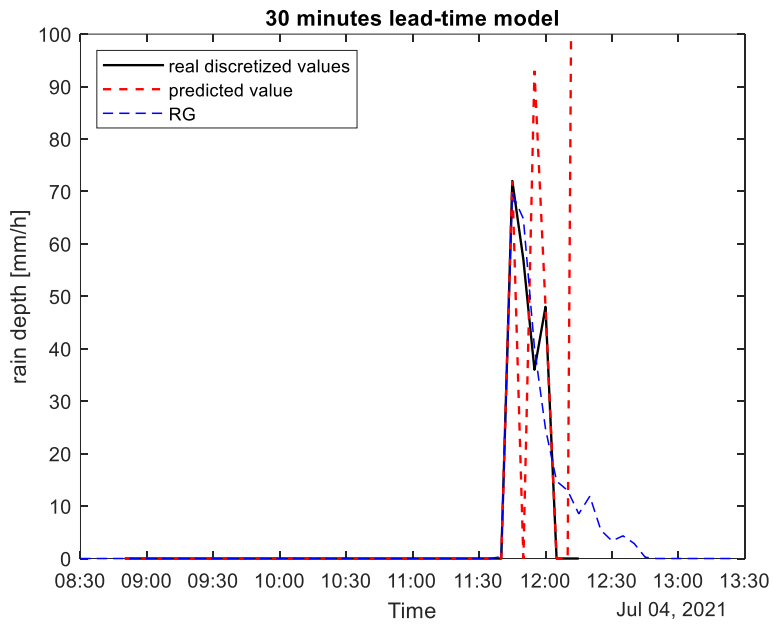


Fig. 6.17 Result of the 30 minutes lead-time model. Comparison between rain gauge measurements (RG), real discretized values, and predicted values for Melsele station.

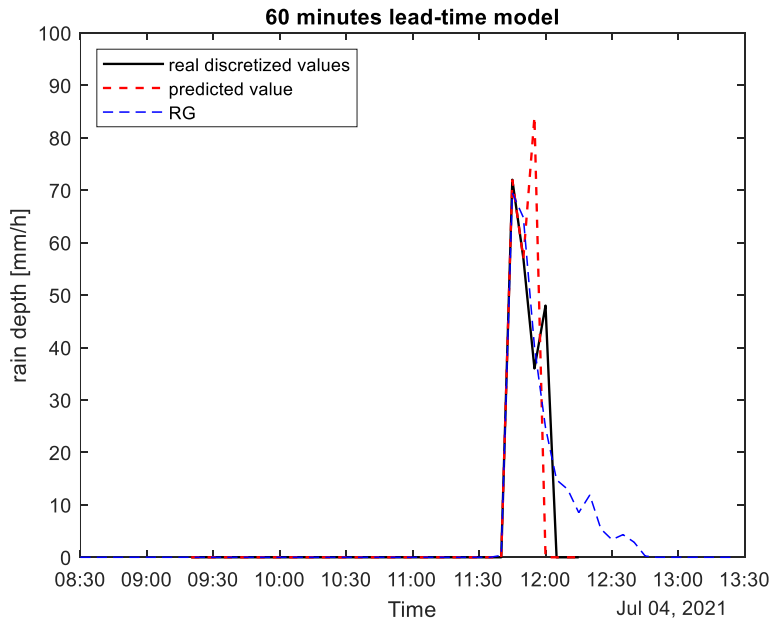


Fig. 6.18 Result of the 60 minutes lead-time model. Comparison between rain gauge measurements (RG), real discretized values and predicted values for Melsele station.

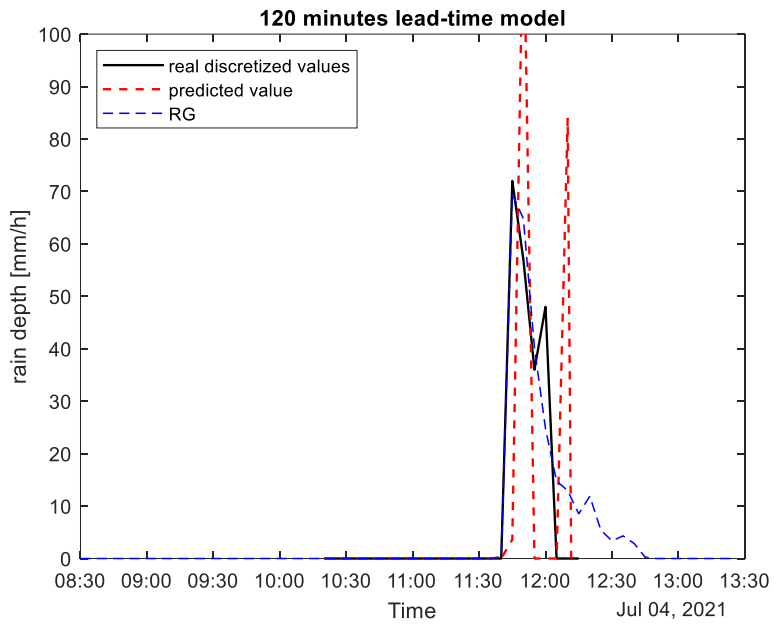


Fig. 6.19 Result of the 120 minutes lead-time model. Comparison between rain gauge measurements (RG), real discretized values and predicted values for Melsele station.

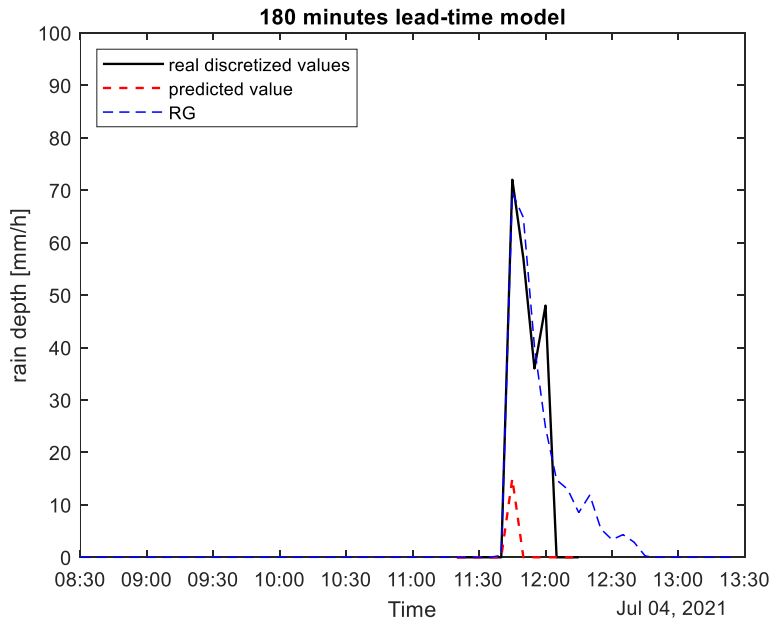


Fig. 6.20 Result of the 180 minutes lead-time model. Comparison between rain gauge measurements (RG), real discretized values and predicted values for Melsele station.

To contrast, the ensemble nowcasts produced by pySTEPS were run using the default configuration listed in **Table 6.4**. According to the registrations at time t_0 , t_0-5 min, and $t_0 - 10$ min, the model produces the nowcasts at time $t_0 + 5$ min up to $t_0 + 3$ hours. The nowcasts are 20-member ensembles produced in real-time at a spatial resolution of 0.9 km^2 and a temporal resolution of 5 min. These ensembles of 20 nowcasts give insight into the forecasted rainfall's uncertainty.

Table 6.4 Default pySTEPS configuration used in the experiments.

Parameter	Value
optical flow	Lucas-Kande
extrapolation	semi-Lagrangian
cascade levels	8
order of the ar(r) model	2
precip. intensity perturbation	non- parametric
value for dry pixels	-15 dBR
ensemble size	24
probability matching	Yes
seed number	24

The results from the 20 ensembles of pySTEPS are illustrated as well in **Fig. 21, Fig. 22, Fig. 23, Fig. 24, Fig. 25, Fig. 26, and Fig. 27**. As previously stated, the event starts at time 8:30, thus according to registration at 8:40, 8:35 and 8:30, the model provided the nowcasts at time 8:45 up to 11:45.

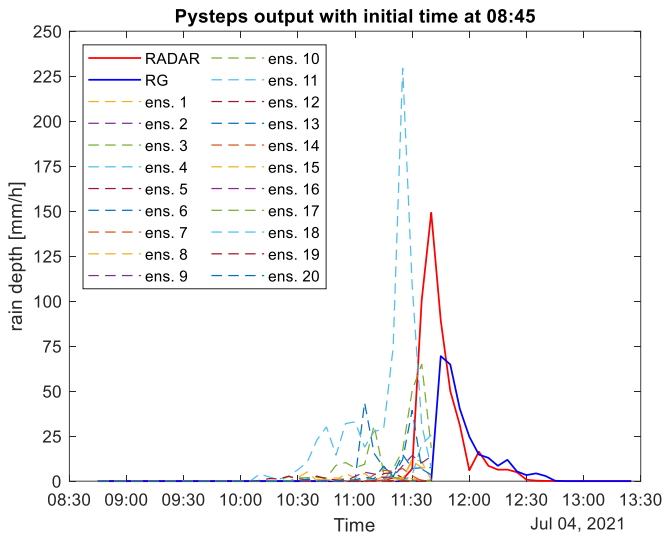


Fig. 6.21 Comparison between 20 ensembles (ens.) from pySTEPS, observed RADAR values and Rain Gauge (RF) with initial time at 08:45⁵.

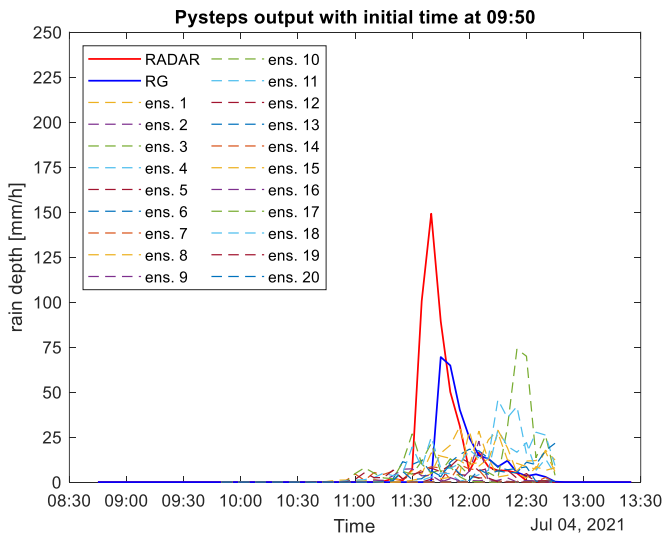


Fig. 6.22 Comparison between 20 ensembles (ens.) from pySTEPS, observed RADAR values, and Rain Gauge (RF) with initial time at 9:50⁶.

⁵ Initial time at 08:45 means that the registration used to obtain the nowcasts are those at time 8:40, 8:35, 8:30.

⁶ Initial time at 09:50 means that the registration used to obtain the nowcasts are those at time 9:45, 9:40, 9:35.

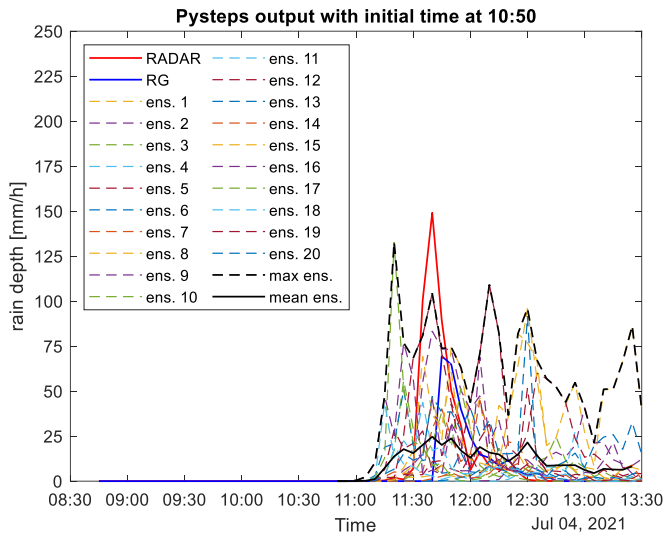


Fig. 6.23 Comparison between 20 ensembles (ens.) from pySTEPS, observed RADAR values and Rain Gauge (RF) with initial time at 10:50⁷.

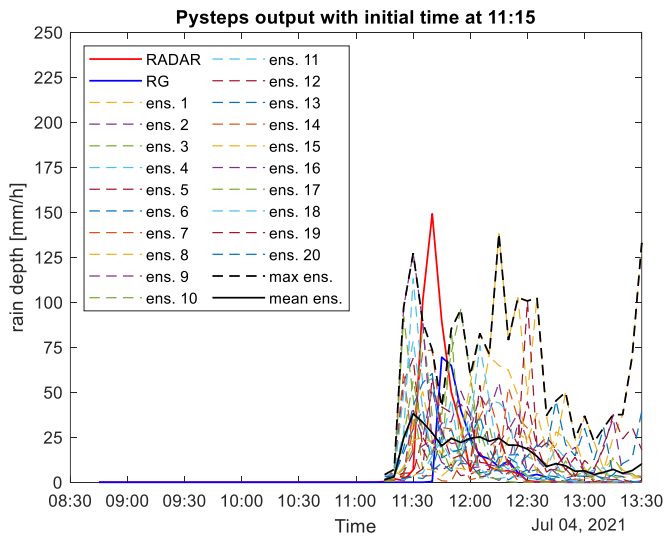


Fig. 6.24 Comparison between 20 ensembles (ens.) from pySTEPS, observed RADAR values and Rain Gauge (RF) with initial time at 11:15⁸.

⁷ Initial time at 10:50 means that the registration used to obtain the nowcasts are those at time 10:45, 10:40, 10:35.

⁸ Initial time at 11:15 means that the registration used to obtain the nowcasts are those at time 11:10, 11:05, 11:00.

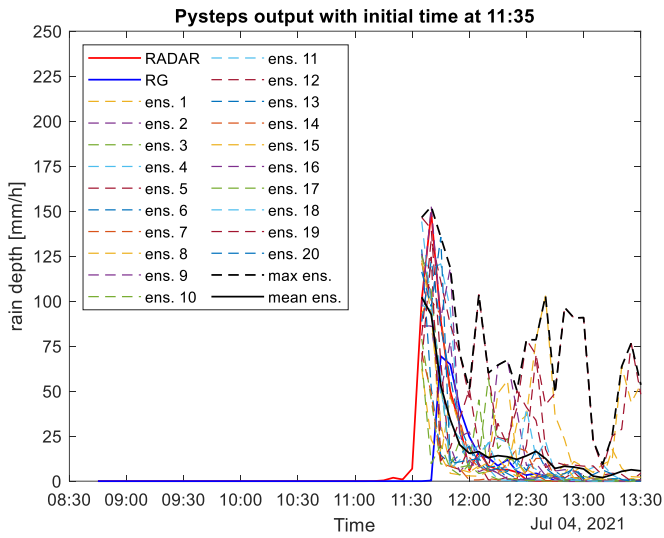


Fig. 6.25 Comparison between 20 ensembles (ens.) from pySTEPS, observed RADAR values and Rain Gauge (RF) with initial time at 11:35⁹.

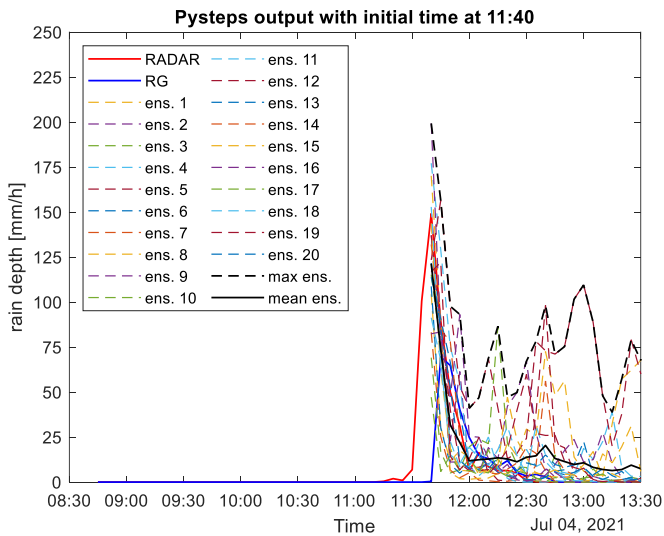


Fig. 6.26 Comparison between 20 ensembles (ens.) from pySTEPS, observed RADAR values and Rain Gauge (RF) with initial time at 11:40¹⁰.

⁹ Initial time at 11:35 means that the registration used to obtain the nowcasts are those at time 11:30, 11:25, 11:20.

¹⁰ Initial time at 11:40 means that the registration used to obtain the nowcasts are those at time 11:35, 11:30, 11:25.

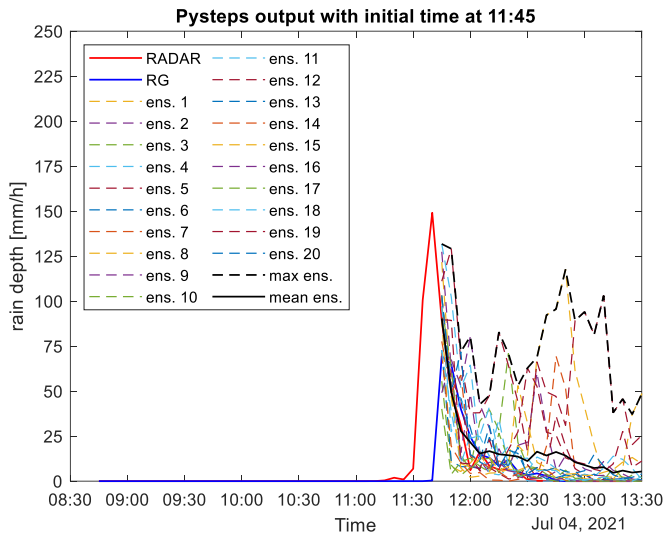


Fig. 6.27 Comparison between 20 ensembles (ens.) from pySTEPS, observed RADAR values and Rain Gauge (RF) with initial time at 11:45¹¹.

As previously stated, comparing pySTEPS outputs with the ones of our models is not entirely fair. Indeed, the nowcasting skills of these two models depend on the user’s focus. Furthermore, the models are based on opposite approaches and use different input data with different spatial resolutions. PySTEPS model uses radar data, which have a higher spatial resolution but lower accuracy than rain-gauge ones. Indeed, regarding the analysed event, radar measurements showed a bias compared to rain-gauge ones. Thus, pySTEPS with radar measurements should be preferred when the achievement concerns quality nowcasts over an area. Alternatively, the user should check the discrepancy between radar and rain gauge measurements beforehand. However, it is broadly known that radars struggle to register convective events and the rainfall is usually overestimated (Asghari et al., 2021). Also, the ensembles of pySTEPS turned out to be reliable up to 15 min ahead. Indeed, for higher lead times, they showed chaotic behaviour.

¹¹ Initial time at 11:45 means that the registration used to obtain the nowcasts are those at time 11:40, 11:35, 11:30.

On the other hand, the proposed approach preferred accuracy at the cost of a lower spatial resolution. It used rain gauge data but is also suitable for radar data. Thus, a more fair valuable evaluation would consider pySTEPS with rain-gauge data or the proposed approach with radar one.

At this research stage, the comparison with pySTEPS showed a clear advantage in using the proposed approach when the target requires accurate data. For most of the lead time, the proposed model outperformed both benchmarks – pySTEPS and EP.

References

- Ayzel, G., Scheffer, T., Heistermann, M., 2020. RainNet v1.0: A convolutional neural network for radar-based precipitation nowcasting. *Geosci. Model Dev.* 13, 2631–2644. <https://doi.org/10.5194/gmd-13-2631-2020>
- Capozzi, V., Picciotti, E., Mazzarella, V., Marzano, F.S., Budillon, G., 2018. Fuzzy-logic detection and probability of hail exploiting short-range X-band weather radar. *Atmos. Res.* 201, 17–33. <https://doi.org/10.1016/j.atmosres.2017.10.006>
- Hosseinzadehtalaei, P., Ishadi, N.K., Tabari, H., Willems, P., 2021. Climate change impact assessment on pluvial flooding using a distribution-based bias correction of regional climate model simulations. *J. Hydrol.* 598, 126239.

Chapter 7 - Synthesis and Conclusions

This chapter provides a synthesis of the research work (**section 7.1**), in which the main findings are summarised and discussed, together with the implications for future research (**section 7.2**). The application of the models to different contexts is discussed and compared: the Italian and the Belgian applications are described, and a comparison of them is provided.

7.1 - Synthesis

This research aimed to investigate rainfall nowcasting performance by exploiting machine learning techniques. First, existing nowcasting models were explored; thus, each approach's weaknesses and strengths were identified. Next, the differences between Model Driven Models (MDMs) and Data-Driven Models (DDMs) and between deterministic and probabilistic approaches were specified. Then, the pros and cons of the data type that could be employed were pointed out; thus, the differences between weather radar measurements and rain gauge ones were examined.

This initial phase allowed identifying the ideal approach to enhance nowcasting techniques. Therefore, according to the outlined requirements, a machine learning

model for probabilistic rainfall nowcasting for short lead times - from a few minutes up to 6 hours - was proposed. A machine learning approach was adopted because they do not require any previous physical assumption. Indeed, short-term prediction is challenging because meteorological variables are strongly interconnected and rapidly change during an event. Thus, machine learning models were preferred since they could identify relevant features in the data and provide reliable and quick forecasts.

The model used cumulative rainfall depths from rain-gauge stations as input. Rain gauge data were used since they are considered reference devices for measuring the amount of precipitation at ground level (Duan et al., 2021; Moraux et al., 2019; Shehu and Haberlandt, 2021). Thus, the preferred feature was accuracy instead of the higher spatial resolution that a weather radar could have given. The idea of using cumulative rain depth from nearby stations was due to the feed-forward neural network's lack of temporal memory. This allowed us to store antecedent time steps and to use only the current rain field as input, resulting in a rapid and easy-replicable method.

Moreover, since precipitation nowcasts issued by ML systems are often uncertain, the proposed models also gave a probabilistic interpretation of the prediction. In particular, the probabilistic nowcast was achieved by employing the Softmax function in the machine learning model, widely used to solve nonlinear multiple classification problems. Therefore, the model supplied the most likely forecast with the associate probability.

To investigate the extendibility of the model, the procedure was applied to two different contexts: in Campania Region (Southern Italy) and Flanders Region (Belgium).

Application in Italy

In Italy, 95 feed-forward neural networks were independently trained and tested on 359 rainfall events over the study area – one of the eight warning zones of the Campania Region in Southern Italy. The model employed cumulative rainfall depths of the recording stations, classified into 20 classes, as an input for the feed-forward

neural network, which nowcast probable rain intervals after 30, 60, 120, 180, and 360 minutes.

The dataset was split into two parts to provide a proper training strategy, avoiding overfitting while preserving generalization abilities: years 2009 to 2016 were used to train the models, while 2017 to 2019 to test. The performance of each model was evaluated and compared using different metrics, both continuous (RMSE and RSE) and categorical (POD, CSI, and FAR). In addition, the Eulerian Persistence (EP) was considered a benchmark model.

Generally, the models with a lead time of up to 2 hours produced consistent nowcasts and learned the complex relationship describing space-time rainfall evolution. As expected, predictive accuracy gradually decreased as the lead time increased, according to physically based models. Notwithstanding the decreasing trend, the performance indicators were all close to their optimal range, confirming the goodness-of-fit of the models. The RMSE mean values increased from 1.67 mm to 6.15 mm, while RSE ranged between 1.58 and 18.64 % from 30-minutes to 6-hours lead time models, respectively. Model accuracy analysis revealed similar trends: POD and CSI decreased from 0.5 h to 6 h lead-time model, while FAR increased. The 30-minutes lead times models achieved the highest CSI (90.94%) and POD (91.64%), and lowest FAR (0.82%), giving better performance. The proposed models outperformed the benchmark EP for all the lead times and performance criteria.

Results showed that it was possible to make a nowcast better than the EP by considering the cumulative rainfall depth from adjacent stations. Thus, using temporal and spatial information for precipitation nowcasting allowed an extension of the lead time up to which a reliable forecast may be issued, providing a quick prediction based solely on actual values.

To the authors' knowledge, this study is the first to present a comparative analysis of the performance of rainfall nowcasting models based on rain gauge information and modern machine learning algorithms in predicting probable rainfall intervals with 10-minutes update frequency.

Moreover, the model's ability to predict different events was investigated. The performances of the proposed nowcasting models were compared for two events of the testing set whose characteristics were similar to convective events - characterized by high intensities and short durations - and stratiform ones - characterized by more significant areas of influences, higher durations, and lower rainfall intensities -, respectively.

According to the results, the models provided better nowcasts when the event extension was homogeneous but failed to catch local precipitation events sufficiently in advance successfully. Thus, as expected, the potential lead time is short for convective rain events, where the rain evolves rapidly. Even though the models detected the increasing rainfall pattern registered, for higher lead-times models, the nowcasts were more significant than the observed values, resulting in an overestimation. To contrast, the stratiform event was better predicted than the convective one. We believe these results were possible thanks to gradual, light rain evolution, consisting of larger, more persistent systems.

Application in Belgium

The model was also applied in the Flanders Region of Belgium. From 2017–2021, 360 rainfall events were selected to test the approach. The model used cumulative rainfall depths as inputs to predict rainfall intervals and the corresponding probability of occurrence in one station after DT lead time. Six models were independently trained for six lead times (5, 10, 30, 60, 120, and 180 minutes). The input data for the considered station model were the cumulative rainfall depths from recording stations within a 50 km radius. The training strategy was the same as the one described in Italy.

The performance of the six models was assessed for training, validation, and testing sets. As expected, the training set achieved the best results, while the performance of validation and testing sets was slightly lower. These trends indicate that the training strategy was successful; thus, the models achieved a competitive generalization ability. Indeed, the results of the validation and testing sets did not overly underperform the training set, but they followed a similar trend. All the indicators

deteriorated with the lead time: POD and Pearson coefficient decreased, while FAR and MAE increased. This also confirmed that the physical behaviour was fulfilled.

Even though the indicators declined with the lead time, they all outperformed the benchmark model EP. In contrast to the trends of the model, the trend of EP with lead times was unstable. Even though for a lead time of 5 minutes, the indicators for EP achieved better results, as soon as the lead time increased, the indicators sharply deteriorated. The main reason for this poor performance was probably due to the chaotic and rapid evolution of the rainfall. Indeed, EP was sensitive to the previous observation; thus, when the rainfall quickly evolved and changed, the values were weakly correlated, and the EP was no longer valuable.

The performance of the models was also compared with the results of another benchmark: Pysteps. The comparison was more qualitative than quantitative. Indeed, the models were based on opposing approaches and used different input data with different spatial and temporal resolutions. Therefore, more than defining the best model, the comparison highlighted their suitability in different contexts. For example, the PySTEPS model used radar data with a higher spatial resolution but lower accuracy than rain-gauge ones. Indeed, regarding the analysed event, radar measurements showed a bias compared to rain-gauge ones. Thus, it allowed deriving that pySTEPS with radar measurements should be preferred when the achievement concerns quality nowcasts over an area. Also, the ensembles of pySTEPS turned out to be reliable up to 15 min ahead since they showed chaotic behaviour for higher lead times. On the other hand, the proposed approach preferred accuracy at the cost of a lower spatial resolution. Furthermore, it used rain gauge data but was also suitable for radar data. Thus, a more fair valuable evaluation would have considered pySTEPS with rain-gauge data or the proposed approach with radar one.

The comparison with pySTEPS showed a clear advantage in using the proposed approach when the target requires accurate data. Furthermore, for most of the lead time, the proposed model outperformed both benchmarks – pySTEPS and EP.

Comparison between the Italian and Belgian applications

The application in Italy and Belgium assessed the extendibility of the procedure to different contexts. Indeed, the considered Regions had different climatic and orographic characteristics. For example, the study area in Italy had a complex highlands system and two main volcanic structures, which enhanced convection systems development, especially in summer. Furthermore, the study area was near the Mediterranean Sea; thus, the prevailing climate was the Mediterranean, characterized by long dry summer periods and rainy winters with mild temperatures. On the other hand, the Belgian Region had a temperate maritime climate with cool summers and, moderate winters, high humidity during the year. Owing to the flat topography, precipitations followed a similar and homogeneous pattern.

Results were promising in both cases. First, the physical behaviour was achieved for both applications: the performance of the models deteriorated with increasing lead times; thus, the nowcasts were physically based. Then, all the models outperformed the benchmarks, especially for higher lead times, which was an important goal, especially for operational early warning purposes. Then, the procedure was tested for convective rainfall events, characterised by rapid and chaotic evolution. They provided notable nowcasts for a lead time of up to 1 hour, which is valuable for dispatching decision-making. POD, CSI, and FAR suggested that the models could support Early Warning Systems to increase preparedness until more data becomes available. We believe these results were possible thanks to the joint use of cumulative rain depth from nearby stations

7.2 - Outlooks or Implications for Future Research

From an operational perspective, the proposed methodology presents some advantages that enable it to be upgraded into an early warning system for hydrological applications. Firstly, it employed punctual rainfall information and did not use areal data, which inevitably provides averaged results. Consequently, it accounts for local

characteristics detected by rain gauges, such as convective cells – which feature high intensity and short durations. Moreover, the model has 10-minutes temporal resolution comparable to convective cell life. Then, the model provided a probabilistic nowcasting of precipitation that allows the assessment of different scenarios. Indeed, the predictions are not specific values, but rain intervals, with associated probabilities of occurrence. Finally, the high update frequency (10-minutes) is a fair trade-off between the optimal (5-minutes) and the sufficient (15–minutes). Consequently, the predicted precipitation fields are available to the forecasters in real time to quickly assess the current weather situation.

For future work, a study will be conducted on how the station's location influences the model performances. One idea is to group the results according to the relative distance between the stations or according to the area of influences of each station – which could be the Thiessen Polygon area. Moreover, the results would also be grouped according to the type of the event (convective, stratiform, or mixed), as well as the duration of the event. This would be an interesting comparison, which may help future research to identify specific patterns that need to be incorporated into future models.

In conclusion, findings suggest that the model is suitable for a real-time early warning system, especially for catchments with small areas and short response times.

Data Availability

Rainfall data will be available on request.

Publications

Pirone, D., Cimorelli, L., Del Giudice, G., Pianese, D., **2023**. *Short-term rainfall forecasting using cumulative precipitation fields from station data: a probabilistic machine learning approach*. J. Hydrol. 617, 128949. <https://doi.org/10.1016/j.jhydrol.2022.128949>.

Pirone, D., Cimorelli, L., Del Giudice, G., & Pianese, D., **2022**. *Rainfall Nowcasting Exploiting Machine-Learning Techniques: A Case Study in Southern Italy*. Environmental Sciences Proceedings, 21 (1), 49.